Restraint Biomechanics in Frontal Impacts with Inboard-Leaning Occupants

A Thesis

Presented to

the faculty of the School of Engineering and Applied Science

University of Virginia

in partial fulfillment
of the requirements for the degree

Master of Science

by

John Paul Donlon

August 2019

APPROVAL SHEET

This Thesis
is submitted in partial fulfillment of the requirements
for the degree of
Master of Science

Author Signature: John Paul Donlon

This Thesis has been read and approved by the examining committee:

Advisor: Richard Kent

Committee Member: Jason Kerrigan

Committee Member: Robert Salzar

Committee Member: Jason Forman

Committee Member: ____________________

Committee Member: ____________________

Accepted for the School of Engineering and Applied Science:

Craig H. Benson, School of Engineering and Applied Science

August 2019

Abstract

Up to one half of drivers swerve before a crash. Pre-crash swerving moves occupants into lateral out-of-position postures, which can affect the interaction of the occupant with the restraint and subsequently the risk of injury. The influence of lateral out-of-position postures on the performance of restraint systems remains poorly understood. Because of this, design and evaluation of restraint systems do not yet account for lateral out-of-position postures. Therefore, the goal of this thesis was to evaluate the effect of a swerve-induced inboard lateral lean on the kinematics and kinetics of an occupant in a frontal crash.

A realistic inboard-leaning posture was quantified from simulated swerving with nineteen human volunteers. Repeated frontal impact tests were then performed with three post-mortem human subjects (PMHS) seated in a neutral, in-position posture and in the inboard-leaning, out-of-position posture obtained from the volunteer tests. The PMHS were restrained by a contemporary three-point seatbelt with a retractor pre-tensioner and a nominal 2.5-kN retractor force-limiter.

Compared to the neutral posture, the inboard-leaning posture increased the initial length of seatbelt webbing from the D-ring to the acromion by 130 mm ± 25 mm (a 32% increase). The increased initial length permitted the head to displace farther forward during the impact by 69 mm ± 13 mm (a 27% increase). Compared to the neutral posture, the inboard-leaning posture also increased the initial angle between the shoulder-to-D-ring seatbelt segment and the impact acceleration vector (the forward-rearward axis) by 16° ± 2° (a 48% increase). The increased initial angle caused the occupant to swing forward and outboard, tracing out a greater displacement than in the neutral tests but without delaying the time of maximum forward displacement. This increased the

maximum resultant velocity of the head by 1.5 m/s ± 0.1 m/s (a 40% increase), which may significantly increase the risk of head injury if the head were to contact another occupant or the vehicle interior. Compared to the neutral-posture tests, the inboard-leaning tests did not significantly change the timing and magnitude of forces in the seatbelt.

This study's results suggest the need for pre-crash safety systems. The postural dependence of occupant restraint biomechanics implies that systems that keep an occupant in a neutral posture before the crash may be more effective than systems that attempt to restrain the occupant during the crash. Future work should explore the effectiveness of pre-crash countermeasures and the consequences of such countermeasures for occupant protection.

Acknowledgements

First, I thank the donors and their families: their precious gift has, I hope, been well employed to save others' lives. Second, I thank Joyson Safety Systems for funding this research and supplying the restraint systems. Next, I must thank my advisor, Rich Kent. He has been a friend and advisor to me, supplying opportunities for personal and professional growth. I also thank my committee: Jason Kerrigan, for teaching me to present research; Rob Salzar, for jumping on at the last minute; and especially Jason Forman, for guiding me through this whole research project (and beyond). Kristy Arbogast, Tom Seacrist, and Christine Holt, of the Center for Injury Research and Prevention at the Children's Hospital of Philadelphia, generously shared their data and analysis from the volunteer tests. I owe a great debt to the diligence and expertise of the team at UVA's Center for Applied Biomechanics in the preparation, execution, and analysis of the PMHS tests: Mohan Jayathirtha, Sara Heltzel Sochor, Kevin Kopp, Brian Overby, Rachel Richardson, Patrick Foltz, Tom Hartka, M.D., Mark Sochor, M.D., and Kristin Schmidt. I owe as great a debt to my fellow "Cabbies" for their open ears: Jacek, Carolyn, Dani, Kasia, Gwansik, Bronek, Meade, Watson, Rachel (again), Sara (again), and so many others. I especially thank Rachel & Carolyn for reviewing this thesis document. After seven years at CAB, and while completing three degrees, I also thank the past Cabbies who got me started—Fran and Damien—and the ones who kept me going—David, Bingbing, Alex, and others. Lastly, I thank my family for their support. In particular, I thank my mother and sister for keeping me fed, my sister also for reviewing the thesis document, and my many nieces and nephews for keeping me sane.

If I have erred in anything I have written, I leave its correction to the Center for Applied Biomechanics at the University of Virginia.

Table of Contents

Table of Figures

Table of Tables

Chapter 1. Out-of-Position Occupants: A Motivation for Expanded Research

1.1. Introduction

Car crashes remain a leading cause of death and injury in the United States (Center for Disease Control and Prevention, 2015) and globally (World Health Organization, 2015). One of the major difficulties in automotive safety design is variability in the posture of the occupant (Searle et al., 1978; Mackay, 1994). Design, evaluation, and regulation of restraint systems have primarily been performed with anthropomorphic test devices (ATD, crash test dummies) placed in a "normal" seated posture—torso and head upright, facing forward, and symmetric (e.g., National Highway Traffic Safety Administration (NHTSA), 1999, 2012). However, studies of field data have found that many crashes involve pre-impact vehicle motions (Ejima et al., 2012; Scanlon et al., 2015), which may cause occupants to be "out-of-position" at the start of the crash (Huber et al., 2014; Graci et al., 2018). Out-of-position postures may change the geometric relationship of the occupant and the restraint before a crash (Parenteau et al., 2002, 2006a, 2006b; Arbogast et al., 2012), and thus may affect the performance of the restraint system during the crash.

Previous studies have found a high incidence of attempted avoidance maneuvers preceding crashes in the field. For example, Thomas et al. (1996) found that 19% of drivers braked, 24% steered, and 18% braked and steered prior to fatal crashes in France. In contrast, Langwieder (1999) found that 25 to 36% of crashes involved pre-crash corrective steering attempts, while 51% involved pre-crash braking. Scanlon et al. (2015) found similar proportions of pre-crash maneuvers in intersection crashes in the United States (14% braked, 10% steered, 57% braked and steered). In contrast, Riexinger and Gabler (2018) found less pre-crash braking in road-departure crashes (6%

braked, 56% steered, 31% braked and steered), as did Viano et al. (2003) in rollover crashes (6% braked, 13% steered, 3% braked and steered). On the other hand, Ejima et al. (2012) found pre-crash braking to be more common (35%) than pre-crash steering (5%) and combined braking and steering (12%). Pre-crash braking was also more common (69%) than steering (4%) and combined braking and steering (24%) for near-crashes in the United States (Seacrist et al., 2018). While the distribution of maneuver type varied greatly among these studies, they all reported a high incidence of pre-crash maneuvers.

Pre-crash braking has been shown to cause occupants to lean or move forward in the vehicle. For example, Kumbfbeck et al. (1999) found that emergency braking from 80 km/h to a standstill caused the occupant to lean forward, decreasing the distance between the volunteer's head and the dashboard from 60 cm to 30 cm for a normal seated posture. Carlsson and Davidsson (2011) further found that the forward displacement of the occupant's head and chest varied with sex (greater for males than for females) and stature (greater for taller occupants, independent of sex). Another study found that the driver's forward head displacement during emergency deceleration was moderately (~6 cm) greater for automatically actuated braking with the driver distracted than for driver-induced braking (van Rooij et al., 2013a). In tests with autonomous emergency braking (AEB), Ólafsdóttir et al. (2013) and Östh et al. (2013) found that activation of a reversible 170 N pretensioner (a "pre-pretensioner") significantly reduced forward displacements of the head and T1 vertebra for all occupants. They also observed significant muscle activation in the hips, abdomen, neck, and shoulders during the tests, with earlier muscle activation in tests with the pre-pretensioner (even earlier for females than for males). Researchers at another institute found greater variability in occupant kinematics for a low-constraint environment (rigid seat with lap seatbelt) when compared to a standard environment (foam-covered seat with lap-shoulder seatbelt) (Kirschbichler et al., 2014; Huber et al., 2014, 2015). They also found that a three-point lap-shoulder seatbelt significantly reduced the forward displacement of the head and chest as compared to a lap-belt. Finally, emergency braking with passengers restrained by a three-point seatbelt was found to cause significant lateral head displacements (up to 11 cm) along with the expected forward head displacements (up to 27 cm) (Jones et al., 2017).

In contrast to braking, evasive steering has been shown to cause occupants to lean or move laterally in the direction opposite to the direction of steering. One research group observed that volunteers leaned outboard—toward the vehicle door—in low speed near-side lateral sled tests (Parenteau et al., 2002), but leaned inboard—away from the vehicle door—in far-side tests (Parenteau 2006a, 2006b). Using the typical three-point seatbelt with outboard D-ring, they also observed that the shoulder-belt moved medially up against the neck when the occupant leaned outboard, while the shoulder-belt moved laterally along or even off the shoulder when the occupant leaned inboard. Dynamic muscle activation in the torso, back, and neck was observed in sinusoidal steering tests (Muggenthaler et al., 2005), a phenomenon which significantly affects occupant motion (Ejima et al., 2012) and varies with age (Graci et al., 2018). The effect of pre-crash steering on changes in occupant posture and seatbelt path have been shown to be sensitive to the restraint design and occupant characteristics. For example, Bohman et al. (2011b) found that the motion of the seatbelt on the shoulder of shorter children during emergency steering depended on the seating condition: the seatbelt slipped off the shoulder for shorter children when they sat on a booster seat, but not when they sat on a highback booster cushion. Bohman et al. (2011b) also observed that the seatbelt moved far laterally along the shoulder of taller children regardless of seating condition (three-point belt only or booster seat). Researchers at another institute found greater variability in occupant kinematics during evasive steering for a low-constraint environment (rigid seat with lap-belt) when compared to a standard environment (foam-covered seat with three-point belt and lateral support structures) (Kirschbichler et al., 2014; Huber et al., 2014, 2015). They also found that the lateral support structures significantly reduced the lateral displacement of the head and chest. Similarly, the addition of a four-point harness was found to reduce lateral displacement of the head significantly in simulated steering tests, and a driver environment (holding the steering wheel) further reduced lateral displacement compared to a passenger environment (van Rooij et al., 2013b). Countermeasures to steering-induced out-of-position postures have also been evaluated. Holt et al. (2018) found that activation of a 200N motorized, reversible pre-tensioner (a "pre-pre-tensioner") significantly reduced lateral displacement of the head and chest, as did active bracing by the volunteers; but increased lateral support structures did not substantially reduce lateral displacements. The reduced lateral displacement observed with a pre-pre-tensioner is consistent across age (Arbogast et al., 2012) and the addition of braking to steering (Ghaffari et al., 2018).

Out-of-position postures have been shown to affect restraint performance in many cases. For example, proximity to frontal airbags has been shown to affect the risk of injury to the head and thorax. In static passenger-side frontal airbag deployment tests with anesthetized baboons, Patrick and Nyquist (1972) found severe displacement and injury outcomes for initial postures near to or against the airbag module. In static airbag deployment tests with the Hybrid III dummy, Horsch and Culver (1979) found significantly higher chest compression for occupants initially placed adjacent to the airbag module (84 mm) compared to occupants initially upright (18 mm). In steering-wheel airbag deployment tests with the Hybrid III dummy and anesthetized swine, Horsch et al. (1990) found that injury risk was highest when the airbag module was centered on the sternum as opposed to the neck or head. Crandall et al. (1999) performed static steering-wheel airbag deployment tests with the Hybrid III 5th-percentile female ATD and seven small female PMHS with the occupant's chest postured directly against the airbag module. They found that this out-of-position posture resulted in multiple rib fractures, and that injury severity may have depended on the pressure onset rate of the airbag. As another example, the posture of the upper extremities relative to frontal airbags or lateral impacting structures has been shown to affect the risk of injury to the upper extremities. In lateral impact drop tests with two human cadavers, or post-mortem human subjects (PMHS), Stalnaker et al. (1979) found that entrapment of the ipsilateral upper extremity decreased the maximum force applied to the thorax. In side impact tests with eight PMHS, Cesari et al. (1981) further observed that the arm distributed the impact force across the chest when the arm was postured between the impactor and the chest. In side impact tests with four adult male PMHS, Kemper et al. (2008) observed that peak forces, peak rib deflections, and peak rib strains were highest when impacting the ribcage alone and lowest when impacting the ribcage and shoulder together. They further found that peak forces, rib deflections, and rib strains were higher when the arm was fully entrapped (parallel to the spine) than when the arm was placed 45° up from the spine. Subit et al. (2010) performed repeated localized lateral impacts on three adult male PMHS and found that the force-deflection and injury response of the thorax was sensitive to the anatomic structures engaged (stiffest when striking the shoulder), the rate of impact (stiffer for a higher velocity), and the direction of impact (more rib fractures for anterolateral impacts than for lateral or posterolateral impacts). In static steering-wheel airbag deployment tests with the 50th-percentile male Hybrid III ATD and dynamic paired tests with the MADYMO™ model of the same ATD, Hault-Dubrulle et al. (2011) found that upper extremities postured adjacent to the airbag module caused not only injurious loading of the forearm, but also injurious head accelerations and neck moments due to arm strikes to the head. The posture of the lower extremities has also been shown to affect injury risk and seatbelt effectiveness. In frontal tests with the Hybrid III dummy, Bacon (1989) found that a decrease in seat cushion angle—and, subsequently, thigh angle—from 4.5° to -5.5° caused the lap-belt to slide over the top of the pelvis and intrude into the abdomen, a phenomenon called submarining. To quantify the effect of hip posture on hip injury tolerance, Rupp et al. (2003) performed dynamic knee loading tests to the right and left lower extremities of 22 PMHS. Using a matched-pair analysis, they found that hip fracture tolerance decreased by 34% for a 30° flexed hip posture and by 18% for a 10° adducted hip posture as compared to a neutral hip posture. As another example, occupant trunk posture has been shown to affect injury risk in rear impacts, where the primary restraint is the seat back. Strother et al. (1994) performed rear impact tests with the Hybrid III in a forward-leaning posture, in both a "yielding" (standard) and a "rigidified" (foamless, rigid) seat. They found that, for the forward-leaning posture, neck forces and moments increased to near-injurious levels in the "rigidified" seat as compared to the "yielding" seat. In rear impact tests with the Hybrid III dummy, Benson et al. (1996) found that forward-leaning postures increased neck forces and moments by as much as 50%, with greater increases in stiffer seats. Viano et al. (2018a; 2018b) performed rear impact tests with 5th-percentile female, 50th-percentile male, and 95th-percentile male Hybrid III ATDs initially leaning forward, inboard, or both. They found that out-of-position postures led to higher forces and moments in the neck, thoracic spine, and lumbar spine. As a final example, several studies have shown that the posture of the occupant's torso affects injury risk in crash modes in which the seat back is not the primary restraint. Bose et al. (2008) simulated frontal impacts with the MADYMO™ multibody human body model (HBM) (TASS, Helmond

Netherlands) in the driver's seat, restrained by a three-point belt and an airbag. They simulated crashes with the occupant in eight out-of-position postures identified from a survey of preferred occupant postures (Zhang et al., 2004), and found that posture significantly affected injury risk. In particular, Bose et al. (2008) found that a "close-to-wheel" posture (moved forward on the seat and leaned forward) yielded one of the two highest whole-body injury risks, with a relatively high risk of head injury, due to deployment of the airbag. The second of the two riskiest postures was an inboard lateral lean, which resulted in significantly increased risk of injury to the head and thorax. However, Bose et al. (2008) also observed a tradeoff: postures that increased risk of injury to the head and thorax typically decreased risk of injury to the lower extremities, and vice-versa. In simulated whole-body side impacts with the 50th-percentile adult male THUMS finite element HBM, Poulard et al. (2014) matched the posture of three PMHS in whole-body side impacts performed by Lessley et al. (2010) and Shaw et al. (2014). They found that the small variations in spine posture observed in the PMHS tests caused a range of reaction forces, rib strains, and predicted injuries in the model equivalent to that observed in the PMHS tests. Kitagawa et al. (2017) simulated frontal crashes with the 50th-percentile adult male THUMS finite element HBM seated in forward- and rear-facing seats with or without recline. They found that the reclined posture resulted in greater displacement of the T1 vertebra for the rear-facing occupant than for the forward facing occupant. Lin et al. (2018) simulated frontal collisions with the 50th-percentile male finite element HBM of the Global Human Body Model Consortium (GHBMC) in various degrees of recline. They predicted that a 40° or 60° recline would cause the lap-belt to slip over the pelvis (submarining) with subsequent serious lap-belt intrusion into the abdomen. Matsuda et al. (2018) simulated pre-crash braking and steering (left and right) with the THUMS midsize adult male finite element HBM in the driver's seat, restrained by a three-point belt, and found that the pre-crash maneuvers greatly changed the posture of the occupant. For both braking- and steering-induced postures, they then simulated a crash (frontal or near-side lateral) with additional deployment of a frontal airbag. Matsuda et al. (2018) found that the seatbelt slipped off the shoulder in combined left steering (which leaned the occupant inboard) and frontal crash, with subsequently increased risk of injury to the head and chest as compared to right steering or braking. They also found that activation of a 65 N pre-pretensioner during the pre-crash phase significantly reduced occupant lateral (for steering) or forward (for braking) displacement at the start of the crash phase; but still the seatbelt slipped off the shoulder for an inboard-leaning occupant in a frontal crash.

Most previous studies that have examined the effect of occupant posture on restraint performance have included a variety of scope and surrogates. Studies of airbag proximity have included PMHS, ATD, and animal surrogates placed in a variety of out-of-position postures (Patrick & Nyquist, 1972; Horsch & Culver, 1979; Horsch et al., 1990; Crandall et al., 1999). Studies of out-of-position postures in rear impacts have relied solely on ATD and HBM (Strother et al., 1994; Benson et al., 1996; Kitagawa et al., 2017; Viano et al., 2018a, 2018b), but have identified seatbelt use and seat stiffness as key factors in occupant response. Using PMHS, ATD, and HBM, many studies have examined the sensitivity of restraint performance and injury outcome to the posture of the upper extremities (Stalnaker et al., 1979; Cesari et al., 1981; Kemper et al., 2008; Subit et al., 2010; Hault-Dubrulle et al., 2011) or the lower extremities (Rupp et al., 2003). However, studies of the effect of trunk posture—recline or lateral lean—on seatbelt restraint have relied solely on simulations with computational HBM (Bose et al., 2008; Poulard et al., 2014; Kitagawa et al., 2017; Lin et al., 2018; Matsuda et al., 2018). HBM simulations are a powerful tool for modeling the broad diversity of occupants (child, elderly, male, female, obese, etc.) and assessing the response of the human body to complex loading scenarios (Crandall et al., 2011). However, refinement and validation of HBM requires data from human volunteer and PMHS tests, and no such data exist for seatbelt-dominated restraint of reclined or lateral-leaning occupants Furthermore, due to the paucity of physical data, it is unknown whether and how occupant trunk posture affects seatbelt performance.

1.2. Goal

Therefore, the goal of this thesis was to quantify the effect of an out-of-position posture on the occupant kinematics and restraint loads in order to evaluate the effect of the out-of-position posture on restraint performance.

Chapter 2 will present a combined strategy using volunteers and PMHS, the methodology and results of volunteer tests used to quantify the out-of-position posture, and the methodology of the PMHS tests used to quantify the effect of the posture on restraint performance. Chapters 3 and 4 will contain the evaluation of the effect of the posture on occupant kinematics (Chapter 3) and on restraint loads (Chapter 4). Chapter 5 will discuss the implications of this thesis for restraint biomechanics.

Chapter 2. Design of Study and Overall Methodology

The goal of the research that this chapter will describe was to design a study of the effect of occupant posture on restraint performance. The first step was to identify a crash mode (frontal, lateral, rollover, etc.) and a pre-crash posture (reclined, leaned, turned, etc.) of interest. The next step was to develop an experimental methodology by which to quantify the effect of the identified pre-crash posture on restraint performance in the identified crash mode. The final step was to perform experiments with this methodology.

2.1. Design of Study

As described in Chapter 1, past studies of the incidence of pre-crash evasive maneuvers in specific crash scenarios (e.g., rollover or road-departure crashes) found a higher proportion of steering than of braking. In contrast, studies not restricted to a specific crash scenario found a higher incidence of braking than of steering before the crash. However, no systematic correlations between pre-crash maneuvers and specific crash modes have yet been identified. Therefore, a frontal (12 o'clock) crash was selected for the current study, since frontal crashes make up 60% of crashes (Ridella et al., 2012). Frontal crashes with pre-crash braking show a reduced incidence of injury, but frontal crashes with pre-crash steering show either no reduction (Talmor et al., 2010) or even increased injury incidence (Ejima et al., 2012). Therefore, a pre-crash steering maneuver was selected for this study.

The goal of this thesis was to evaluate the effect of an out-of-position posture on restraint performance. To achieve this goal, a combined approach using volunteers and post-mortem human subjects (PMHS, cadavers) was used.

Pre-crash evasive steering may occur over two or three seconds, during which active and reactive musculature may affect occupant kinematics (Ólafsdóttir et al., 2013; Kirschbichler et al., 2014). Furthermore, the attendant accelerations of evasive steering may not exceed 1 g, which is within amusement park safety standards (ASTM F2291). Therefore, simulated evasive swerving tests with volunteer human subjects were performed to identify a potential worst-case out-of-position posture due to pre-crash swerving. Section 2.2. presents the methodology and results of the volunteer tests.

To maximize applicability of the out-of-position crash tests, a reasonable target crash velocity would be the median ΔV of frontal crashes, which in the United States is in the range of 30 to 44 km/h (Flannagan & Rupp, 2009). However, this velocity range corresponds to around a 15% probability of severe injury (MAIS 3+, Augenstein et al., 2003) in frontal crashes, and so is unsafe for volunteers. PMHS, while having many limitations in comparison to the response of living humans, are an accurate anatomic and structural surrogate for impact and injurious testing (Crandall et al., 2011). Therefore, simulated frontal crash tests with PMHS were performed to evaluate the effect of an out-of-position posture on restraint performance. Section 2.3. presents the methodology and initial positions of the PMHS tests, and Chapters 3 and 4 contain an examination of the resulting occupant kinematics and restraint mechanics.

2.2. Volunteer Testing Methodology

A series of simulated evasive swerving tests was performed using 19 adult male volunteers (Table 1). Subjects were recruited and handled with the approval of an Institutional Review Board at the Children's Hospital of Philadelphia. Informed consent was obtained from all volunteers. Subjects were confirmed free of past injury to or pathology of the head, neck, and spine. During the tests, subjects wore an athletic compression shirt and a pair of athletic shorts.

Table 1. Volunteer information. The target volunteer (Subject 42) and the PMHS are shown for comparison.

	Age [yr]	Mass [kg]	Stature [cm]	BMI [kg/m^2]	Seated Height [cm][a]
volunteer mean ± s.d.	26 ± 7	76 ± 12	176 ± 6	24 ± 3	86 ± 4
Subj. #42	26	86	176	28	87
PMHS 778	19	72	182	21	99
PMHS 816	37	73	178	23	103
PMHS 899	51	82	175	28	990

[a] Seated height of PMHS was estimated from supine pre-test CT scans as distance from top of head to pubic symphysis.

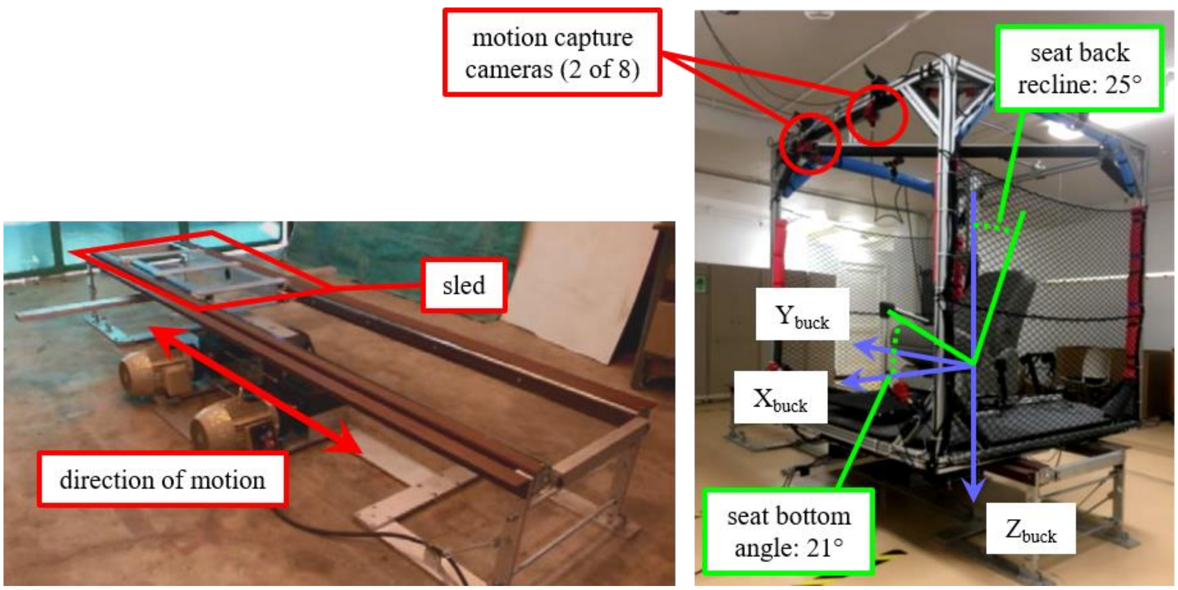

Figure 1. Scotch yoke mechanism (left) with occupant compartment (right) of the lateral acceleration device used in the volunteer tests (Seacrist et al., 2016; Holt et al., 2018).

Tests were performed with a lateral acceleration device (Seacrist et al., 2016). The sled consisted of an occupant compartment driven by a Scotch yoke mechanism on low-friction Teflon shoes along parallel steel rails (Figure 1). To simulate evasive swerving, the device imparted a sinusoidal lateral acceleration to the occupant compartment. For these tests, subjects were exposed to four periods of 0.75 g, 0.5 Hz sinusoidal lateral acceleration (Figure 2). This acceleration input was representative of closed-track and on-road tests of swerving and steering maneuvers (Seacrist et al., 2016). Lateral acceleration of the sled was measured by an onboard accelerometer at 10 kHz and filtered with a 4-pole Butterworth filter.

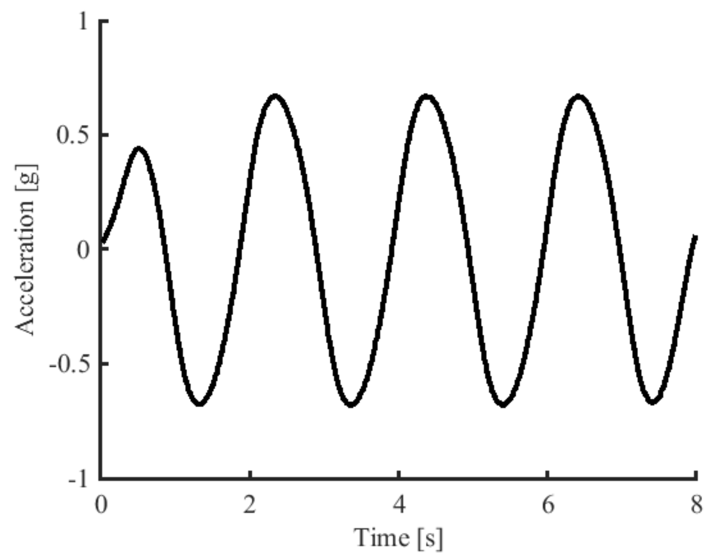

Figure 2. Lateral acceleration input for volunteer tests; average for all tests shown (Holt et al., 2017).

Subjects sat on a second-row captain's chair from a recent model year passenger van (2015 Toyota Sienna) (Figure 1, right). The seat bottom was angled 21° from horizontal and the seat back was angled 25° from vertical. After the volunteer tests, the seat pan angle of 21° was discovered to exceed the actual in-vehicle seat bottom angle of 15°. The PMHS tests used 15°. Subjects were restrained by a production 3-point seatbelt with an inactive pre-tensioner. The retractor included an inertial locking mechanism, activation of which was observed in overhead videos of the volunteer tests. The buckle and anchor were positioned to replicate a mid-track seat position. The lap-belt was placed below the anterior superior iliac spines. The D-ring was adjusted for each subject so that the shoulder-belt crossed mid-clavicle. Subjects sat centered on the seat, face forward, feet flat and centered on the footrest, with hands on thighs (Figure 3).

Reflective markers were attached to the head, torso, and upper and lower extremities (Figure 3). Eight Optitrack Flex 13 (NaturalPoint, Inc., Corvallis, OR) infrared cameras recorded the motions of the markers during the test at 120 Hz. The motions of the markers were reported with respect to a global coordinate system (GCS) on the buck, with axis polarities according to SAE J211 (X_{buck} positive forward, Y_{buck} positive to the right, Z_{buck} positive down; Society of Automotive Engineers (SAE), 2007). The origin of the buck GCS was placed on top of the undeformed seat, in the midline of the seat, at the target h-point fore-aft position (Figure 1, right).

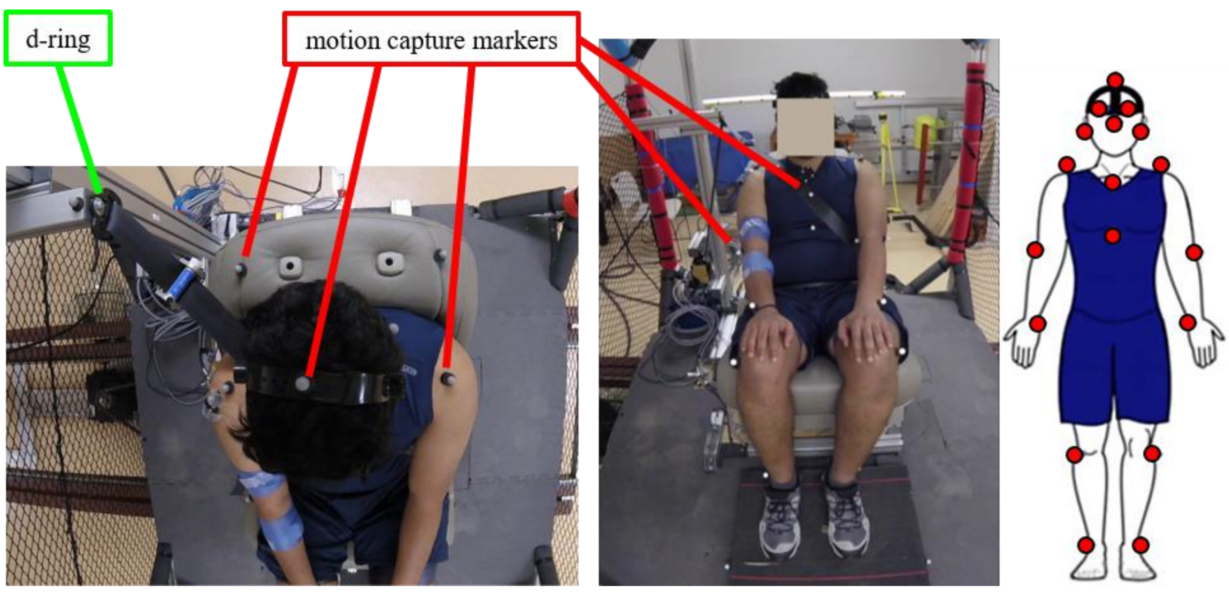

Figure 3. Initial position of volunteers and locations of motion capture markers (Holt et al., 2018).

2.3. Volunteer Testing Results and Identification of Target PMHS Posture

Figure 4 shows still photos of volunteer Subject 42 at key points during the first two cycles. The volunteer's maximum inboard and outboard displacements occurred out-of-phase (around 0.5 s lag) with the acceleration input. Figure 5 shows the time-history of the head lateral displacement of Subject 42 compared with the mean and ± 1 standard deviation corridor of all the subjects.

Subject 42 consistently displaced more than the mean, and displaced significantly more than the mean in every inboard peak. This implies that Subject 42 represented a worst-case scenario. Therefore, Subject 42 was selected to identify target postures for the PMHS tests. The inboard posture from the second cycle was selected as the target posture (Figure 4, 2.5 s), to avoid the startup effect of the first cycle (Figure 4, 0.5 s) and to avoid the possibility of learning effects in the third and fourth cycles.

The target posture was simplified from the second-cycle inboard posture of Subject 42 to calculate target lateral positions for the head and shoulders of the PMHS (Figure 4, 2.5 s). The volunteer's inboard posture included not only an inboard lean of the torso, but also an inboard turn of the whole body (Figure 4, 2.5 s). The whole-body turn was neglected for the PMHS to isolate the effect of the inboard lean. In addition, the neuromuscular state of the volunteer was neglected since it could not be replicated in the PMHS. The forces in the seat and seatbelt, though measured during the volunteer test, were reduced to a nominal value that represented a possible worst-case scenario for the occupant. The retractor locked in the volunteer tests due to the accelerations; this was not implemented in the PMHS tests, although a pre-tensioner was implemented at the start of the test. Two complementary targeting schemes were implemented for the PMHS: first to match the lateral displacements of the volunteer's head top and shoulders; and second to compare against the inboard lean angle of the volunteer. The head top and shoulders were selected as targets because the PMHS were to be supported by the head and shoulders.

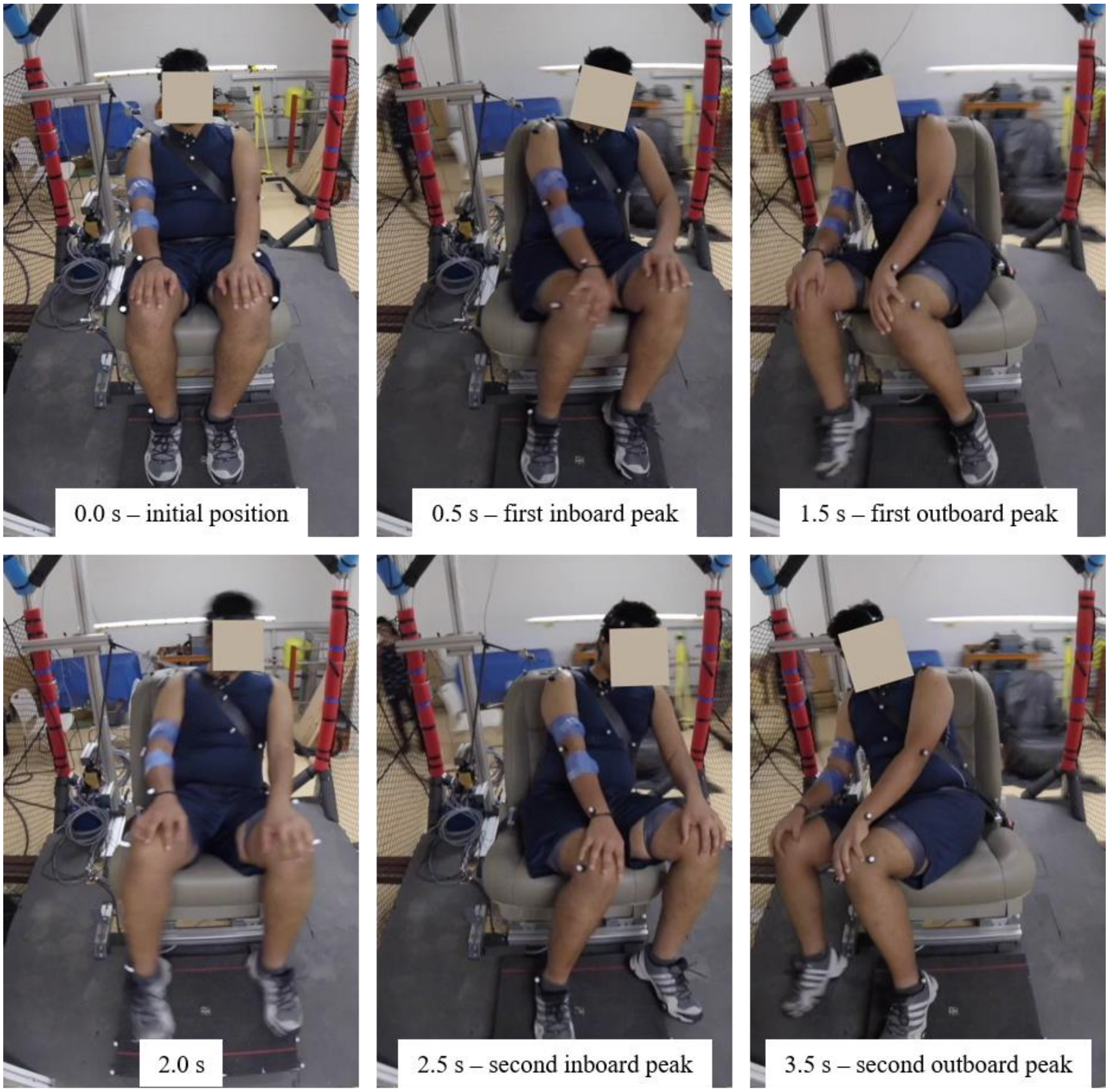

Figure 4. Video frames illustrating motion of volunteer Subject 42 in first two cycles of lateral acceleration.

The lateral displacements of the volunteer's head and shoulders from the neutral posture to the inboard posture were scaled to the PMHS according to seated height:

$$\Delta y_{PMHS} = \Delta y_{S42} \frac{h_{PMHS}}{h_{S42}}$$

where Δy_{PMHS} is the lateral displacement from neutral of a given point (head, left shoulder, or right shoulder) on the PMHS, Δy_{S42} is the lateral displacement from neutral of the same point on Subject 42, h_{PMHS} is the seated height of the PMHS (estimated from pre-test CT scans), and h_{S42} is the seated height of Subject 42. Table 1 lists the seated heights of Subject 42 and the PMHS, and Table 5 lists the lateral displacements of Subject 42 and the PMHS.

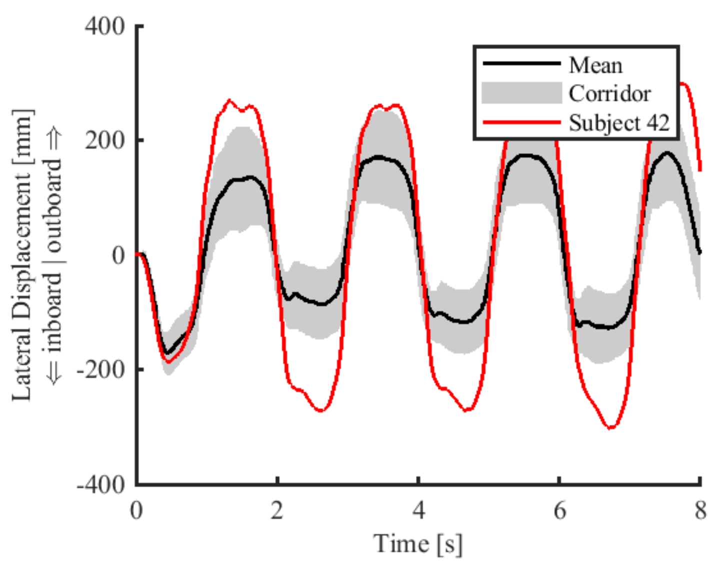

Figure 5. Mean head lateral displacement from volunteer tests with corridor (±1 standard deviation) and response of Subject 42 (Holt et al., 2018).

Since no markers were attached to the pelvis, buttocks, or thighs of the volunteer, the volunteer's torso lateral lean angle was calculated in the neutral and inboard postures as

$$\theta_{lat} = -\operatorname{atan}\left(\frac{y_{head,S42}}{z_{head,S42}}\right)$$

where the negative sign ensures that an outboard lateral lean angle is positive. Table 5 lists the torso lateral lean angles of Subject 42 and the PMHS.

2.4. PMHS Testing Methodology

A series of repeated neutral and inboard frontal sled impacts was performed using three midsize adult male PMHS (Table 2). The subjects were acquired and handled with the approval of and in accordance with the policies and procedures of the UVA Center for Applied Biomechanics Oversight Committee. The PMHS were frozen until testing. PMHS were ensured free of blood-borne pathogens including HIV and Hepatitis B and C. A full body computed tomography (CT) scan confirmed the absence of bone injury, and dual-energy X-ray absorptiometry (DXA) was used to evaluate bone quality.

Table 2. PMHS information.

PMHS #	Test #	Age [yr]	Sex	Cause of Death	Mass [kg]	Stature [cm]	BMI [kg/m^2]	BMD Total [g/cm^2]	BMD Ribs [g/cm^2]	Total T-score*
778	S0500 S0501 S0502	19	Male	Chemical (non-traumatic) asphyxia	72	182	21	1.255	0.861	†
816	S0503 S0504 S0505	37	Male	Alcoholic cirrhosis	73	178	23	1.199‡	1.294‡	0.7‡
899	S0506 S0507 S0508	51	Male	Unknown	82	175	28	1.461	1.241	2.6
mean	-	36	-	-	76	178	24			

* World Health Organization (WHO) criteria for post-menopausal, Caucasian Women:

Normal: T-score ≥ -1

Osteopenia: -1 > T-score > -2.5

Osteoporosis: -2.5 ≥ T-score

† T-score not computed because age < 21

‡ PMHS #816:

Total body BMD not measured; Total Mean Dual Femur results reported instead for BMD and T-score

Rib BMD not measured; AP Spine results reported instead

Each PMHS was subjected to three tests (Table 3). The first test was performed with the PMHS in a standard seated posture ("neutral"), and the second and third tests were performed with the PMHS in the inboard-leaning posture ("inboard") identified from volunteer Subject 42. After each test, the PMHS was palpated to assess overall changes in ribcage and neck stability. After the final test, rib and spinal injuries were identified via a CT scan and an autopsy. Each PMHS was wrapped with Coban™ (3M, St. Paul, MN) self-adhering wrap prior to testing to minimize fluid leakage and to cover and strain-relieve instrumentation cables. Anthropometry of each PMHS is included in Appendix A.

Table 3. PMHS test matrix.

Test Number	PMHS Number	Impact Velocity [km/h]	Torso Posture
S0500	778	30	Neutral
S0501	778	30	Inboard
S0502	778	41	Inboard
S0503	816	30	Neutral
S0504	816	30	Inboard
S0505	816	41	Inboard
S0506	899	30	Neutral
S0507	899	30	Inboard
S0508	899	41	Inboard

A trapezoidal reverse acceleration pulse was used in each test (Figure 6) using a Seattle Safety (Kent, WA) 1.4 MN ServoSled®. For the first two tests, a 9-g, 30-km/h pulse was used. For the third test, a 14-g, 41-km/h pulse was used. These crash velocities levels correspond to 12% and 34% probability of MAIS2+ (Stigson et al., 2012) and to 14% and 29% probability of MAIS3+ (Augenstein et al., 2003) in frontal crashes. The pulse shape, magnitudes, and durations were chosen based on past PMHS frontal sled tests (Shaw et al., 2009; Montesinos-Acosta et al., 2016), and represent a mid-size passenger car rigid barrier frontal crash pulse.

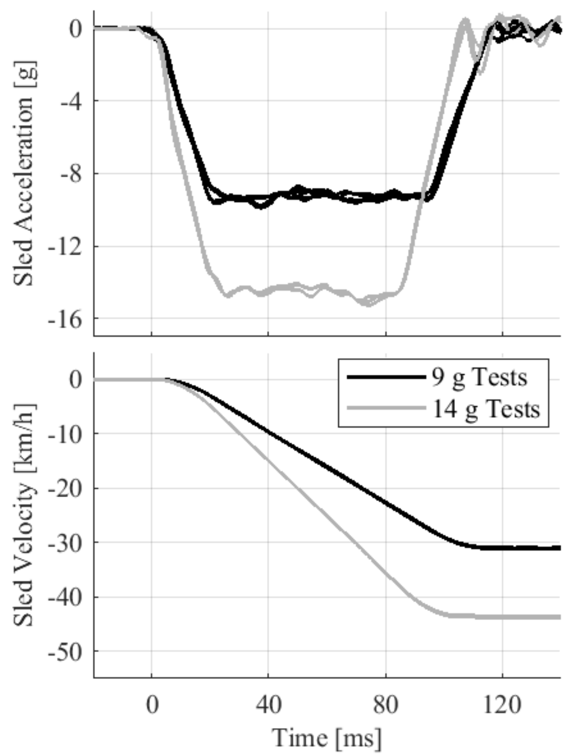

Figure 6. Acceleration (top) and velocity (bottom) inputs for the PMHS tests.

The sled test fixture ("buck") approximated a vehicle restraint environment while permitting motion capture visibility (Figure 7). The PMHS was seated on a second-row passenger-side seat cushion from a 2015 Toyota Sienna. The seat frame was reinforced with two transverse steel bars to ensure rigidity in the repeated tests without affecting the interaction of the cushion and frame. The seat was mounted to the buck via an aluminum baseplate and a 6-axis load cell. A pair of foam blocks attached to struts connected to the seat baseplate provided posterior support to the buttocks to maintain the fore-aft location of the bilateral greater trochanters (the hip-point or "h-point") (Figure 8).

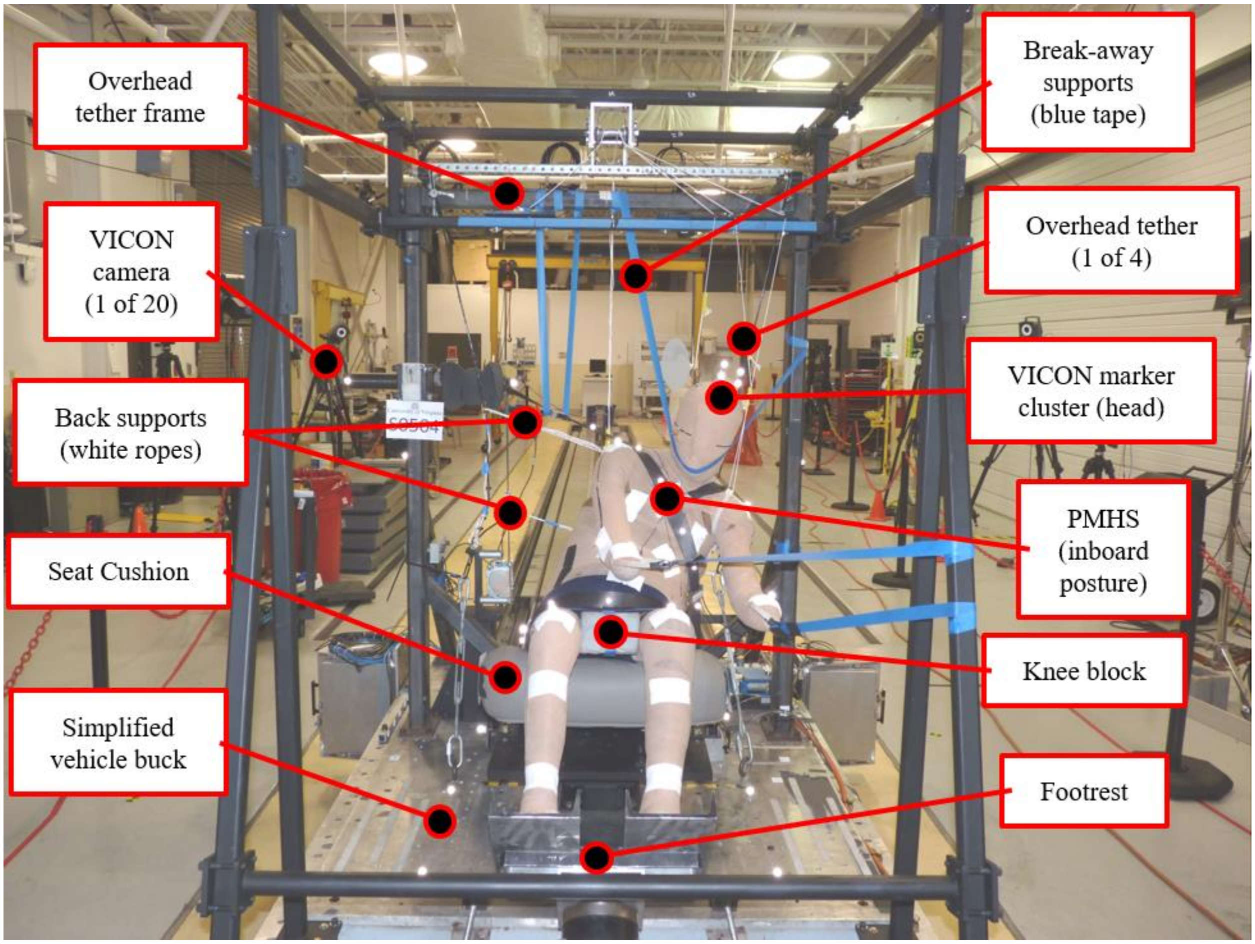

Figure 7. Front view of vehicle buck used in PMHS tests.

The target h-point with respect to the seat was calculated and marked on the seat based on measurements in an available 2017 Toyota Sienna and the initial ATD position reported in the Side Impact New Car Assessment Program (SINCAP) test report for the 2015 Toyota Sienna (NHTSA, 2015). The relevant structures (vehicle frame and seats) were identical for Toyota Sienna model years 2015-2017. The SINCAP test was selected because it was the only NHTSA-regulated test of the 2015 Toyota Sienna with a second-row occupant. The SINCAP test used a 5th-percentile female side-impact ATD (the SID-IIIsD), but the target h-point fore-aft position was the same as would have been achieved with a midsize male ATD (NHTSA, 2012). The seats in the available

2017 Toyota Sienna were configured as reported from the SINCAP test (Table 4). The h-point fore-aft position of the SID-IIIsD was then marked on the seat cushion in the 2017 Toyota Sienna, and this mark was duplicated on the seat cushion used in the tests (Figure 9). With the top of the seat cushion at the 15° angle observed in the available 2017 Toyota Sienna, the h-point fore-aft location corresponded with a transverse seam on the top of the seat cushion cover.

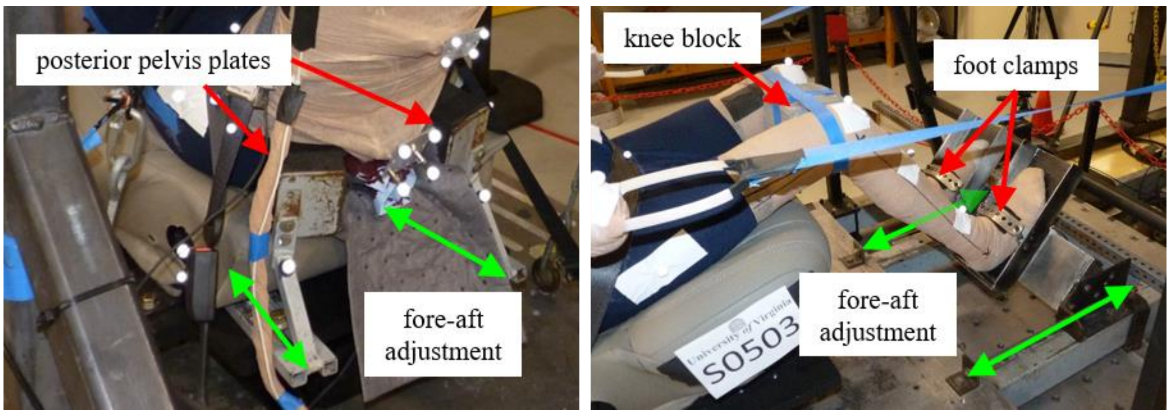

Figure 8. Mechanisms to constrain lower extremity posture: adjustable posterior pelvis plates (left), knee block and adjustable foot clamps (right).

To reduce the rearward displacement of the subject in the rebound after each test, the subject's feet were secured in a pair of aluminum channels, which were mounted via a 6-axis load cell to a baseplate that could be moved forward and backward on the buck (Figure 8). A 6-inch wide foam block was secured by frangible tape between the knees to keep the thighs parallel (Figure 8)

Table 4. Seat configurations and h-point location from SINCAP test report for the 2015 Toyota Sienna (NHTSA, 2015).

Value	Configuration/Measurement
Driver Seat Fore-Aft Detent	13th of 25 detents from the front
Driver Seat Back Recline	5th of 26 detents from upright
Second-row Passenger Seat Fore-Aft Detent	24th of 24 detents from the front
Second-row passenger Seat Back Recline	1st of 15 detents from upright
H-point location forward of c-pillar striker plate	280 mm

Two horizontal ropes supported the back of the PMHS, and a set of overhead ropes supported the head and shoulders of the PMHS (Figure 10). Each overhead rope passed through a sheave plate (Figure 10). The sheave plates were attached to a slotted lateral strut and could be independently adjusted laterally (Figure 10). The strut was attached to a frame and could be adjusted forward and backward (Figure 10). For each PMHS, the strut was secured in position above the head in the neutral posture of the first test, and left in that position for the subsequent tests. The sheave plates were centered laterally in the first test with each PMHS, and were shifted laterally according to the target lateral displacements calculated from Subject 42.

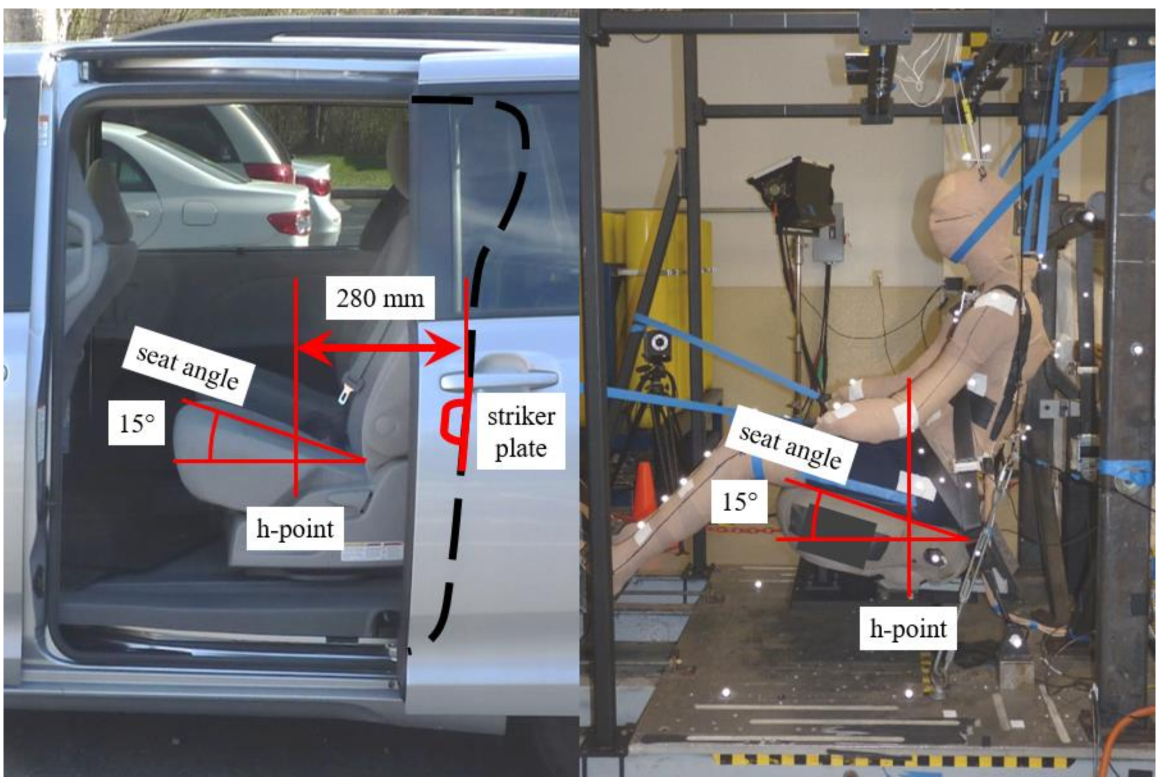

Figure 9. H-point location and seat angle in the target passenger vehicle (left) and in the buck (right).

A three-point seatbelt restrained the PMHS (Figure 7). The lap-belt anchor and buckle positions approximated those in the available 2017 Toyota Sienna when the second-row passenger seat was placed mid-track. The D-ring location was adjusted for each PMHS as described below (2.5. Positioning Procedure). The restraint was a custom-made (non-production) three-point belt system with a shoulder-belt pretensioner, which was activated 10 ms after the start of the test, and an approximately 2-kN load limiter (Joyson Safety Systems, Auburn Hills, MI). The restraint system was replaced after every test.

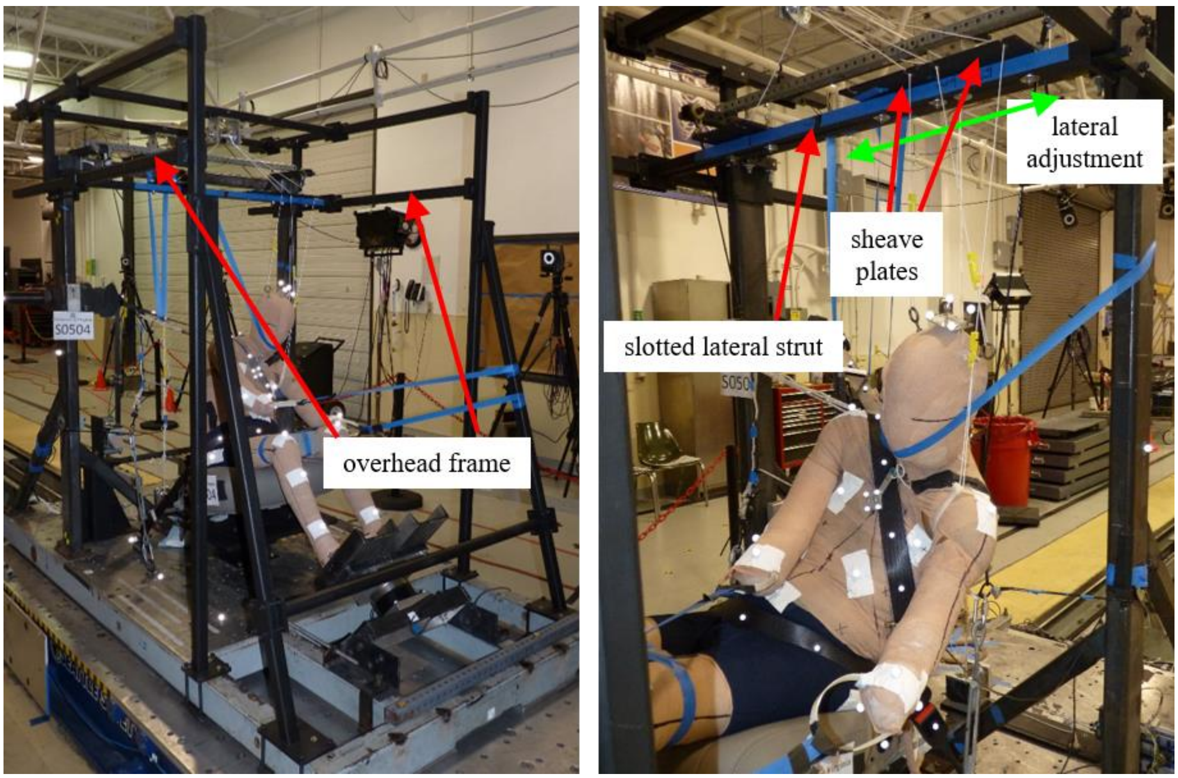

Figure 10. Posture maintenance system used in PMHS tests. Left: overhead frame attached to buck. Right: adjustable tether guides.

2.5. Positioning Procedure

The PMHS was lifted in from the front of the buck, supported by a tether under the thighs and a tether under the arms. The PMHS was set upon the seat such that the h-point was vertically above the h-point mark on the seat cushion. The posterior pelvis plates were placed to maintain the PMHS in the target fore-aft position, and the lifting tether under the thighs was removed. The feet were secured in the footrest clamps. The footrest was then moved forward or backward to attain the target femur and tibia angles of 18° and 50° (Schneider et al., 1983, pp. H-64 & H-65). For the second and third tests, the PMHS was already in the seat, so the h-point was re-aligned with the h-point mark on the seat cushion, and the posterior pelvis plates and footrest were left in the same position as in the first test. The foam block was secured between the knees.

With the lower body positioned, the back-support ropes were adjusted and tightened to support the upper body. The lateral positions of the drop-release tether guides were adjusted to the targets scaled from the target volunteer, and the drop-release tethers were attached to the head (via the head rings) and the shoulders (via large cable-ties beneath the armpits and above the shoulders). In some cases, the left (inboard) shoulder required no drop-release tether, and in all cases, the head required breakaway tape to maintain the target head posture. In both neutral and inboard postures, the target torso sagittal angle was 10° from the vertical and the target Frankfurt plane angle was 0° from the horizontal. The upper extremities were supported by breakaway tape such that the arms were up and out from the thighs to approximate the posture of volunteer Subject 42 and to permit visibility of the VICON markers on the lap-belt.

While the buckle and anchor positions were constant for all tests, the D-ring position and belt path were adjusted for each PMHS' neutral posture so that the shoulder-belt crossed the middle of the clavicle and the middle of the sternum and the lap-belt in front of the iliac crests. For each PMHS, the D-ring was positioned with the PMHS in the neutral posture and then left the same for that PMHS' second and third tests. In the volunteer tests, the D-ring was positioned 6 in. above the acromion, 11 in. rear of the external auditory meatus, and laterally such that the mid-line of the shoulder-belt fell on the center of the clavicle (Holt et al., 2018). In the PMHS tests, the D-ring could not move forward or backward; so the angle along the shoulder-belt as it ascended from the shoulder to the D-ring was defined as the target, which was 30° in the sagittal plane (Figure 11).

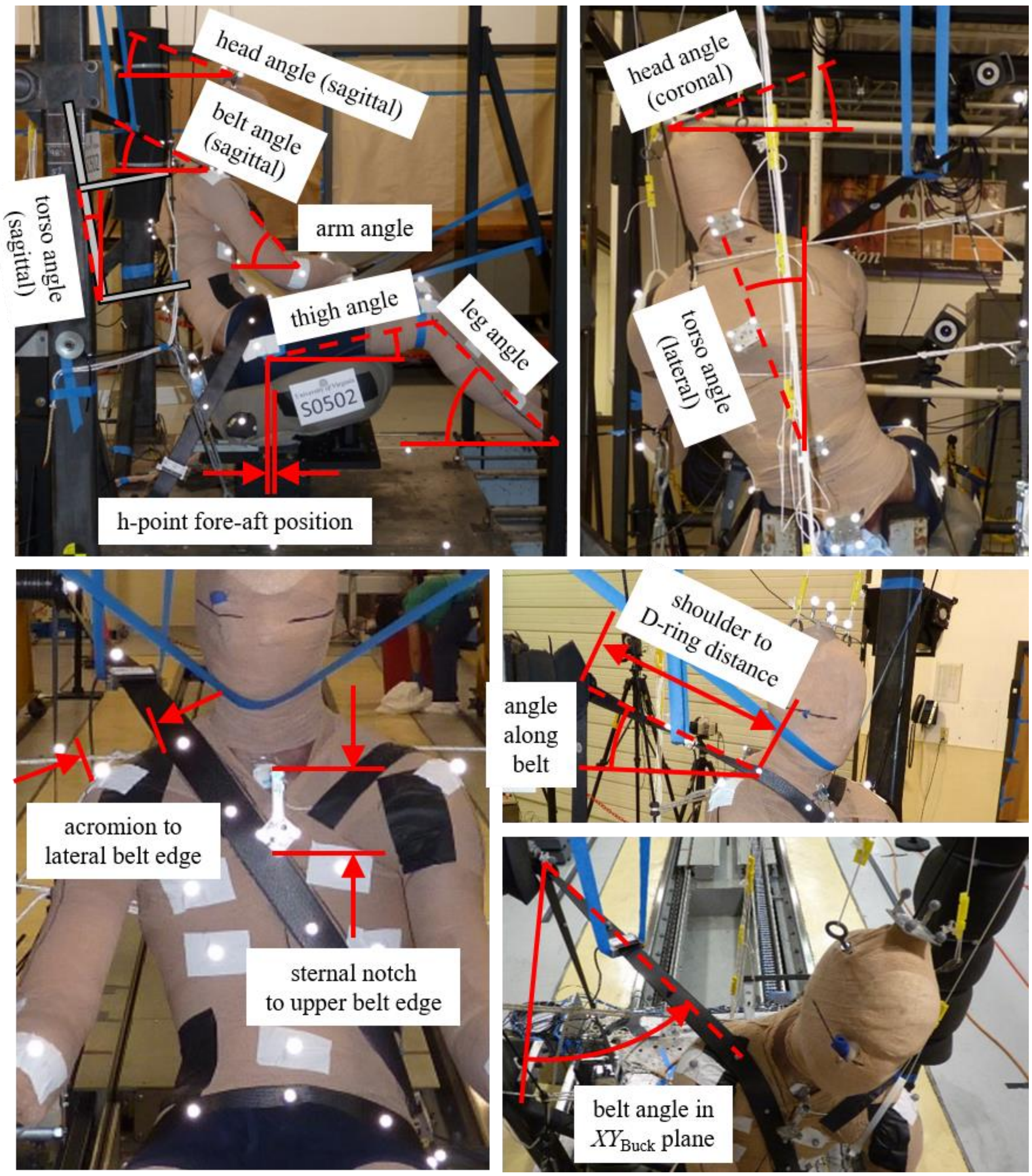

Figure 11. Definitions of PMHS posture measurements.

After positioning and shortly before the test, the PMHS' lungs were inflated with 2.5 liters of air through a tracheal tube inserted during PMHS preparation. The tube was covered with a filter and was left open after inflation.

2.6. Initial Positions

Figure 12 shows a front-view photograph comparison of the volunteer and PMHS in the inboard posture, and Appendix B shows the initial position photographs of the PMHS in each test. Table 5 compares the initial positions of the target volunteer and the PMHS in the neutral (NL) and inboard (IB) postures in the 9 g and 14 g tests. Table 6 reports additional measurements of the initial postures and belt paths of the PMHS, and Figure 11 depicts the measurements. The lateral positions of the head and shoulders in the second and third tests for each PMHS were within 16 mm of each other, but the torso lateral angle of the PMHS exceeded those of the volunteer by 0° to 7°.

This chapter has presented a combined strategy using volunteers and PMHS, the methodology and results of the volunteer tests used to quantify the inboard-leaning posture, and the methodology of the PMHS tests used to quantify the effect of the posture on restraint performance. The next chapter (Chapter 3) will describe the methods used to quantify PMHS kinematics and the evaluation of the effect of the inboard-leaning posture on PMHS kinematics.

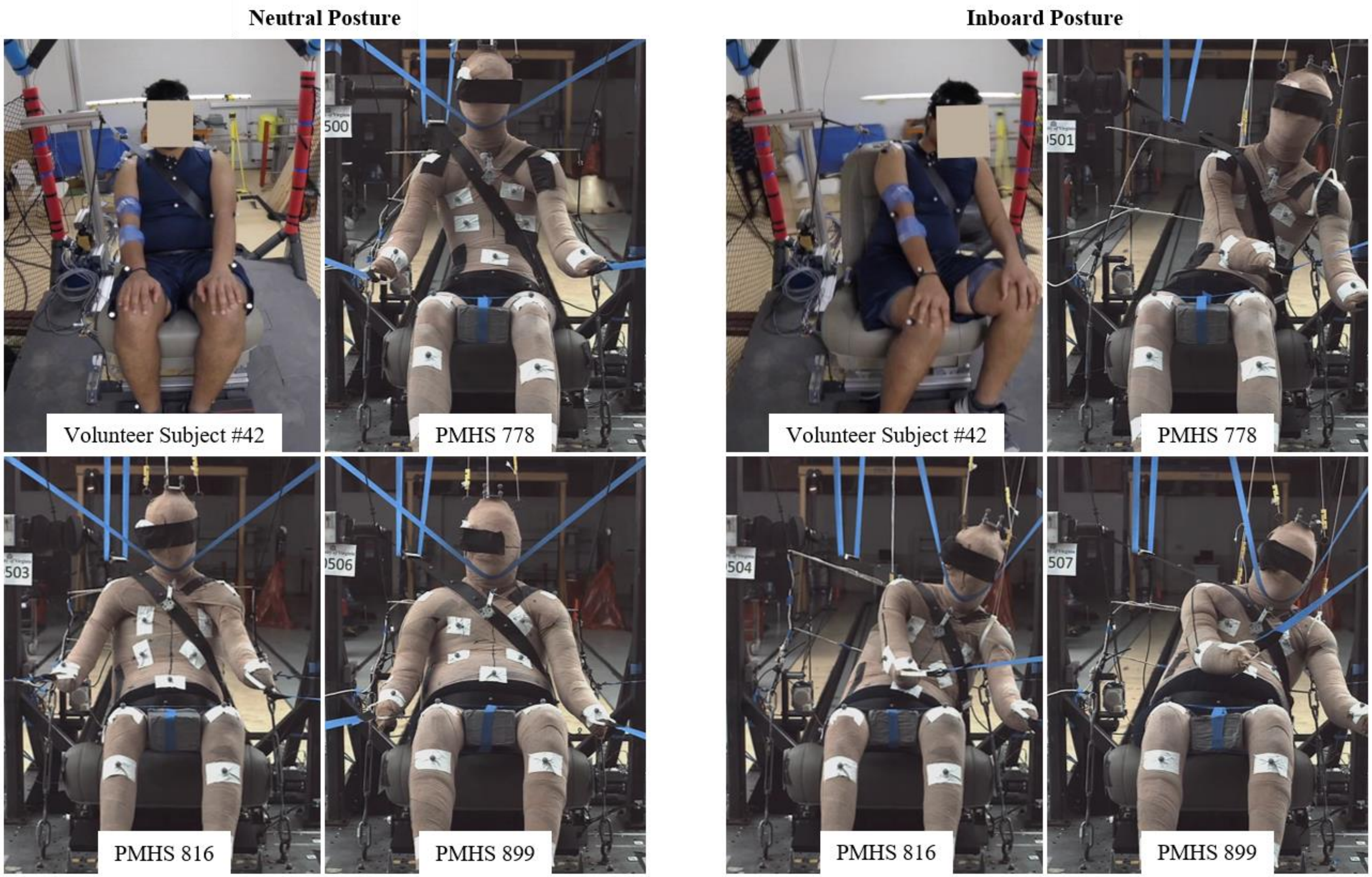

Figure 12. Front view of neutral (left) and inboard-leaning (right) postures for volunteer Subject #42 and PMHS.

Table 5. Initial positions of PMHS and volunteer Subject 42 in neutral (NL) and inboard (IB) postures. Data are reported with respect to the buck GCS.

		Subject #42		S1				S2				S3			
		NL	IB	IB target	NL 9g	IB 9g	IB 14g	IB target	NL 9g	IB 9g	IB 14g	IB target	NL 9g	IB 9g	IB 14g
Head Top [mm]	x	-353	-291	nt	-143	-103	-87	nt	-180	-145	-110	nt	-146	-151	-141
	y	32	-238	-306	0	-321	-328	-318	-18	-301	-304	-284	4	-268	-265
	z	733	-730	nt	-889	-827	-806	nt	-813	-708	-681	nt	-786	-726	-713
Right Shoulder [mm]	x	-289	-245	nt	-221	-166	-154	nt	-258	-229	-196	nt	-179	-167	-162
	y	177	10	-190	204	-17	-18	-198	183	-37	-47	-177	215	33	48
	z	-453	-518	nt	-578	-595	-579	nt	-548	-563	-550	nt	-508	-553	-542
Left Shoulder [mm]	x	-292	-285	nt	-215	-149	-149	nt	-242	-208	-191	nt	-192	-203	-187
	y	-165	-326	-182	-221	-417	-418	-189	-214	-383	-381	-169	-213	-363	-355
	z	-469	-465	nt	-585	-497	-492	nt	-537	-399	-375	nt	-517	-427	-422
Torso Angle [°]		2	-18	-19	0	-21	-22	-19	0	-23	-26	-19	0	-20	-22

nt = no target

Table 6. PMHS initial positions and seatbelt measurements.

	S1			S2			S3		
	NL 9g	IB 9g	IB 14g	NL 9g	IB 9g	IB 14g	NL 9g	IB 9g	IB 14g
Right h-point fore-aft [mm]	-7	nm	-6	-10	-16	-8	0	0	0
Left h-point fore-aft [mm]	-10	nm	-10	-12	-9	-14	0	0	2
Right thigh angle [°]	17	13	13	19	20	17	19	13	13
Left thigh angle [°]	18	20	18	19	16	19	19	13	17
Right leg angle [°]	55	52	50	57	57	52	56	59	51
Left leg angle [°]	49	48	48	54	46	47	51	52	48
Torso Sagittal Angle [°]	8	3	1	10	8	3	10	10	8
Torso Lateral Angle [°]	0	-21	-22	0	-23	-26	0	-20	-22
Head Plate Sagittal Angle [°]	4	-5	-5	-8	-10	-9	-2	-5	-2
Head Plate Coronal Angle [°]	-2	-23	-23	-4	-25	-26	-3	-26	-28
right arm angle [°]	nm	nm	nm	59	40	38	57	35	36
left arm angle [°]	nm	nm	nm	58	42	30	54	34	37
Acromion to lateral belt edge [mm]	82	68	50	73	37	35	88	70	55
Sternal notch to upper belt edge [mm]	65	59	90	20	15	nm	17	nm	nm
Belt sagittal angle from shoulder [°]	26	30	28	28	31	30	31	27	29
Angle along belt from shoulder [°]	24	18	22	23	14	19	21	17	14
Shoulder-to-D-ring distance [mm]	385	541	543	359	490	507	463	568	548
Belt angle in XY_{Buck} plane [°]	27	43	44	34	51	49	37	50	49

nm = not measured

Chapter 3. Occupant Kinematics

The goal of this thesis was to evaluate the effect of an out-of-position posture on restraint performance. The previous chapter established a study design and quantified an initial inboard-leaning posture. This chapter will aim to quantify the kinematics of the PMHS in the tests described in Chapter 2, and to assess the effect of the inboard-leaning posture on the kinematics.

3.1. Introduction

A fundamental challenge in restraint design is to limit the motion of the occupant, thus preventing injuries due to impact with the vehicle interior, while also limiting the forces applied to the occupant by the restraint system, thus preventing restraint-induced injuries. Many studies have examined this tradeoff in frontal crashes for an occupant seated "normally"—upright, symmetric, and forward-facing, as it is affected by seat stiffness (e.g., Adomeit & Heger, 1975; Shaw et al., 2018) or by seatbelt pre-tensioning and force-limiting (e.g., Kent et al., 2007; Forman et al., 2008). Few studies have done so for out-of-position occupants in frontal crashes (e.g., submarining risk due to slouching, Luet et al., 2012; Uriot et al., 2015), and none have done so for lateral out-of-position occupants in frontal crashes. Out-of-position postures may change the geometric relationship of the occupant with the restraint system. This may in turn alter the capacity of the restraint system to limit the occupant's motion and the restraining forces simultaneously.

Severe injuries to the head and thorax in frontal crashes have been attributed to lateral out-of-position postures. (Bohman et al., 2011a). Such postures have been shown to result from pre-crash evasive steering maneuvers (Muggenthaler et al., 2005; Kirschbichler et al., 2014; Ghaffari et al., 2018; Graci et al., 2018). An outboard-leaning out-of-position posture may increase proximity to the door, window, and other vehicle structures (Parenteau et al., 2002). An inboard-leaning out-of-position posture may increase the risk of the shoulder-belt slipping off (Parenteau 2006a, b; Arbogast et al., 2012).

Two past studies have examined the kinematics of restrained occupants in inboard-leaning postures with computational human body models. Bose et al. (2008) predicted injury risk to be highly sensitive to pre-crash posture in frontal crash simulations with a MADYMO human body model restrained by seat, seatbelt, and steering-wheel airbag. Matsuda et al. (2018) too predicted injury risk to be sensitive to pre-crash posture in frontal crash simulations with a THUMS human body model restrained by seat, seatbelt, and steering-wheel airbag. In particular, both studies predicted that an inboard-leaning pre-crash posture would greatly increase risk of injury to the head—due to increased excursion of the head and subsequent strikes to the vehicle interior. However, these computational models have only been validated against physical tests with normally seated occupants. Therefore, computational models may not accurately predict occupant kinematics in out-of-position postures. Post-mortem human subjects (PMHS, cadavers) may still be the most biofidelic surrogate for impact tests (Crandall et al., 2011).

The research described in this chapter aimed to quantify the motions of lateral out-of-position occupants in a frontal crash using the study design described in Chapter 2. Specifically, this chapter will describe the displacement trajectories of the head, spine, pelvis, and shoulders of the PMHS.

3.2. Methods

Three offboard high-speed video cameras recorded each impact at 1 kHz from the front and both sides (Figure 13). An additional high-speed video camera was placed downstream on the driver side to record the rebound of the subject (Figure 13).

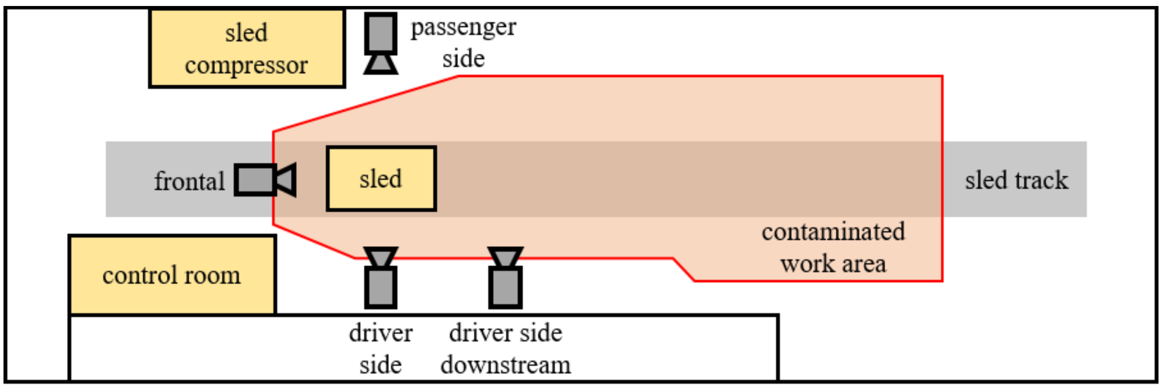

Figure 13. Arrangement of offboard high-speed video cameras in PMHS tests.

An optoelectronic stereophotogrammetric system consisting of 20 VICON MX^{TM} (Oxford, UK) cameras measured the motions of retroreflective markers inside a calibrated three-dimensional space containing the buck. Motion data were collected at 1 kHz. Markers were attached at regular intervals along the belt. Markers were also placed on the buck. The buck markers were used to define the buck global coordinate system (GCS) in which to describe the motions of the subject. The origin of the buck GCS was on the top of the undeformed seat, in the midline of the seat, at the target h-point fore-aft position (Figure 14). The GCS polarities conformed to SAE J211 (SAE, 2007): forward (+X_{Buck}), backward (-X_{Buck}), rightward/outboard (+Y_{Buck}), leftward/inboard (-Y_{Buck}), downward (+Z_{Buck}), and upward (-Z_{Buck}).

The system of VICON cameras also measured the motions of clusters of retroreflective markers surgically attached to the skull, T1, T8, and L2 vertebrae, pelvis, and sternum (Figure 15). The motions of the bones were calculated from the motions of the marker clusters based on pre-test computed tomography (CT) scans of the instrumented PMHS and laser surface scans of the motion-cluster assemblies (Figure 15) following the procedure presented by Shaw et al. (2009). The motion of each bone was expressed as the motion of a local coordinate system (LCS), with respect to the buck GCS. LCS were defined from anatomic landmarks: the head origin was at the midpoint of the bilateral zygomatic processes; the vertebral origins were at the midpoint of the centers of the endplates; the pelvis origin was at the midpoint of the posterior superior iliac spines; and the sternum origin was at the midpoint of the centers of the 4th-rib sterno-costal joints (Appendix C). Single markers were also taped to the bilateral acromia and the extremities.

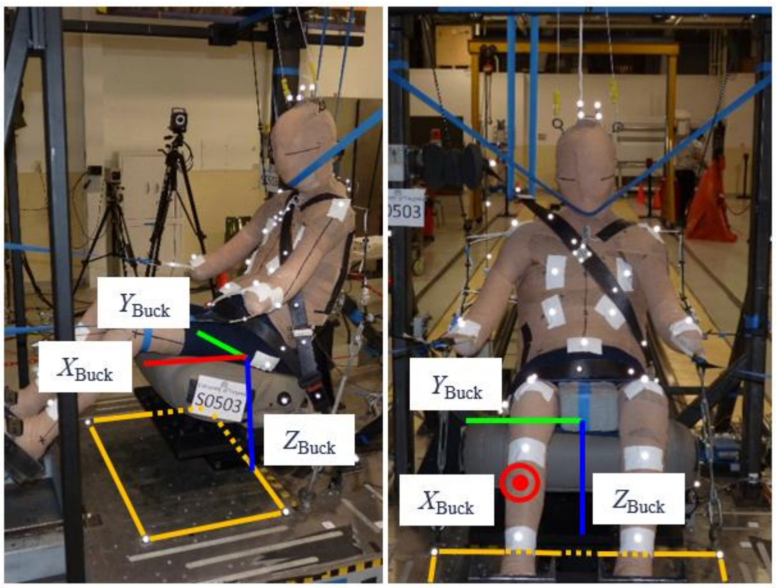

Figure 14. Buck markers and definition of buck global coordinate system.

Inertial sensors were also attached to the VICON-tracked bones: combined three-accelerometer and three-angular rate sensor packages (6DX Pro, DTS, Seal Beach CA) were attached to the head and T1; triaxial accelerometer packages were attached to T8, L2, and pelvis; and a single anterior-facing accelerometer was attached to the sternum. Inertial data were collected at 10 kHz. Accelerations and angular rates were debiased by subtracting out the average of the signal before time zero. Accelerations were filtered following channel filter class (CFC) recommendations of SAE J211 (SAE, 2007): CFC 1000 for head, pelvis, and sternum, and CFC 180 for T1, T8, and L2. SAE J211 does not contain CFC recommendations for angular rate; but the bandwidth of the angular rate signals fell well within the 600 Hz limit of CFC 180, so the angular rate signals were filtered at CFC 180. The accelerations of the head LCS were calculated from the head sensor signals using the method described in Appendix E.

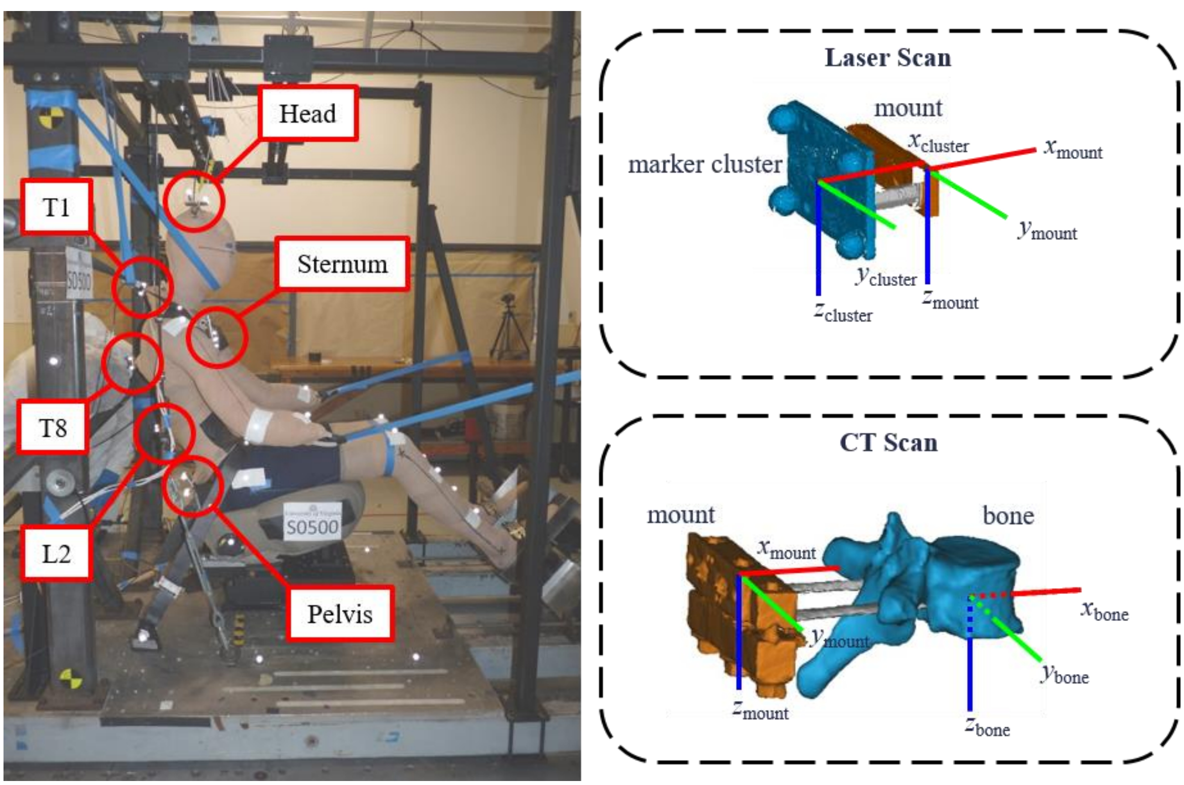

Figure 15. Motion-capture marker clusters (left) and motion-capture assemblies (right) in PMHS tests.

Past studies have proposed scaling methods for PMHS kinematics to calculate what the kinematics would have been for a standard anthropometry (Eppinger et al., 1984). Since the current study involved repeated tests on each PMHS, scaling was not used. Instead, the difference in results (e.g., change in maximum forward head displacement) between test conditions (e.g., neutral 9 g vs. inboard 9 g) was calculated for each PMHS, and paired-sample Student's *t*-tests were performed to quantify the statistical significance of the differences.

3.3. Results

The kinematics of the PMHS in the neutral posture followed the characteristic motion sequence established in past studies of seatbelt-restrained PMHS in frontal impacts (Forman et al., 2006a; Forman et al., 2009b; Ash et al., 2012; Montesinos-Acosta et al., 2016). The head followed a curvilinear trajectory forward, down, and laterally toward the right (belted) shoulder until the head reached maximal forward displacement of 205 to 224 mm at 116 to 118 ms. The lap-belt arrested the forward motion of the pelvis (101 to 107 ms) and lumbar spine (90 to 107 ms), while the shoulder-belt arrested the forward motion of the thoracic spine (T1 and T8: 94 to 118 ms). In all tests, the shoulder-belt remained on the shoulder. The maximum forward displacement of the left (unbelted) shoulder (170 to 227 mm) was greater than that of the right (belted) shoulder (41 to 146 mm). This caused the torso to twist as if the PMHS was turning to face outboard. During rebound—the period after maximum forward head displacement—the head continued to move down and to the right, achieving maximum outboard (right lateral) displacement of 183 to 339 mm at 254 to 286 ms.

When the PMHS were placed in the inboard-leaning initial posture, the head was 215 to 289 mm inboard from its initial position in the neutral tests. For the 9 g, 30 km/h pulse, the head followed a forward, downward, outboard trajectory. The time of maximum forward displacement in the inboard 9 g tests (116 to 125 ms) was similar to that observed in the neutral tests (116 to 118 ms), but the maximum forward displacement increased from 205–224 mm to 258–294 mm. As in the neutral tests, the left (unbelted) shoulder displaced farther forward than the right (belted) shoulder (left: 228 to 257 mm; right: 47 to 154 mm). In all tests, the shoulder-belt remained on the shoulder. The maximum outboard (right lateral) displacement also increased from neutral (183 to 339 mm) to inboard (498 to 623 mm), but this did not yield an increase in outboard position since the head was initially inboard (left lateral), and it did not greatly increase the time (274 to 312 ms).

When the PMHS was placed in the inboard-leaning initial posture and tested with a more severe crash pulse (14 g, 41 km/h), the motion sequence was similar to the inboard-leaning, lower severity test: the head and torso swung forward and outboard. From the lower-severity to the higher-severity inboard tests, the maximum forward head displacement increased from 258–294 mm to 307–378 mm, and the time to maximum forward head displacement decreased from 116–125 ms to 104–116 ms. The lateral position of the head at the time of maximum forward displacement did not change from lower- to higher-severity inboard test.

Figure 16, Figure 17, and Figure 18 show high-speed video captures which illustrate the kinematics observed in the 9 g, 30 km/h neutral and inboard tests. As described above, the inboard-leaning initial posture did not change the time of maximum forward head displacement (around 120 ms, Figure 16) or the time of maximum outboard (rightward) head displacement (around 280 ms,

Figure 17). The inboard-leaning initial posture of the PMHS did change the position of the head at the time of maximum forward displacement (around 120 ms, Figure 16), but not at the time of maximum outboard (rightward) displacement (around 280 ms, Figure 17). The PMHS re-engaged the back support structures by around 180 ms (Figure 18). Sequences of high-speed video stills up to the time of maximum forward head displacement are shown in Appendix D for all tests with PMHS from the frontal view (Figure 56, Figure 57, Figure 58), the passenger-side view (Figure 59, Figure 60, Figure 61), and the driver-side view (Figure 62, Figure 63, Figure 64).

Figure 19, Figure 20, and Figure 21 show graphical "stick-figure" plots that further illustrate the kinematics observed in the PMHS tests. The overhead view (Figure 19) shows the increase in head forward displacement from 9-g neutral to 9-g inboard to 14-g inboard, and the difference in forward displacement of the left (unbelted) and right (belted) shoulders that caused the torso to turn to the right (outboard) in all tests. The side view (Figure 20) shows that the head displaced further forward in the inboard test than in the neutral test, but the spine and pelvis did not. The front view (Figure 21) shows that, at the time of maximum forward head displacement, the spine was centered laterally in the neutral test but leaned inboard in both lower- and higher-severity inboard tests.

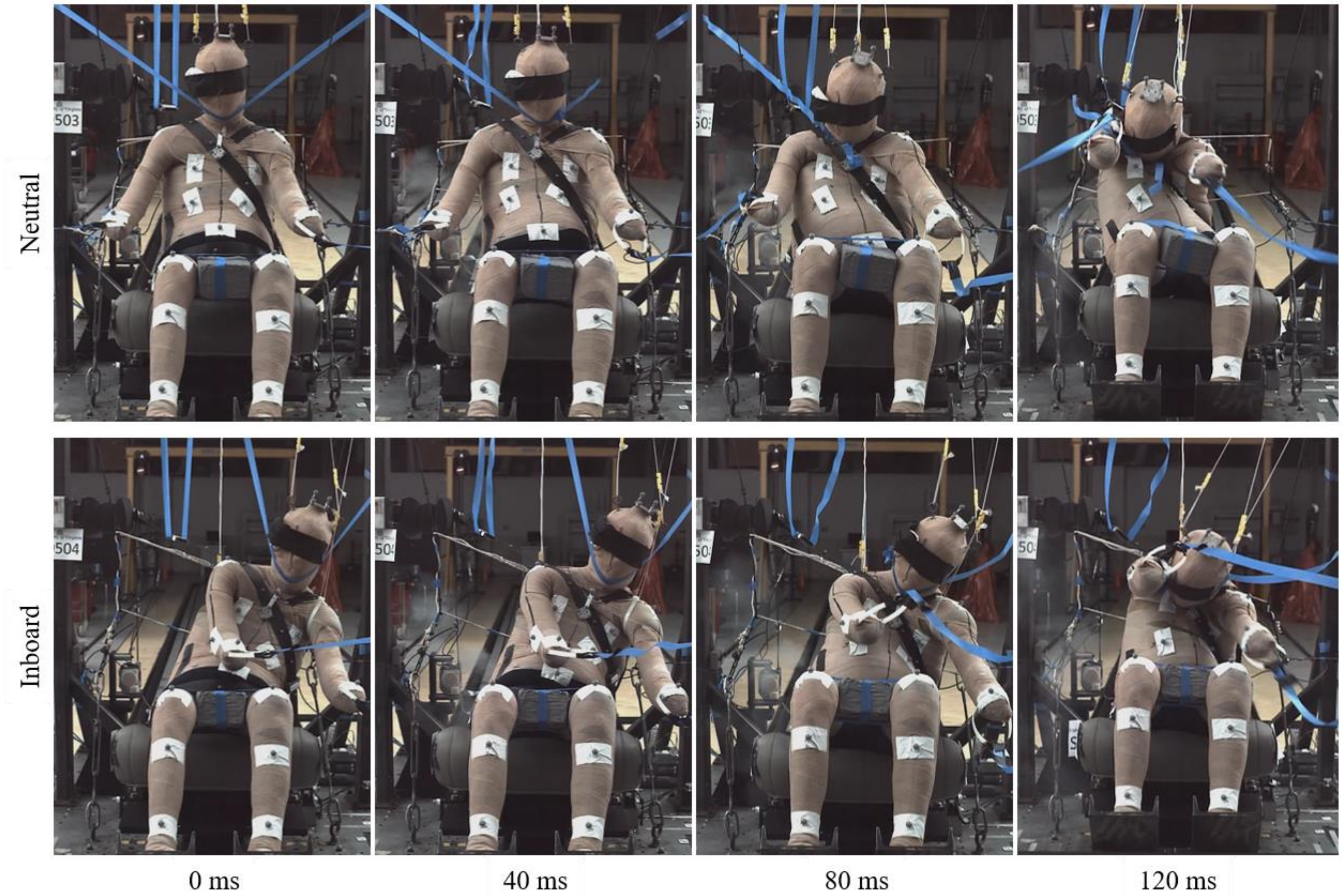

Figure 16. High-speed frontal video captures of PMHS S2 at 40-ms intervals illustrating the characteristic motion of the PMHS in the neutral 9 g (top) and inboard 9 g (bottom) tests up to the time of maximum forward head displacement.

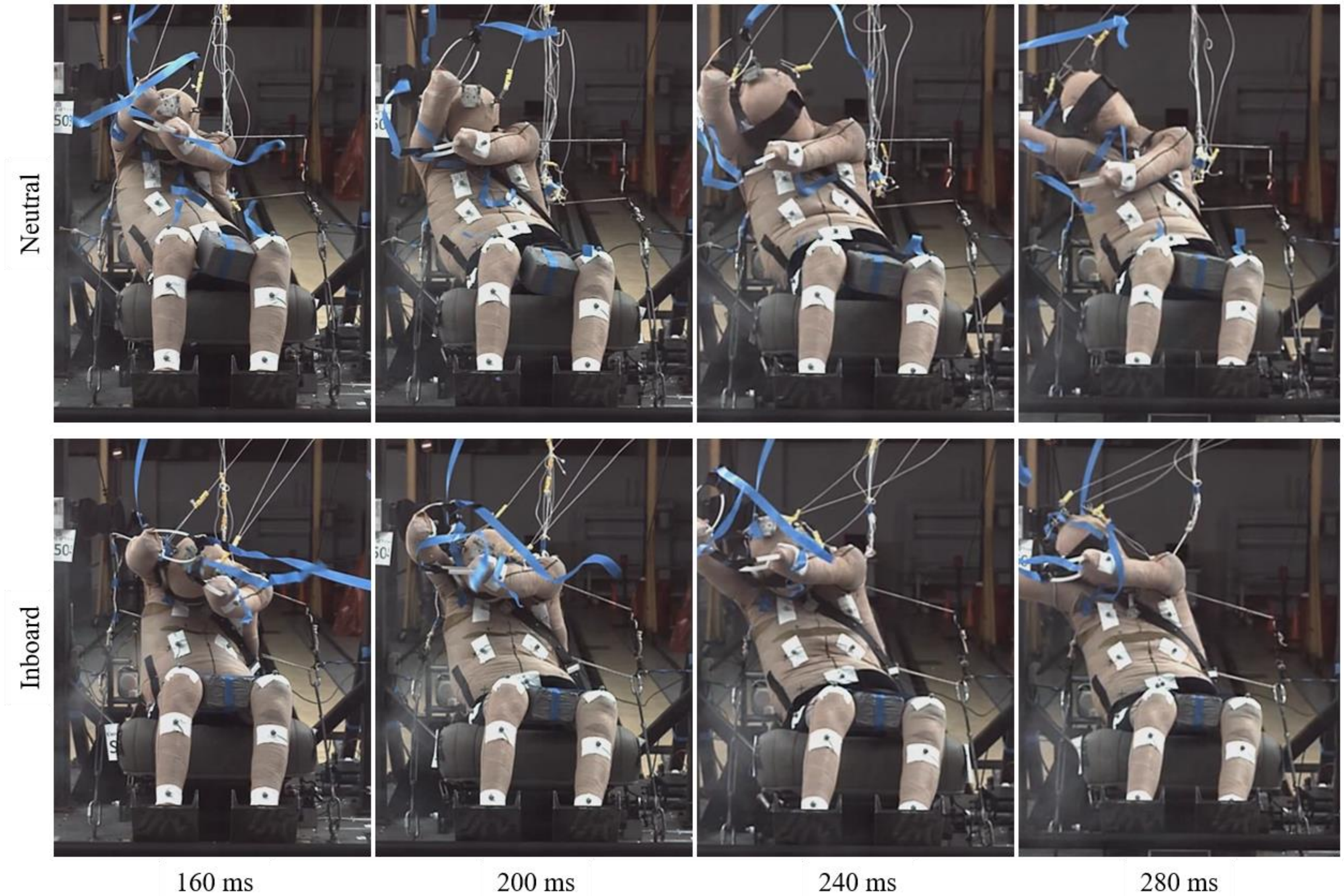

Figure 17. High-speed frontal video captures of PMHS S2 at 40-ms intervals illustrating the characteristic motion of the PMHS in the neutral 9 g (top) and inboard 9 g (bottom) tests during rebound (after the time of maximum forward head displacement).

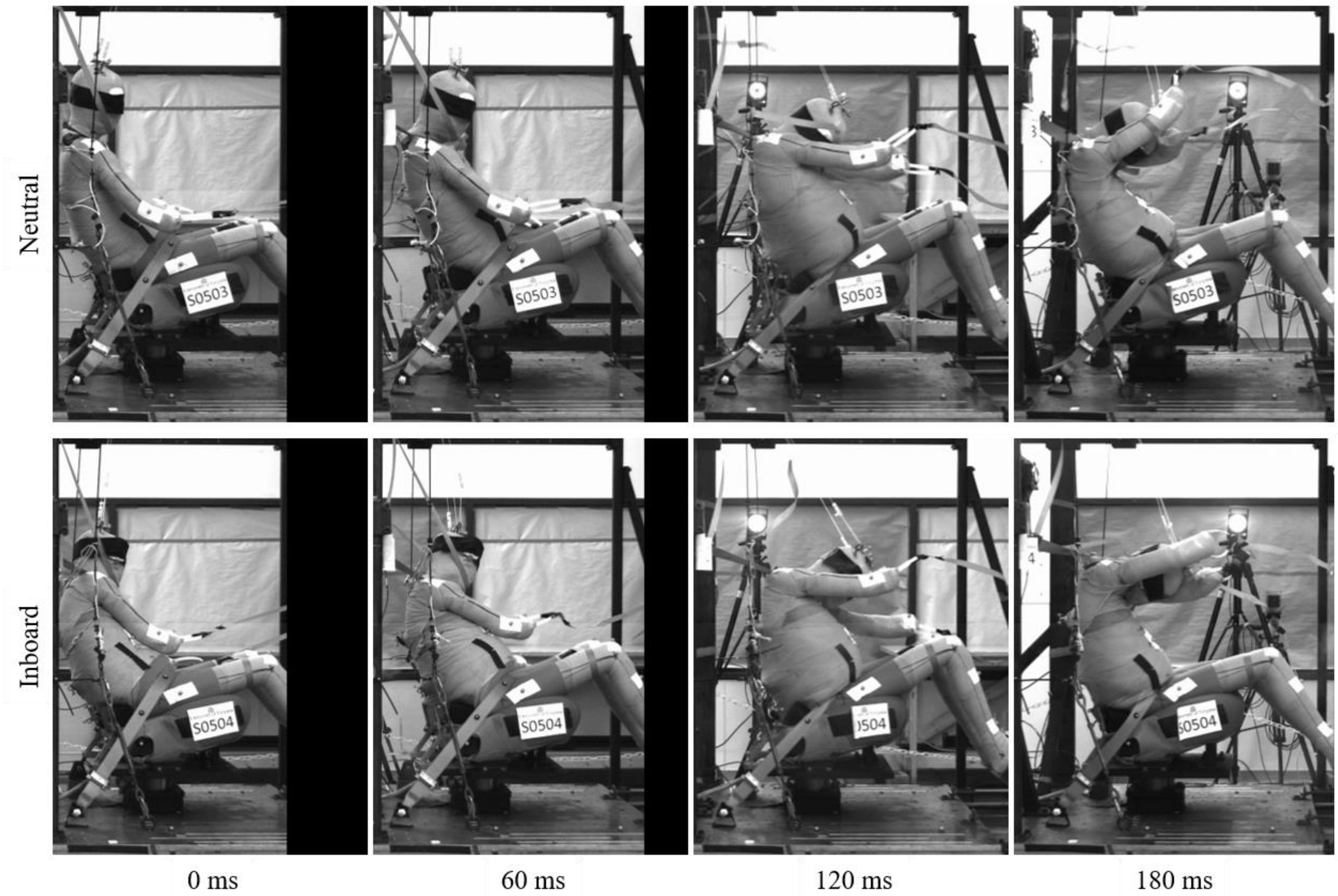

Figure 18. High-speed passenger-side video captures of PMHS S2 at 60-ms intervals illustrating the characteristic motion of the PMHS in the neutral 9 g (top) and inboard 9 g (bottom) tests.

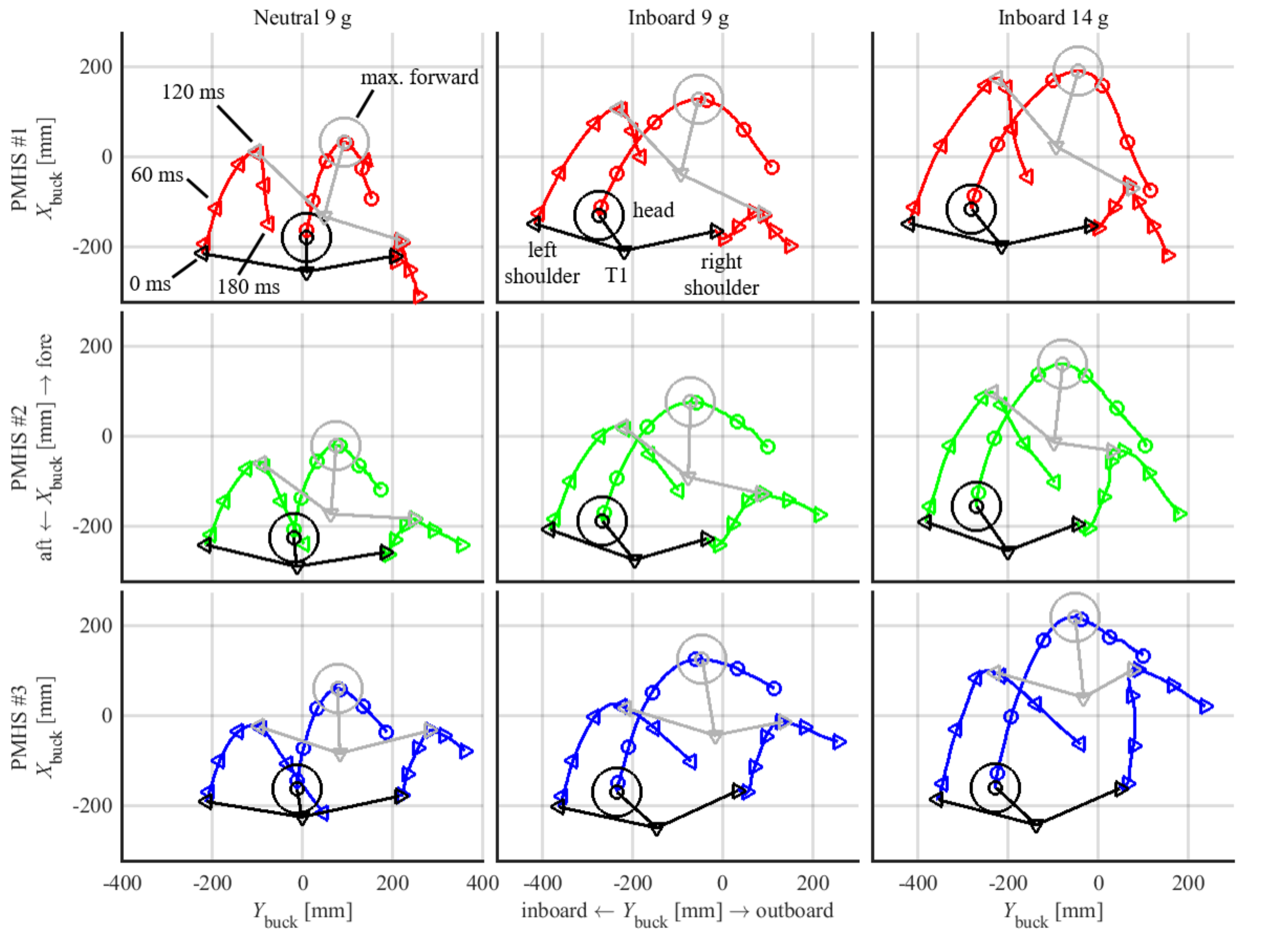

Figure 19. Overhead ($X_{Buck}Y_{Buck}$) view of the head and shoulder motions in the PMHS tests. Points are plotted at 30-ms intervals.

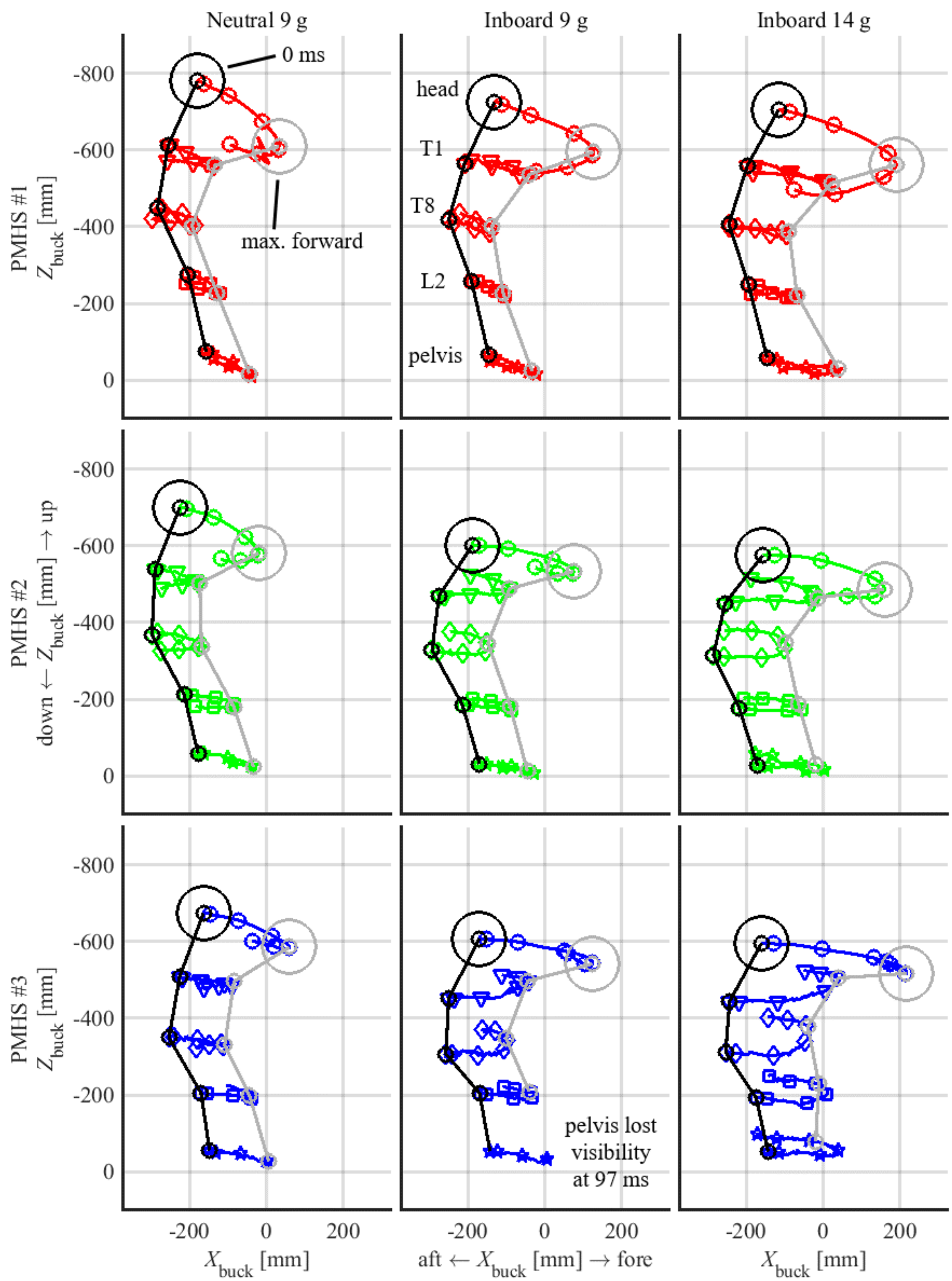

Figure 20. Right side ($Z_{Buck}X_{Buck}$) view of the head, spine, and pelvis motions in the PMHS tests. Points are plotted at 30-ms intervals.

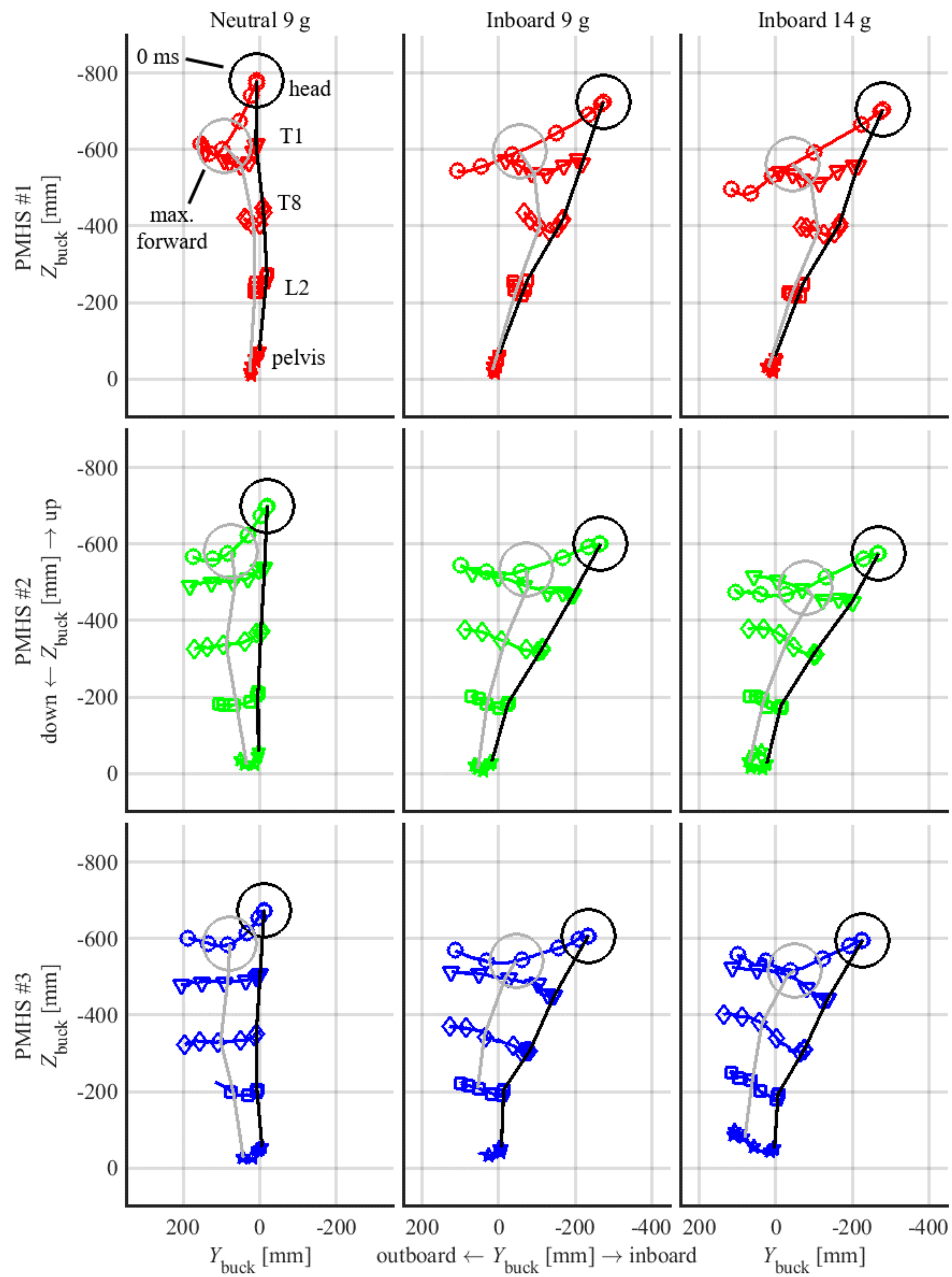

Figure 21. Front ($Y_{Buck}Z_{Buck}$) view of the head, shoulders, spine, and pelvis motions in the PMHS tests. Points are plotted at 30-ms intervals.

Figure 22 shows the time-histories of the anterior-posterior (X_{Buck}) and lateral (Y_{Buck}) displacements and positions of the head in the neutral and inboard 30 km/h tests. The maximum forward head displacement and position were greater for inboard than for neutral, but the time of maximum forward head displacement was the same regardless of initial posture (Figure 22a, b). In addition, the inboard-leaning posture changed the lateral position of the head at the time of maximum forward head displacement, from around Y_{Buck} = 80 mm (outboard) to around Y_{Buck} = -60 mm (inboard) (Figure 22c). The maximum outboard (right lateral) position was the same for inboard as for neutral, but the time of maximum outboard position was later for inboard than for neutral (Figure 22c). The observed large change in maximum outboard displacement was due to the change in the initial position of the head in the inboard-leaning posture (Figure 22d).

As stated above (Section 3.2), statistical tests were performed on the mean of the differences rather than on the difference of the means. For the head, statistical tests were performed on the maximum forward (+X_{Buck}) displacements and the time of maximum forward (+X_{Buck}) and outboard (+Y_{Buck}) displacement. However, since the initial lateral position of the head was deliberately changed, statistical tests were performed on the maximum outboard (+Y_{Buck}) position but not displacement. Additionally, statistical tests were performed on the lateral (Y_{Buck}) and vertical (Z_{Buck}) position of the head at the time of maximum forward (+X_{Buck}) displacement. Statistical tests on maximum forward (+X_{Buck}) displacement and time of maximum forward displacement were also performed for T1, T8, L2, and pelvis. Statistical tests on maximum downward (+Z_{Buck}) displacement were only performed for pelvis. Table 7 shows the results of statistical tests on the kinematics. From neutral to inboard, the maximum forward (+X_{Buck}) displacements increased significantly for the head (59 mm ± 13 mm, p = 0.015), T1 (60 mm ± 10 mm, p = 0.010), and T8 (17 mm ± 3 mm, p =

0.014), but not for L2 (p = 0.552) and the pelvis (p = 0.570). At the time of maximum forward head displacement, the head was significantly farther inboard (-139 mm ± 13 mm, p = 0.003), but not significantly farther down (p = 0.081) in the inboard test than in the neutral test. The maximum outboard (+Y_{Buck}) position of the head occurred during rebound and did not change significantly from neutral to inboard (p = 0.121). The maximum downward (+Z_{Buck}) displacement of the pelvis decreased (-11 mm ± 5 mm, p = 0.054). The time of maximum forward displacement did not change significantly for the head (p = 0.434), T1 (p = 0.826), T8 (p = 0.480), L2 (p = 0.208), and pelvis (p = 0.081). In contrast, the time of maximum head outboard displacement increased (24 ms ± 10 ms, p = 0.052). Finally, statistical tests were performed to assess the differences between lower- and higher-severity inboard tests. However, the only notable results were the increased forward head displacement (61 mm ± 19 mm, p = 0.031), increased forward T1 displacement (59 ± 15 mm, p = 0.020), and decreased downward pelvis displacement (-11 mm ± 5 mm, p = 0.058).

Table 7. Statistical analysis of selected kinematic results from the neutral and inboard 30 km/h PMHS tests.

		Neutral			Inboard			Inboard - Neutral			
		S1	S2	S3	S1	S2	S3	$\bar{d}$	$\bar{d}$ [%]	$s_{\bar{d}}$	p
Head	max. +ΔX_{Buck}	213	205	224	258	264	294	59	27	13	0.015
	time of max. +ΔX_{Buck}	116	115	117	115	116	124	2	2	4	0.434
	Y_{Buck} at time of max. +ΔX_{Buck}	93	75	78	-54	-72	-45	-139	-170	13	0.003
	Z_{Buck} at time of max. +ΔX_{Buck}	-609	-581	-586	-595	-533	-542	35	-6	19	0.081
	max. +Y_{Buck}[a]	191	267	328	224	281	388	35	14	24	0.121
	time of max. +Y_{Buck}	253	273	285	285	286	311[b]	24	9	10	0.052
T1	max. +ΔX_{Buck}	123	122	141	172	187	209	60	47	10	0.010
	time of max. +ΔX_{Buck}	112	109	117	113	110	114	0	0	2	0.826
T8	max. +ΔX_{Buck}	97	137	148	115	150	168	17	13	3	0.014
	time of max. +ΔX_{Buck}	93	105	109	105	106	107	4	4	7	0.480
L2	max. +ΔX_{Buck}	84	136	138	89	132	145	2	2	6	0.552
	time of max. +ΔX_{Buck}	89	102	106	94	105	106	3	3	3	0.208
Pelvis	max. +ΔX_{Buck}	119	150	161	126	143	152	-3	-2	8	0.570
	time of max. +ΔX_{Buck}	100	102	106	97	95	96	-7	-6	4	0.081
	max. +ΔZ_{Buck}	63	41	36	54	25	28	-11	-23	5	0.054

Positions and displacements reported in [mm] and times reported in [ms] unless otherwise indicated.
Percent mean of differences ($\bar{d}$ [%]) was calculated as $\bar{d}$/mean(Neutral)
[a] value occurred during rebound
[b] value occurred at end of visibility

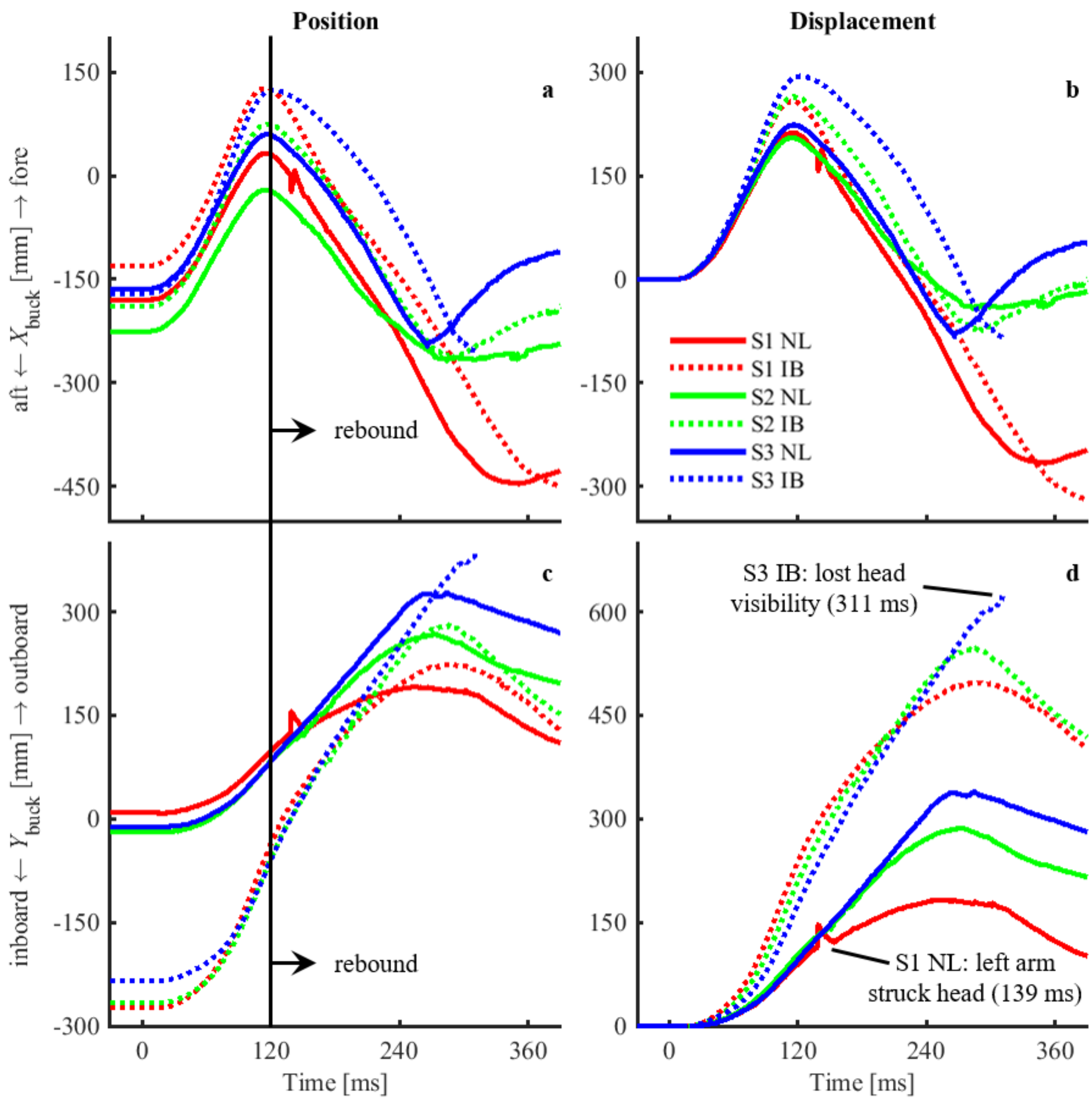

Figure 22. Time-histories of head anterior-posterior (X_{buck}) and lateral (Y_{buck}) position (left) and displacement (right) for the neutral (NL) and inboard (IB) 9g, 30 km/h tests with the three PMHS (S1, S2, S3).

Time-histories of the component and resultant acceleration of the head center of gravity in the head LCS are shown in Figure 23. The head acceleration was primarily anterior ($+x_{Head}$) and superior ($-z_{head}$), with maximum accelerations at or before the time of maximum forward ($+X_{Buck}$) and downward ($+Z_{Buck}$) displacement of the head (~120 ms). The large spike in acceleration at the end of the neutral 9 g test with S1 occurred when the right forearm struck the sensor hardware.

Figure 24 shows a passenger-side view for all tests at the approximate time of maximum forward excursion (120 ms), with an estimation of the pelvis posture and lap-belt path. The lap-belt slipped over the top of the pelvis ("submarined") in all three tests with PMHS #1, but in no tests with PMHS #2 or #3 (Figure 24). This phenomenon has profound consequences for whole-body kinematics and will be explored further in Chapter 5.

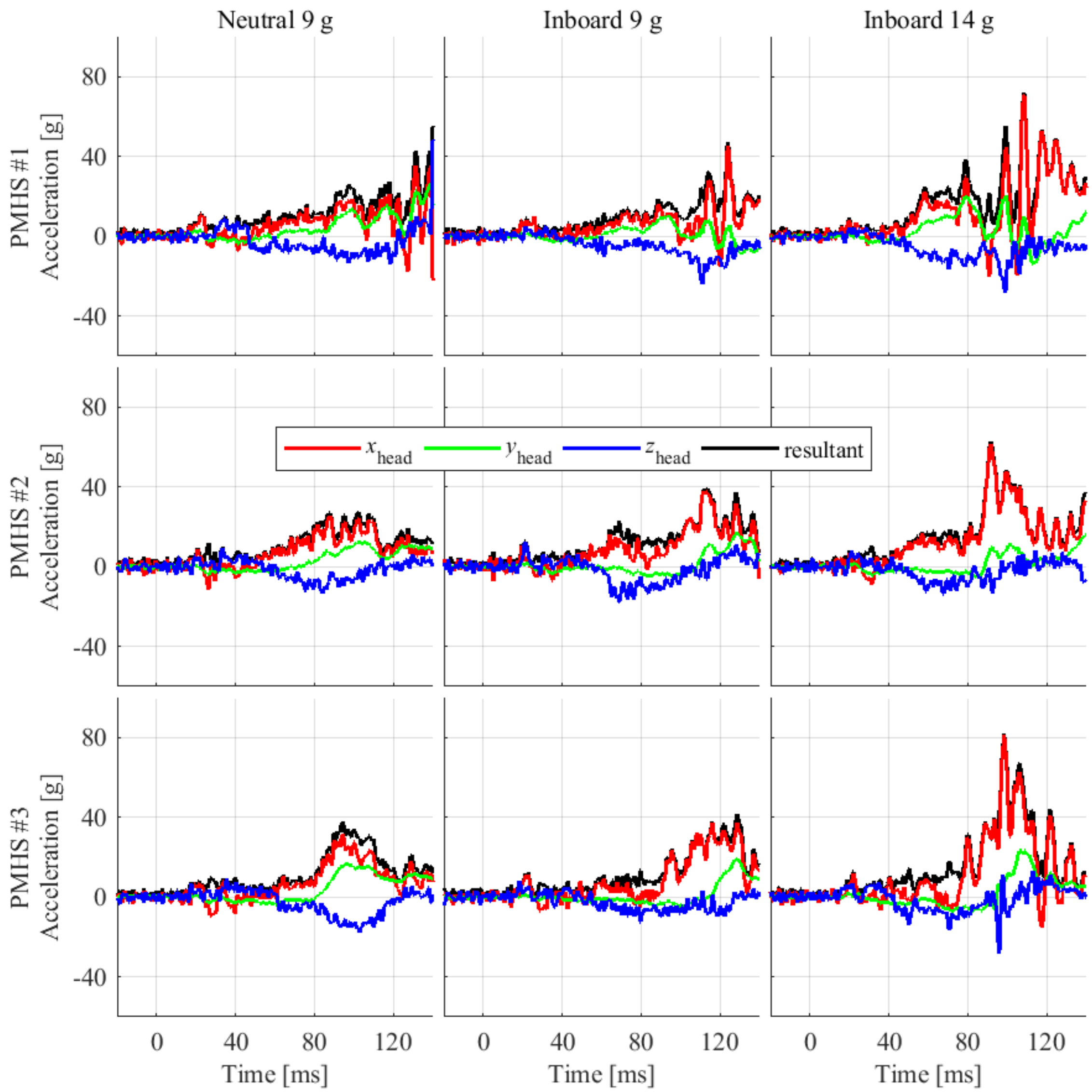

Figure 23. Accelerations of the head center-of-gravity in the head LCS for the PMHS tests.

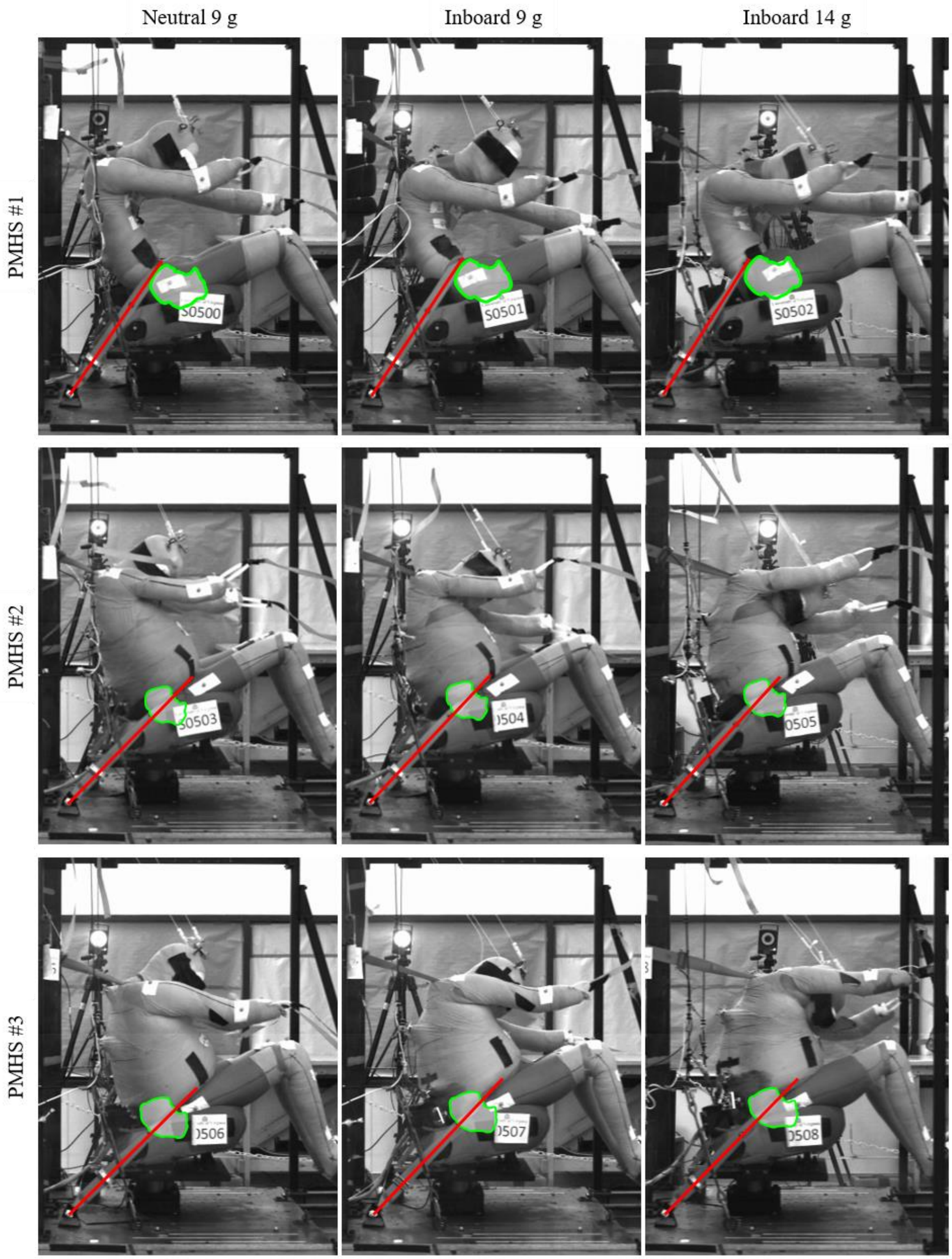

Figure 24. High-speed stills from passenger-side view of all tests about the time of maximum forward excursion (120 ms). The red lines estimate the path of the lap-belt and the green outlines estimate the posture of the pelvis. The shoulder-belt remained on the shoulder in all tests.

3.4. Discussion

Occupant Posture and Seatbelt Geometry

It is often asserted that the seatbelt geometry—the locations of the anchor, buckle, and D-ring—heavily influences the occupant kinematics in a frontal crash (Adomeit & Heger, 1975; Haight et al., 2013; Kent & Forman, 2015). In this study, the 105- to 155-mm increase in initial length of seatbelt between the shoulder and D-ring due to the inboard-leaning posture (Table 6) allowed the 45- to 71-mm increase in forward head displacement (Table 7). The effect is demonstrated in Figure 25. If the D-ring position relative to the seat is the same, and if the shoulder retains the seatbelt, then an inboard lean pulls out more seatbelt webbing (Figure 25a). If the seatbelt has an inertial locking mechanism but neither pretensioner nor force-limiter, then the increased initial shoulder-to-D-ring length due to the inboard-leaning posture permits the occupant to displace farther forward (Figure 25b). In this study, the difference between the increased initial shoulder-to-D-ring length (105 to 105 mm) and the increased maximum forward head displacement (45 to 71 mm) may have been due to the pretensioner, which may have pulled in the seatbelt, and the force-limiter, which may have let out the seatbelt. The contributions of the pretensioner and force-limiter will be discussed in Chapter 4. The fact that the inboard-leaning posture did not significantly change the maximum outboard displacement during rebound suggests that the seatbelt may mitigate the effects of posture on kinematics over time. However, the occupant re-engaged the back-support structures well before the time of maximum outboard displacement (around 180 ms vs. around 280 ms), so this result may not be due solely to the seatbelt.

Despite the posture-induced increase in forward displacement, the inboard posture did not change the timing of the motion sequence: maximum forward head displacement occurred at the same time (neutral: 115 to 117 ms; inboard: 115 to 124 ms), and maximum outboard head displacement during rebound was not greatly delayed (neutral: 253 to 285 ms; inboard: 285 to 311 ms). Given the same time to traverse a greater displacement, the velocity of the occupant must have increased in the inboard test. This effect was most evident for the head (Figure 26). The increased resultant displacement (Figure 26a) due to the inboard-leaning posture occurred within the same time as in the neutral test, which yielded an increased resultant velocity (Figure 26b).

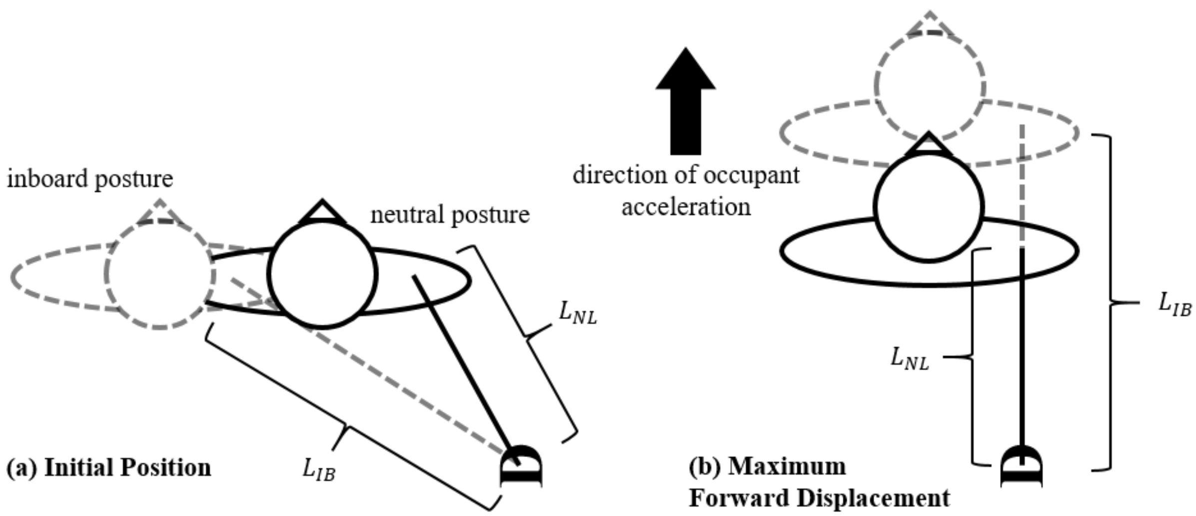

Figure 25. Greater initial shoulder-to-D-ring length allows greater forward displacement (overhead view).

In a frontal crash with a three-point seatbelt, the occupant moves laterally toward the belted shoulder (Ash et al., 2012; Montesinos-Acosta et al., 2016). The magnitude of lateral displacement is generally much less than that of forward displacement, especially at the time of maximum forward displacement. In this study, the neutral posture resulted in maximum forward head displacement of 205 to 224 mm and lateral head displacement at the same time of 84 to 95 mm. In contrast, the inboard-leaning posture changed the proportion of head displacements: 258 to 294 mm forward and 189 to 220 mm lateral. The increase in lateral displacement considerably reduced the difference in lateral head position from initial time (215 to 289 mm between neutral and inboard) to time of maximum forward head displacement (123 to 147 mm between neutral and inboard). Regardless of the initial posture, the occupant moved laterally toward the belted shoulder to achieve the most stable configuration of the three-point seatbelt.

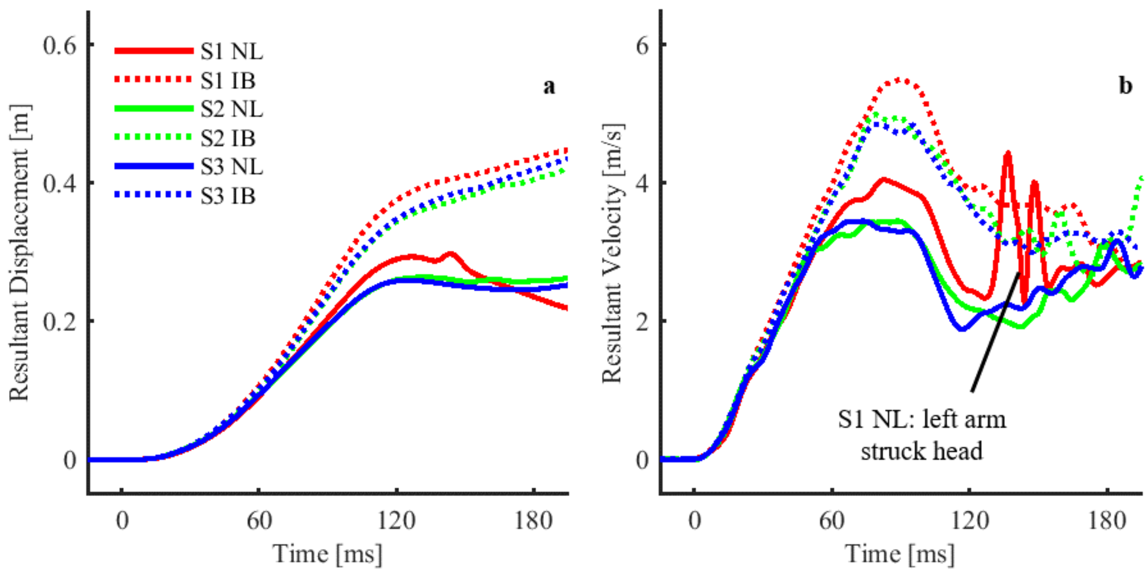

Figure 26. Time-histories of resultant head displacement (a) and resultant head velocity (b) in the buck GCS.

Putting the seatbelt on in the inboard-leaning tests pulled some additional webbing from the retractor (39 mm ± 32 mm) compared to the neutral tests (Table 10). This may have contributed to the increased shoulder-D-ring belt segment length discussed above. The additional belt pull-out may not have occurred in the volunteer test, in which the inertial lock of the retractor may have activated. Nonetheless, the length of belt webbing between the D-ring and the acromion may have increased in the volunteer test when the belt slipped over the anterior surface of the torso. This limitation in approximating the volunteer tests will be examined in more detail in the final chapter, and highlights the need for future work to understand the sensitivity of seatbelt forces and occupant kinematics to variations in belt payout, belt positioning, belt slip, and belt spooling.

Shoulder-Belt Retention and Stability

The seatbelt is a tension-only member, and so it is only stable—that is, it will not displace perpendicular to its path—when its path aligns with the direction of the applied force (Figure 27). When the direction of the applied force is different from the direction of the seatbelt (Figure 27a), the seatbelt realigns to recover the stable configuration (Figure 27b). This is why an occupant restrained by a three-point seatbelt moves laterally toward the belted shoulder in a frontal crash (Figure 27c). In this study, the inboard-leaning posture not only increased the initial length of the shoulder-to-D-ring seatbelt segment, but also the initial angle between this seatbelt segment and the sled acceleration vector (Figure 28): the initial angle was 29° to 39° in the neutral tests, but 43° to 52° in the inboard tests (Table 6). Despite the difference in its initial angle, the shoulder-to-D-ring seatbelt segment in the inboard-leaning test aligned with its direction in the neutral test (Figure 28). The fact that the shoulder-to-D-ring seatbelt angle did not decrease to zero by the time of maximum forward head and torso displacement indicates that the most stable configuration of the seatbelt depends on the whole shoulder-belt and not just on the upper portion (Figure 29c). The difference in initial angle may also have affected the development of force within the seatbelt, which will be examined in Chapter 4. The fact that the seatbelt realignment moved the occupant laterally toward the belted shoulder indicates that the three-point seatbelt is an asymmetric restraint that causes asymmetric kinematics. This phenomenon will be discussed further in Chapter 5.

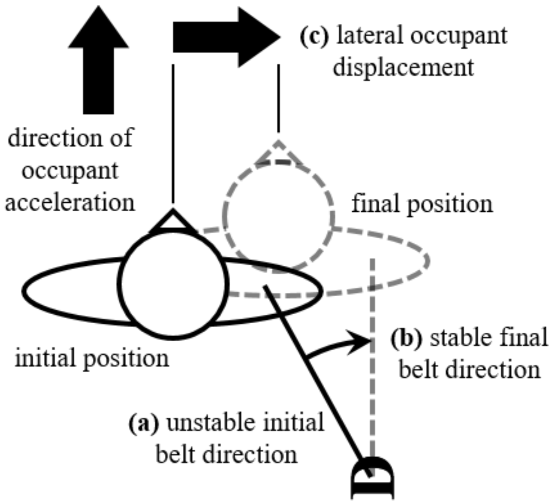

Figure 27. Self-stabilization of the three-point seatbelt in a frontal crash causes lateral displacement of the occupant toward the belted shoulder, even for in-position occupants (overhead view).

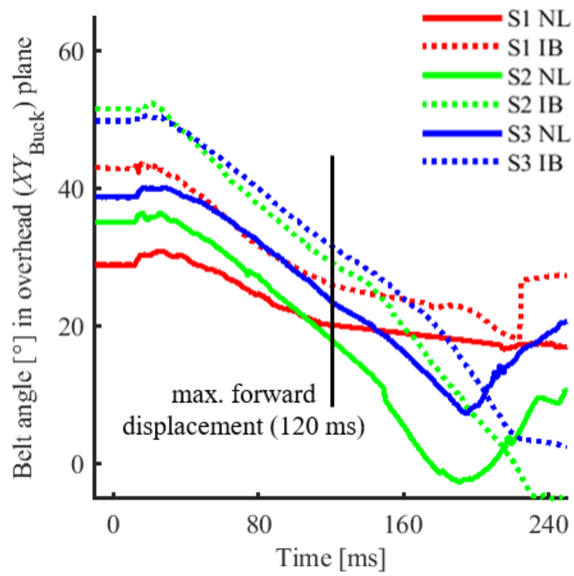

Figure 28. Shoulder-to-D-ring seatbelt angle in overhead plane.

Retention of the seatbelt on the shoulder is a key factor in occupant motion and subsequent injury risk. Most studies of shoulder-belt retention have focused on far-side lateral impacts (e.g., Arbogast et al., 2012; Forman et al., 2013). In frontal collisions with pre-crash steering, shoulder-belt slip-off has been identified as a contributing cause of serious head injuries for children (Bohman et al., 2011a). Simulations of frontal crashes with pre-crash inboard leaning have predicted shoulder-belt slip-off (Matsuda et al., 2018). In this study, the greater forward excursion of the left (unbelted) shoulder relative to the right (belted) shoulder caused the torso to turn outboard (Figure 19). This rotation could permit the seatbelt to slide laterally along the shoulder. Combined with the 14- to 36-mm more lateral initial position of the seatbelt on the shoulder in the inboard tests (Table 6), the seatbelt was expected to slip off the shoulder in the inboard-leaning tests. However, regardless of posture and crash velocity, the seatbelt remained on the shoulder in all tests well beyond the time of maximum forward displacement of the head and torso (Figure 24). The retention of the shoulder-belt may be due to the flexibility of the shoulder and the inertia of the arm (Tornvall et al., 2005): in the tests, the shoulder and arm moved superiorly, creating a stable, concave-up geometry to "cup" the shoulder-belt (Figure 29). This is consistent with the behavior of Subject 42 in the volunteer tests, who, as observed in Chapter 2, elevated the belted shoulder and so retained the seatbelt (Figure 4). This is also consistent with past PMHS tests in far-side frontal oblique tests: Kallieris et al. (1982) observed that the seatbelt remained on the shoulder in 9-12 g, 30 km/h far-side frontal oblique sled tests even up to 45°. In addition to the cupping of the seatbelt in the shoulder, the friction of the seatbelt on the PMHS may have contributed to shoulder-belt retention, as will be discussed further in Chapter 5.

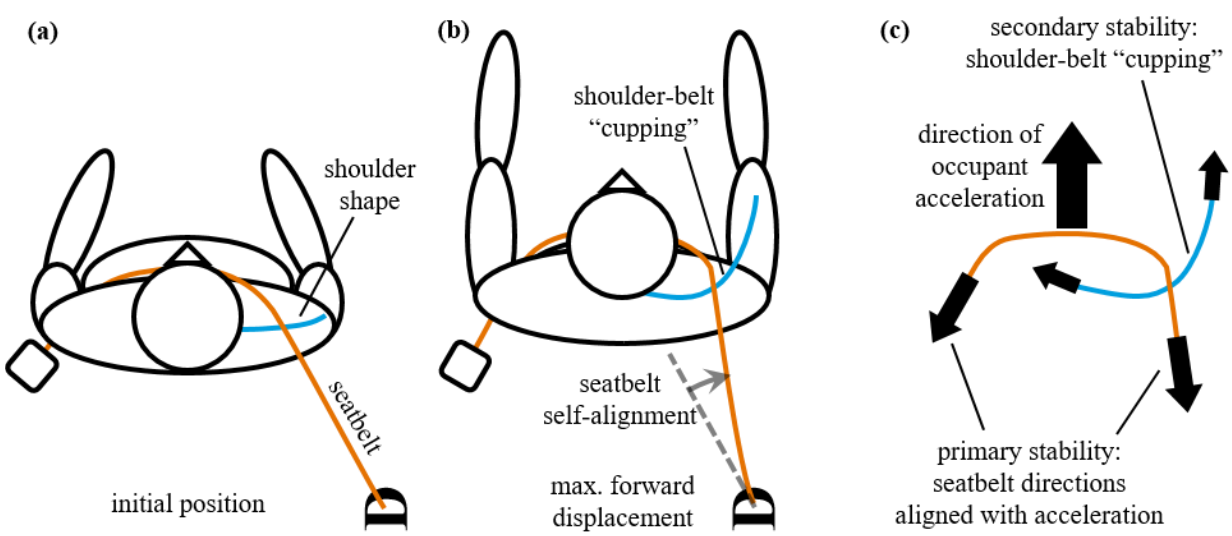

Figure 29. From (a) the initial position to (b) the position of maximum forward displacement, the seatbelt and shoulder geometry align to (c) a stable configuration.

Consequences of the Inboard Posture for Occupant Protection

The posture-induced changes in the timing and magnitude of motions yield significant consequences for occupant protection. The 58 mm ± 13 mm increase in maximum forward head displacement from neutral to inboard, and the additional 61 mm ± 19 mm increase from inboard 30 km/h to inboard 40 km/h, suggest an increased risk of head strikes to interior structures for inboard-leaning occupants. However, the interpretation of these displacements depends on the amount of initial space. Consider, for example, the passenger van second-row occupant environment selected as the basis for seat and seatbelt geometry for the volunteer and PMHS tests performed for this study (Figure 30). With the second-row (occupied) seat placed in its rearmost position, the clearance between the head (assuming around 100 mm up from the head center-of-gravity to the top of the head) and the back of the first-row seat (assuming it did not deflect forward in the crash) would be around 50 mm if the first-row seat was placed in the mid-track fore-aft position (Figure 30b). If the first-row seat was placed in its rearmost position (120 mm back from mid-track), then the head would have struck the back of the first-row seat (Figure 30b). Thus, a steering-induced inboard-leaning posture may increase risk of head injury for a second-row passenger even if the seatbelt does not slip off the shoulder.

The inboard-leaning posture did not increase the maximum outboard displacement of the head during rebound. As stated above, the interaction of the PMHS with the back support structures started around 180 ms, shortly after maximum forward displacement (around 120 ms) and well before maximum outboard displacement (around 280 ms). Therefore, the post-rebound outboard displacement observed in these tests may not be representative of in-vehicle occupant kinematics, and an assessment of the post-rebound outboard displacement's effect on occupant contact with the vehicle interior was beyond the scope of this thesis.

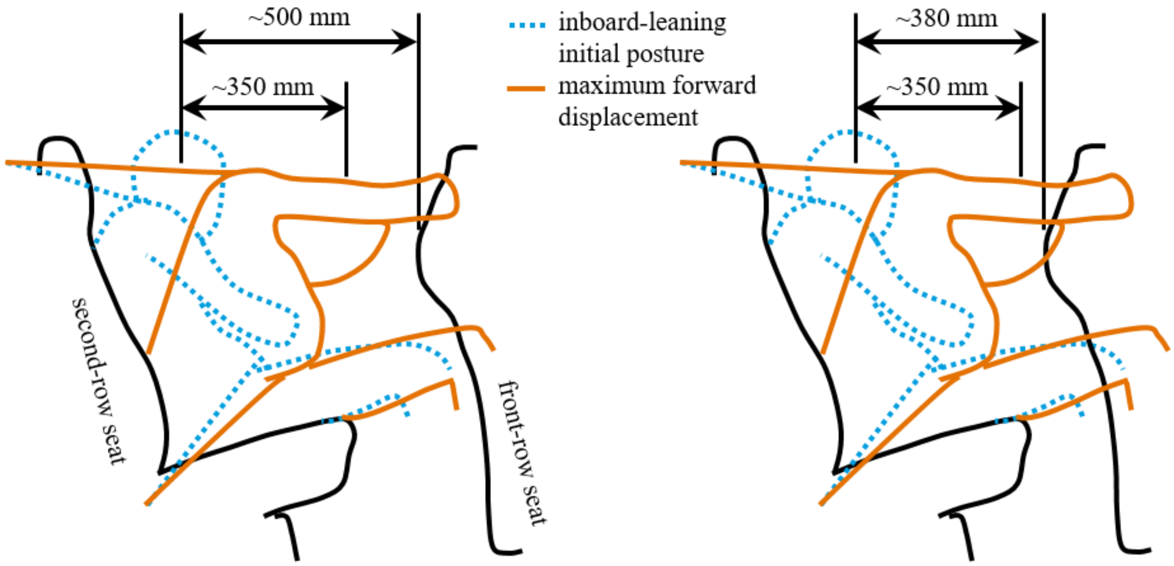

Figure 30. Tracings from passenger-side high-speed video of PMHS S2 in 14 g inboard test overlaid on outline of second-row environment from passenger van used as the basis of seat and seatbelt geometry for volunteer and PMHS tests.

This study found that the inboard-leaning posture significantly changed the magnitude of maximum forward head displacement, but not the time. This means that at the time when an airbag would have contacted the head and face of an in-position occupant, the head and face of an inboard-leaning occupant would have been significantly farther forward (Figure 22a) and inboard (Figure 22b). Consider a steering-wheel airbag module around 300 mm in front of the driver's chest and a dashboard airbag module around 500 mm in front of the right front passenger's chest (Figure 31). Driver-side frontal airbags generally deploy far back enough to begin loading the chest and head before the driver starts to displace forward (Kent et al., 2000), so the initial inboard lean would be of greater concern than the subsequent greater forward displacement (Figure 31a, b). In contrast, a right front passenger typically has a greater initial distance from the airbag module. Since the seatbelt self-alignment decreased the posture-induced difference in lateral head position over time, the effect of the inboard-leaning posture may not change airbag engagement as much for a right-front passenger as for a driver (Figure 31c, d). In either case, the airbag would have to be wide enough to account for the inboard-leaning posture (Figure 31b, d). While these examples remain hypothetical, they demonstrate the importance of considering an inboard-leaning pre-crash posture for synergistic seatbelt and airbag design.

This chapter (Chapter 3) has quantified and assessed the effect of an inboard-leaning pre-crash posture on PMHS kinematics in a frontal crash. A statistically significant effect of initial posture on the occupant's position and posture at the time of maximum forward excursion was observed. An inboard-leaning posture resulted in a more forward and inboard position of the head and thoracic spine (represented by the T1 and T8 vertebrae), while the position of the lumbar spine and pelvis did not significantly change. This implies that the inboard-leaning initial posture changed the geometric relationship of the seatbelt and the thorax. The angle of the torso in the sagittal plane has long been asserted to impose a strong effect on the distribution of seatbelt loads on the thorax and subsequent risk of rib fracture (Adomeit & Heger, 1975). As such, past studies have focused on occupant kinematics solely within the sagittal plane (e.g., Forman et al., 2006a; Arbogast et al., 2009; Lopez-Valdes et al., 2010). However, the inboard-leaning posture yielded demonstrably three-dimensional occupant kinematics. The lateral, non-sagittal component of motion may affect the restraining loads that the seatbelt imparts to the thorax. Therefore, the next chapter (Chapter 4) will quantify and assess the effect of the inboard-leaning pre-crash posture on the seatbelt forces.

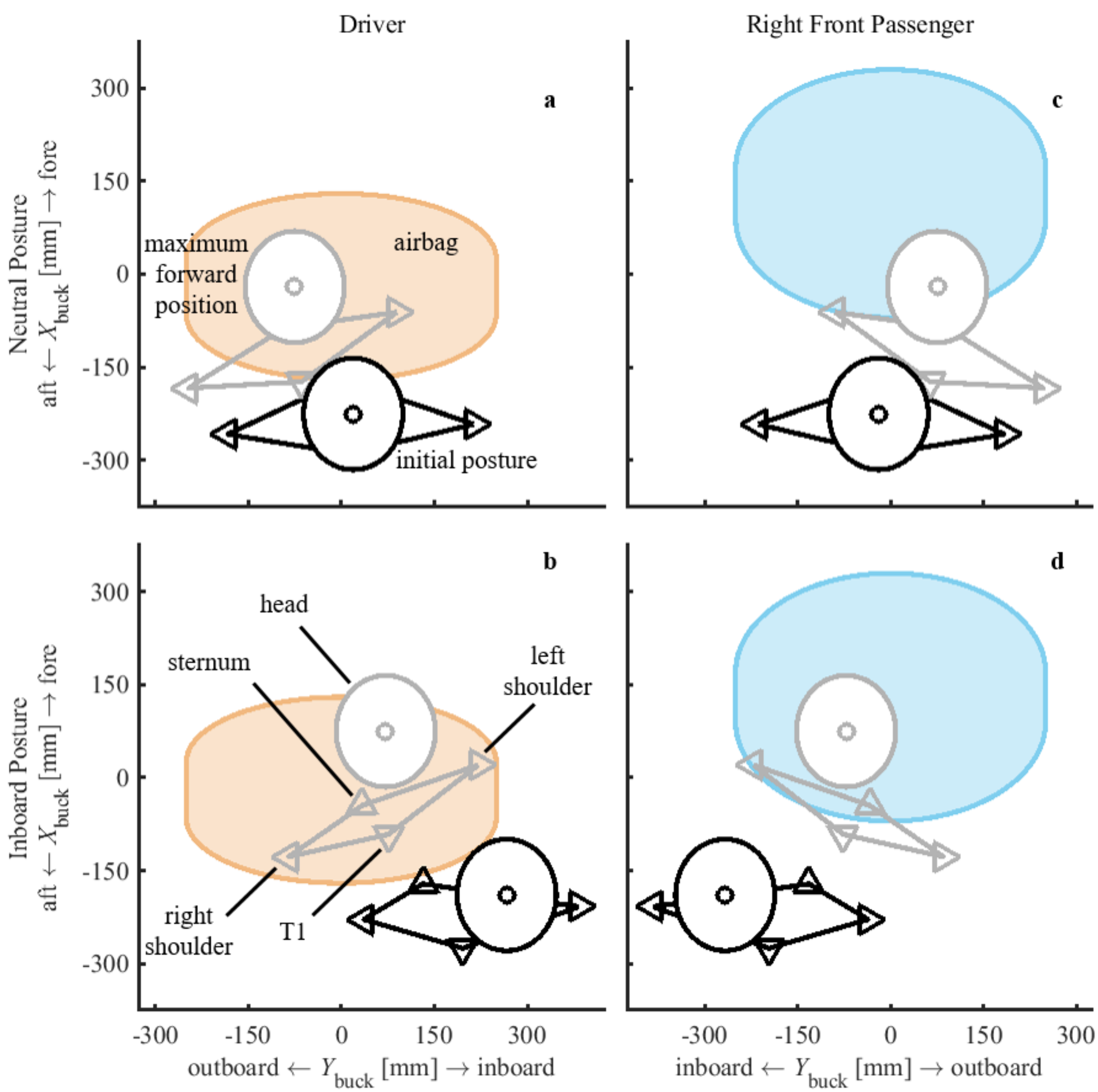

Figure 31. Overhead view of PMHS #2 kinematics in neutral (top) and inboard (bottom) 30 km/h tests, overlaid with approximate fully-deployed airbag shape in driver (left) and right front passenger (right) configurations. The PMHS kinematics were reflected around the sagittal (Z_{Buck} X_{Buck}) plane for the driver configuration.

3.5. Conclusions

The goal of this chapter was to quantify and assess the effect of an inboard-leaning pre-crash posture on the kinematics of the occupant in a subsequent frontal crash. The inboard-leaning posture increased forward displacement of the head and thoracic spine, but did not change the time to reach maximum forward displacement. This was attributed to the increased length of seatbelt between the shoulder and the D-ring. Outboard lateral displacement during rebound (after maximum forward displacement) did not change between neutral and inboard tests, but significant outboard displacements were observed in both test conditions. This was attributed to the asymmetry of the three-point seatbelt. The seatbelt did not slip off the shoulder in any test, which demonstrated the stability of the three-point seatbelt. To build from this chapter's assessment of occupant motion, the next chapter will examine the seatbelt forces and their sensitivity to the change in initial posture.

Chapter 4: Belt Mechanics

As stated in Chapter 1, the goal of this thesis was evaluate the effect of an out-of-position posture on occupant kinematics and restraint loads. In Chapter 2, a steering-induced inboard lateral lean was identified from volunteer tests and used as the initial posture of PMHS in frontal crash tests. Analysis of the PMHS kinematics in Chapter 3 showed that the pre-crash inboard lean changed the physical relationship between the occupant the restraint. This may change the contact surfaces, forces, and event timings in a crash. Therefore, the goal of the research described in this chapter was to evaluate the effect of the out-of-position posture on restraint loads in the PMHS tests.

4.1. Introduction

Although many studies have examined restraint of in-position occupants in frontal crashes using post-mortem human subjects (PMHS) (e.g., Kallieris et al., 1982; Vezin et al., 2002; Forman et al., 2006a, 2009b; Shaw et al., 2009; Ash et al., 2012), none have used PMHS specifically to study the restraint of lateral out-of-position occupants in this crash mode. Several studies have examined occupant restraint in frontal-oblique crashes, where the combined frontal and lateral motions may suggest possible effects on restraint due to a pre-crash lateral posture. Kallieris et al. (1982) and Kent et al. (2003) found that rib fracture patterns—and, therefore, thoracic loading—were similar in 0° (frontal) up to 30° (far-side frontal oblique), but concentrated on the upper ribcage in 45° tests. In contrast, PMHS tests in near-side frontal oblique tests showed a shift in seatbelt forces from the upper shoulder-belt to the lower shoulder-belt, which implies a change in how the seatbelt forces are transferred to the ribcage (Lopez-Valdes et al., 2016; Montesinos-Acosta et al., 2016). It is unknown how an inboard-leaning posture in a frontal crash would affect the distribution of belt forces and subsequent injuries.

Past frontal-oblique tests also examined the containment of the shoulder-belt. In near-side frontal oblique tests with PMHS, the shoulder-belt moved medially toward the neck (Lopez-Valdes et al., 2016; Montesinos-Acosta et al., 2016), but the shoulder-belt moved laterally in far-side frontal oblique tests (Kallieris et al., 1982; Kent et al., 2003). Despite this lateral motion, the seatbelt did not slip off the shoulder, even up to a 45° impact angle. This suggests that human occupants tend to contain the shoulder-belt within the concave geometry of the shoulder-arm complex (Tornvall et al., 2005). In Chapter 3, it was shown that the seatbelt remained on the shoulder in a frontal crash with an inboard-leaning pre-crash posture. However, it is unknown whether the kinematics of the inboard-leaning occupant changed how the seatbelt transfers load to the shoulder.

Several studies have suggested a strong relationship between the anatomic structures engaged by the seatbelt and the level of force sustained by the thorax without injury in frontal collisions. In quasi-static tests with PMHS, Cavanaugh et al. (1988) found that the stiffness of the thorax under localized loading was greatest at the sternum, less at the upper ribcage, and still less at the lower ribcage. Shaw et al. (2007) found the same result in dynamic tests with PMHS. Additionally, Kent et al. (2004) found that, for the same level of chest deflection, the force applied through a diagonal belt (which engaged the clavicle, sternum, and many ribs) or through a distributed, airbag-like load (which engaged the sternum and many ribs) was approximately twice the force applied through a hub (which engaged only the sternum). These studies suggest that thoracic restraint mechanics may depend on the posture of the occupant relative to the restraint.

Two computational studies predicted significantly increased risk of thoracic injury for inboard-leaning occupants in a frontal crash as compared to normally-seated occupants. In simulated frontal impacts with a 50th-percentile adult male MADYMO™ multibody model (TASS, Helmond, Netherlands), Bose et al. (2008) found that a 15° inboard lateral lean increased chest deflection by 11%. Matsuda et al. (2018) also predicted an 11% increase in chest deflection for the THUMS midsize adult male finite element model in an inboard lateral lean due to simulated pre-crash steering. Both studies also predicted belt slip-off of the shoulder. However, since no lateral-leaning frontal crash tests with PMHS had been performed before this study, it is unknown whether those simulation studies accurately predicted risk of thoracic injury.

Therefore, the goal of the research described in this chapter was to quantify the effect of an inboard-leaning posture on the locations, magnitudes, and directions of restraint forces for occupants in frontal impacts.

4.2. Methods

The detailed test methodology was given in Chapter 2. The kinematics measurement methodology was given in Chapter 3. This section describes additional instrumentation used in the tests presented in earlier chapters, and the data processing and reduction methods applied to the signals from the additional instrumentation.

Sensor Locations

Belt tension gauges were placed between the retractor and the D-ring ("pre D-ring"), between the D-ring and the shoulder ("upper shoulder-belt"), between the chest and the sliding latch-plate on the shoulder-belt ("lower shoulder-belt"), and between the lap and the outboard anchor on the lap-belt ("lap-belt") (Figure 32; Table 8). To measure the direction of the belt force vectors with respect to the laboratory reference frame, single reflective markers were placed before and after the belt tension gauges along the centerline of the seatbelt (Figure 33). In cases where markers could not be placed both before and after the belt tension gauges, markers were placed in alternate locations (e.g., on the outboard anchor or on the D-ring).

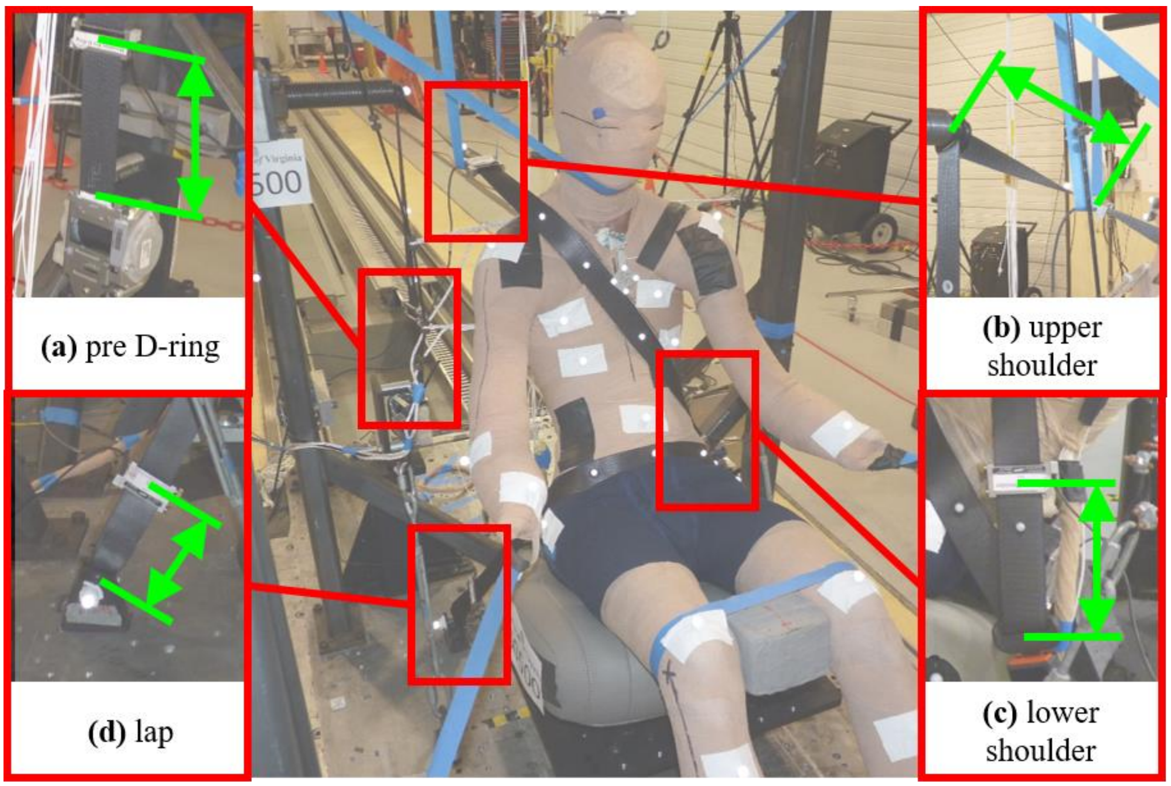

Figure 32. Locations of belt tension gauges.

Table 8. Reference distances of belt tension gauges.

[mm]	**Neutral 30 km/h**			**Inboard 30 km/h**			**Inboard 41 km/h**		
	S1	**S2**	**S3**	**S1**	**S2**	**S3**	**S1**	**S2**	**S3**
(a) distance after retractor	200	200	200	200	200	200	200	200	200
(b) distance after D-ring	200	200	200	200	200	200	200	200	200
(c) distance before buckle	155	155	105	155	155	100	155	110	100
(d) distance before anchor	120	120	120	120	120	120	120	120	120

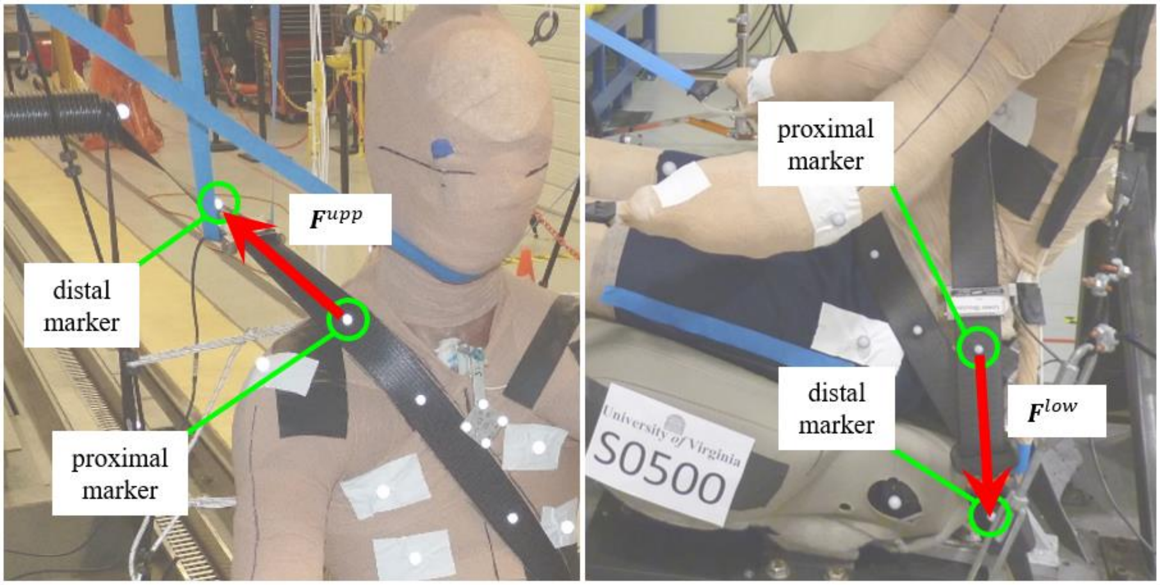

Figure 33. Motion-capture markers used to calculate upper shoulder-belt (F^{upp}) and lower shoulder-belt (F^{low}) force directions.

In order to distinguish changes in mechanical response due to loading condition from changes in mechanical response due to biological variability among specimens, geometric and inertial scaling has often been applied to PMHS test results (Eppinger et al., 1984). In this study, each PMHS was subjected to all loading conditions. Therefore, the effect of loading condition on mechanical response did not require scaling, but rather could be determined through matched-pair analysis. As with the kinematics in Chapter 3, paired-sample Student's *t*-tests were performed to quantify the statistical significance of the differences in seatbelt forces. Analyzed restraint mechanics quantities included maximum force (all belt gauges), time to maximum force (all belt gauges), force-limit level (pre D-ring gauge only), pre-tension force (pre D-ring gauge only), and loading rate (upper shoulder-belt only) (Figure 34). Force-limit level was calculated as the average force between the time when force ceased to increase and the time when force began to decrease (Figure 34d). Load rate was calculated as the slope of the line between the minimum force after pre-tensioning and the force identified as the start of force-limiting (Figure 34e).

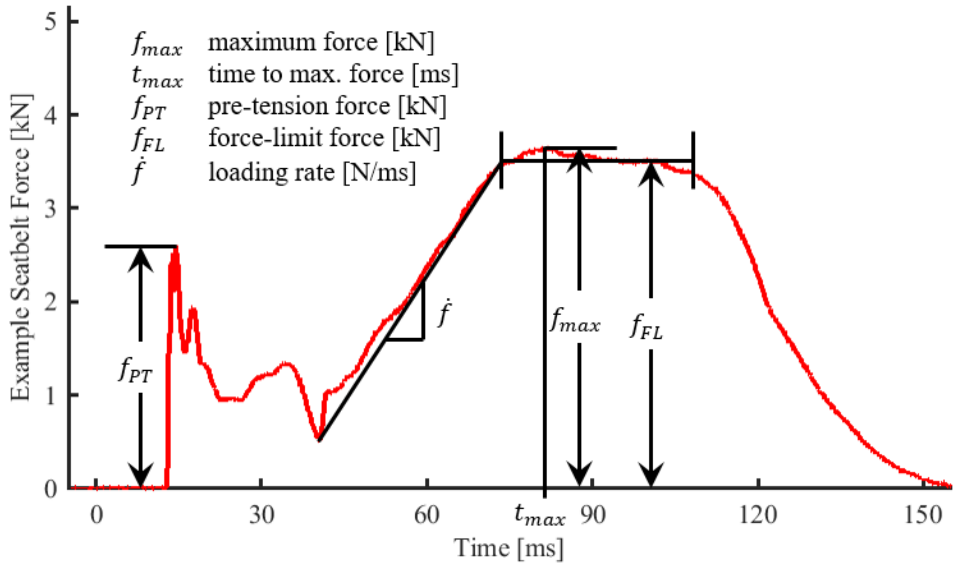

Figure 34. Analyzed restraint mechanics quantities.

Shoulder-Belt Force Components with respect to the Thorax

The components of the upper and lower shoulder-belt forces were calculated with respect to the T8 coordinate system. The T8 coordinate system was chosen to represent the thorax, with x_{T8} positive anteriorly, y_{T8} positive to the right, and z_{T8} positive caudally (Figure 35; SAE, 2007). The transformation matrix time-history of T8 ,$\boldsymbol{T}_{Buck/T8}(t)$, and the position time-histories of the belt markers with respect to the buck coordinate system ,$\boldsymbol{P}_{-/Buck}(t)$, were calculated as described in Chapter 3, Section 2. The position time-histories of the belt markers with respect to the T8 coordinate system, $\boldsymbol{P}_{-/T8}(t)$, were then calculated using Equation (1):

$$\boldsymbol{P}_{-/T8}(t) = \boldsymbol{T}_{Buck/T8}(t) * \boldsymbol{P}_{-/Buck}(t) \tag{1}$$

For each tension gauge, a pair of markers was selected to define the direction of the belt tension vector (Figure 33). A unit vector along the line connecting the pair of markers, $\boldsymbol{u}_{-/T8}(t)$, was calculated at each time-step for each gauge. The belt tension time-history, $F(t)$, was down-sampled from the DAS sampling rate of 10 kHz to the VICON sampling rate of 1 kHz. The components of the upper and lower shoulder-belt forces with respect to the T8 coordinate system, $\boldsymbol{F}_{-/T8}(t)$, were then calculated using Equation (2):

$$\boldsymbol{F}_{-/T8}(t) = F(t) * \boldsymbol{u}_{-/T8}(t) \tag{2}$$

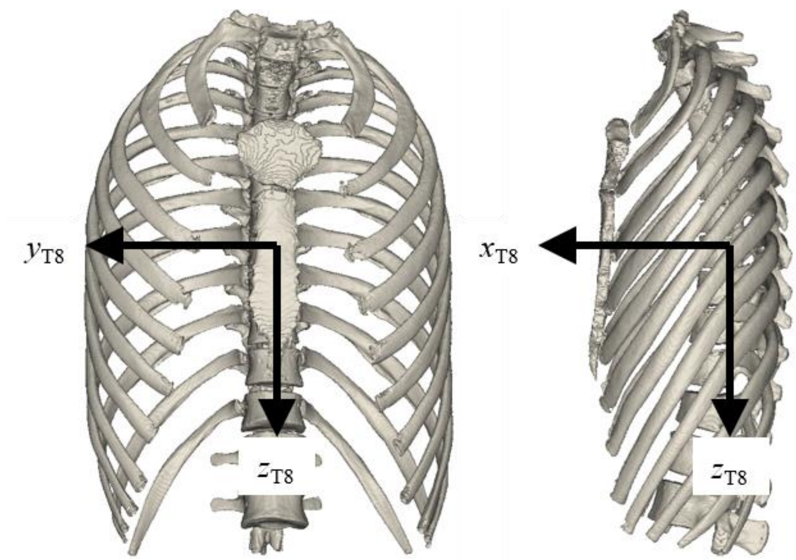

Figure 35. T8 local coordinate system used as the thorax local coordinate system.

Length of Spooled Belt

For the torque bar type force-limiter used in these tests, the actual force-limit depends on the moment arm from the torque bar to the seatbelt as it exits the retractor. Thus, if more belt is spooled around the torque bar, then the moment arm will be greater and the force-limit less. The length of belt in the retractor was calculated both for the initial position (time = 0 ms) and for the brief phase after pre-tensioning and before force-limiting (Figure 36). Shortly before the test, the belt webbing was marked where it exited the retractor (Figure 36a), and the length of belt in the retractor up to this line was measured after the tests (Figure 36b). The payout of the belt during the test was calculated as the vertical displacement of a motion-capture marker on the pre-D-ring portion of the belt Figure 36c). The length of belt after pre-tensioning was the sum of the initial length and the payout at the time immediately after pre-tensioning.

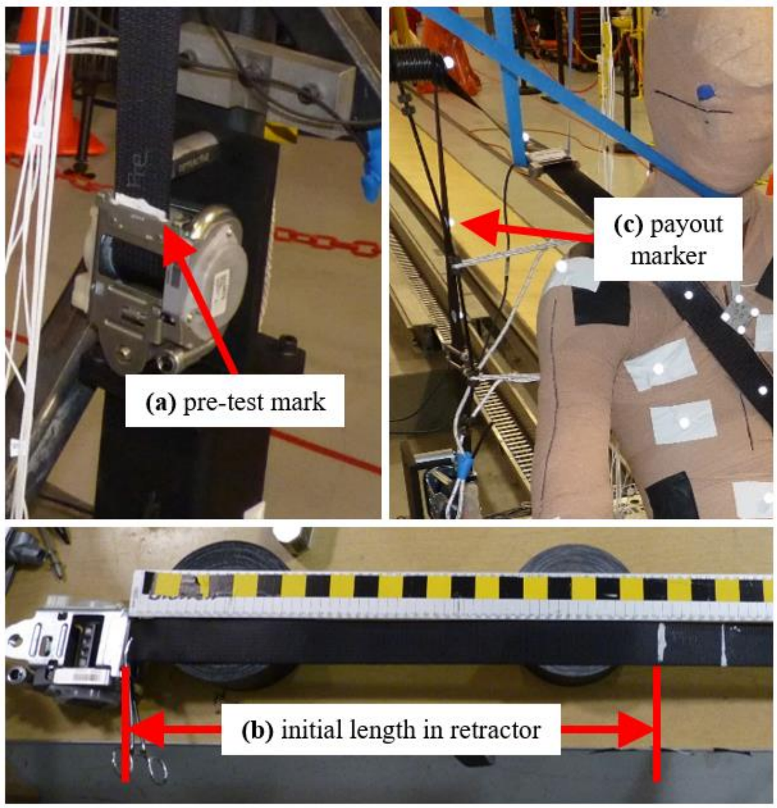

Figure 36. Measurement of length of belt in retractor before and after pre-tensioning.

4.3. Results

The seatbelt force time-histories in all tests exhibited the characteristic sequence of events observed in past PMHS frontal crash tests with pre-tensioned, force-limited three-point seatbelts (Kent et al., 2000; Forman et al., 2009b). The pre-D-ring tension gauge demonstrated the dynamics of the pre-tensioner and force-limiter (Figure 37a). The pre-tensioner activated at 10 ms and reached maximum pre-tensioning force (f_{PT}, as defined in Figure 34) of 4.1 to 4.3 kN within 5 ms of activation (Table 9). The pre-tensioner pulled 59 to 74 mm of belt into the retractor (Table 10). After the pre-tensioning peak, the force decreased to around 1 kN until 40 ms after the start of the test. The force then increased to a plateau of 2.4 to 3.1 kN (f_{FL}, as defined in Figure 34; Table 9), which indicated that the force-limiter was engaged. The force-limiter let 11 to 35 mm of belt out of the retractor (Table 10). At around 120 ms—the time of maximum forward displacement of the occupant—the force began to decrease from the force-limit threshold (Figure 37a). A similar sequence of events occurred at the upper and lower shoulder-belt tension gauges: pre-tension at 10 ms to about 1 kN until 40 ms, increase to maximum force around 100 ms, and unloading after 120 ms (Figure 37b, c). The lap-belt tension showed little evidence of pre-tensioning, but otherwise followed the same sequence (Figure 37d).

Table 9. Summary of belt force data in the neutral and inboard 30km/h PMHS tests.

	Neutral			**Inboard**			**Inboard - Neutral**			
	S1	**S2**	**S3**	**S1**	**S2**	**S3**	$\bar{d}$	$\bar{d}$ [%]	$s_{\bar{d}}$	p
Max. pre D-ring [kN]	2.84	3.20	3.44	2.56	2.97	3.52	-0.15	-5	0.20	0.331
time of max. [ms]	75	101	88	96	94	95	7	7	14	0.500
Max. upper shoulder-belt [kN]	3.65	4.01	4.29	3.08	3.46	4.29	-0.37	-10	0.32	0.182
time of max. [ms]	82	100	92	95	95	95	4	4	9	0.541
Max. lower shoulder-belt [kN]	2.11	2.46	2.87	2.27	3.15	3.72	0.57	25	0.36	0.113
time of max. [ms]	75	83	91	103	94	97	15	17	12	0.162
Max. lap-belt [kN]	1.81	2.00	2.12	1.25	1.92	2.51	-0.08	-5	0.48	0.802
time of max. [ms]	81	101	100	78	92	95	-5	-6	3	0.099
Pre-tension force [kN]	4.34	4.28	4.11	4.27	4.26	4.18	-0.01	0	0.07	0.874
Force-limit force [kN]	2.71	3.04	3.15	2.41	2.77	3.11	-0.20	-7	0.15	0.138
Upper sh.-belt load rate [N/ms]	88	61	56	38	45	56	-22	-35	25	0.271

Percent mean of differences ($\bar{d}$ [%]) was calculated as $\bar{d}$/mean(Neutral)

The inboard-leaning posture caused a trade-off in force between the upper and lower shoulder-belt. The maximum force (f_{max}, as defined in Figure 34) in the upper shoulder-belt (Figure 37b) decreased from the neutral tests (3.7 to 4.3 kN) to the inboard tests (3.1 to 4.3 kN), while the maximum force in the lower shoulder-belt (Figure 37c) increased from the neutral tests (2.1 to 2.9 kN) to the inboard tests (2.3 to 3.7 kN). In the neutral tests, the upper shoulder-belt force acted posteriorly ($-x_{\mathrm{T8}}$) and superiorly ($-z_{\mathrm{T8}}$), but in the inboard tests, it acted posteriorly ($-x_{\mathrm{T8}}$) and laterally ($+y_{\mathrm{T8}}$) (Figure 38). The inboard-leaning posture increased the lateral ($-y_{\mathrm{T8}}$) and inferior ($+z_{\mathrm{T8}}$) components of the lower shoulder-belt force (Figure 39). The force-limit force (f_{FL}) decreased from neutral (2.7 to 3.1) to inboard (2.4 to 3.1) (Figure 37a), although the length of spooled belt after pre-tensioning also decreased (Table 10). The force-limit plateau was also not as apparent in the inboard-leaning tests as in the neutral tests, nor was it sustained as long (Figure 37a). No consistent trend was observed across PMHS in the maximum force of the lap-belt. The sudden threshold or decrease of force in the lower shoulder-belt and lap-belt in both tests with PMHS #1 (Figure 37c, d) indicates the submarining observed in the kinematics (Figure 24).

Table 10. Length of belt in retractor at key points in neutral and inboard 30 km/h PMHS tests.

All lengths in [mm]	**Neutral**			**Inboard**			**Inboard - Neutral**		
	S1	**S2**	**S3**	**S1**	**S2**	**S3**	$\bar{d}$	$s_{\bar{d}}$	p
At start of test	554	599	324	479	572	309	-39	32	0.167
After pre-tensioning	624	661	387	554	643	368	-36	30	0.173
Change due to pre-tensioning	70	62	63	74	71	59	3	7	0.537
After force-limiting	589	642	363	540	632	346	-25	21	0.175
Change due to force-limiting	-35	-20	-24	-14	-11	-22	11	10	0.191

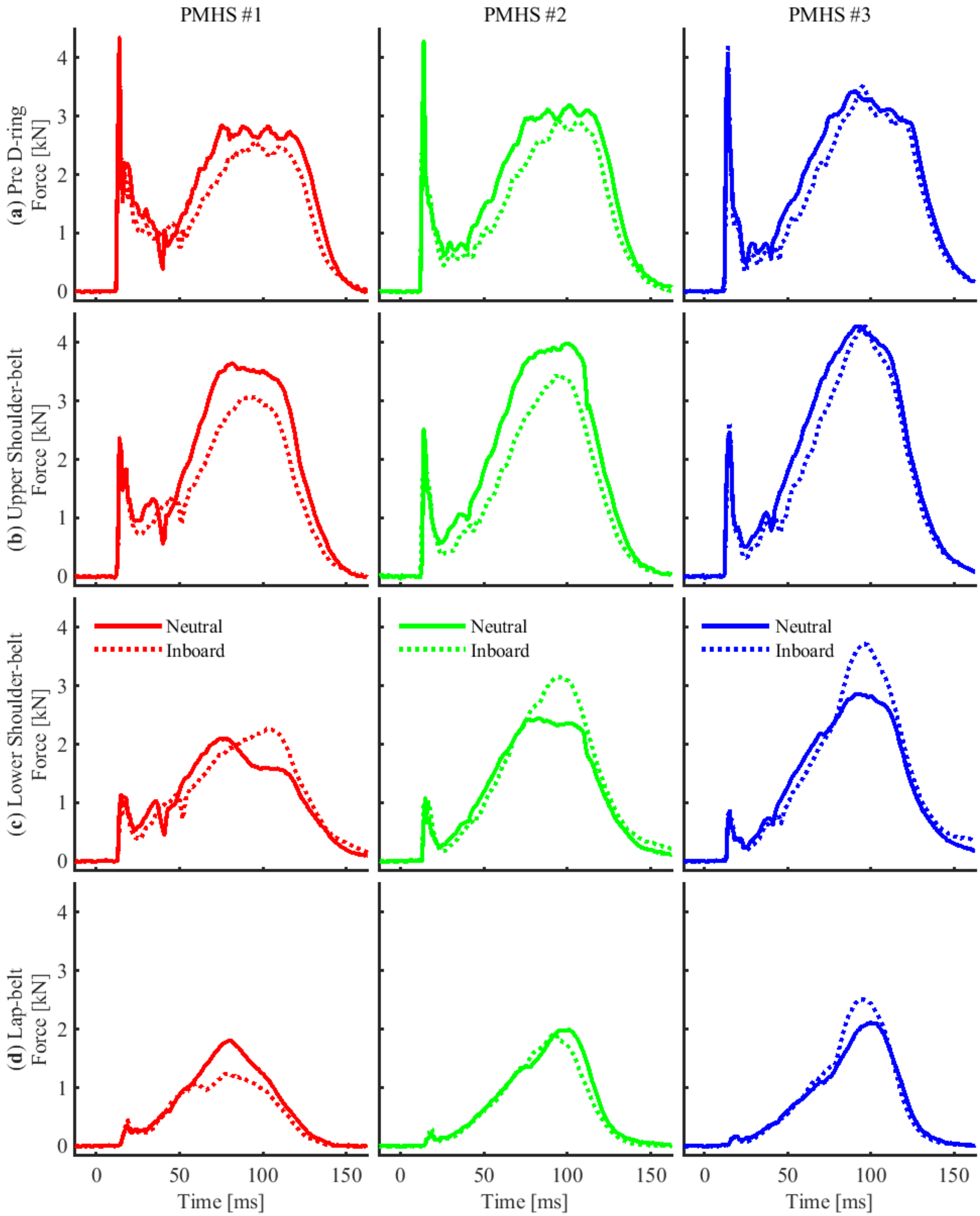

Figure 37. Belt force time-histories from neutral and inboard 30 km/h tests for each PMHS (columns) at each measurement location (rows).

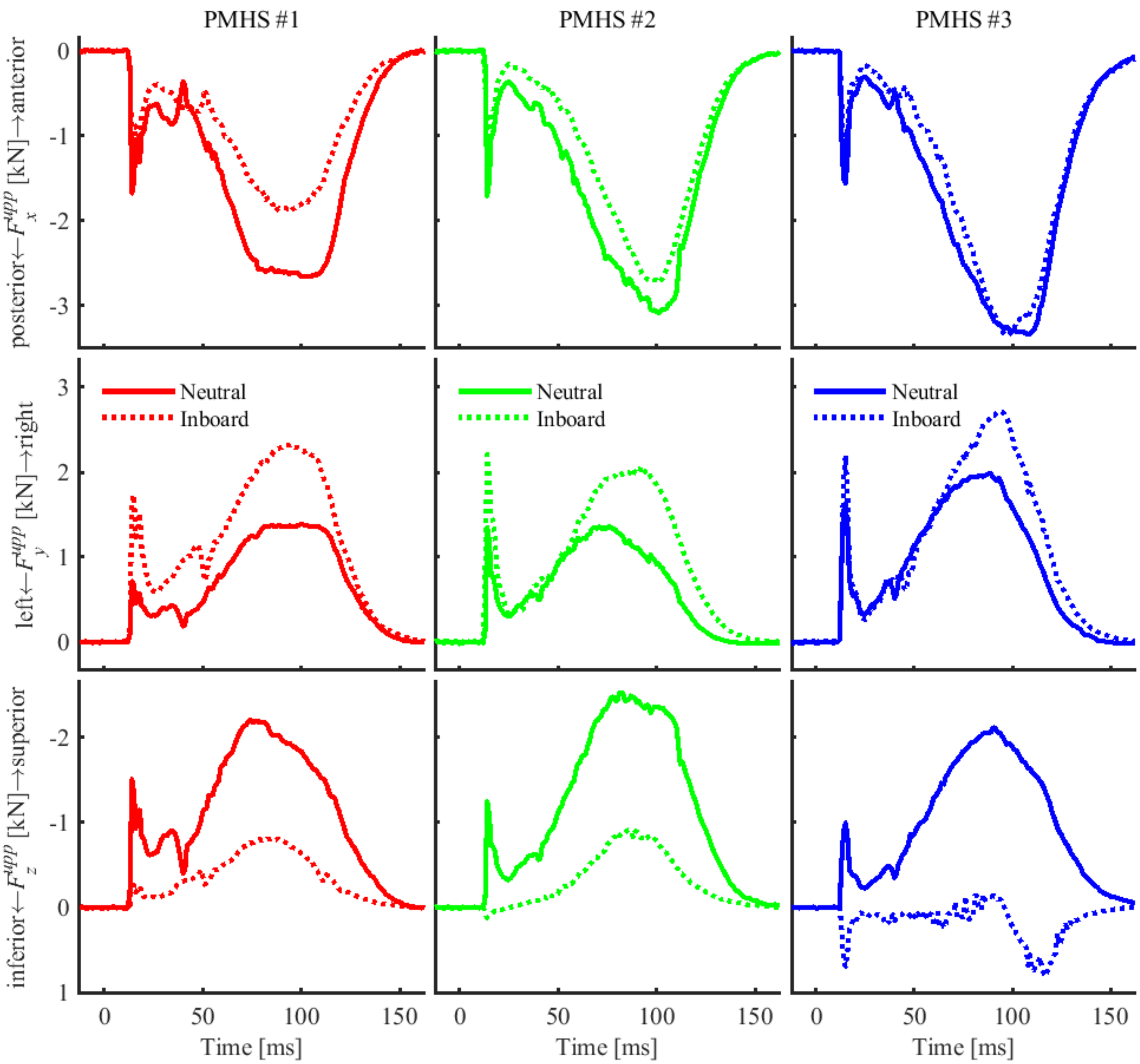

Figure 38. Upper shoulder-belt force components with respect to the T8 LCS in 30 km/h neutral and inboard PMHS tests.

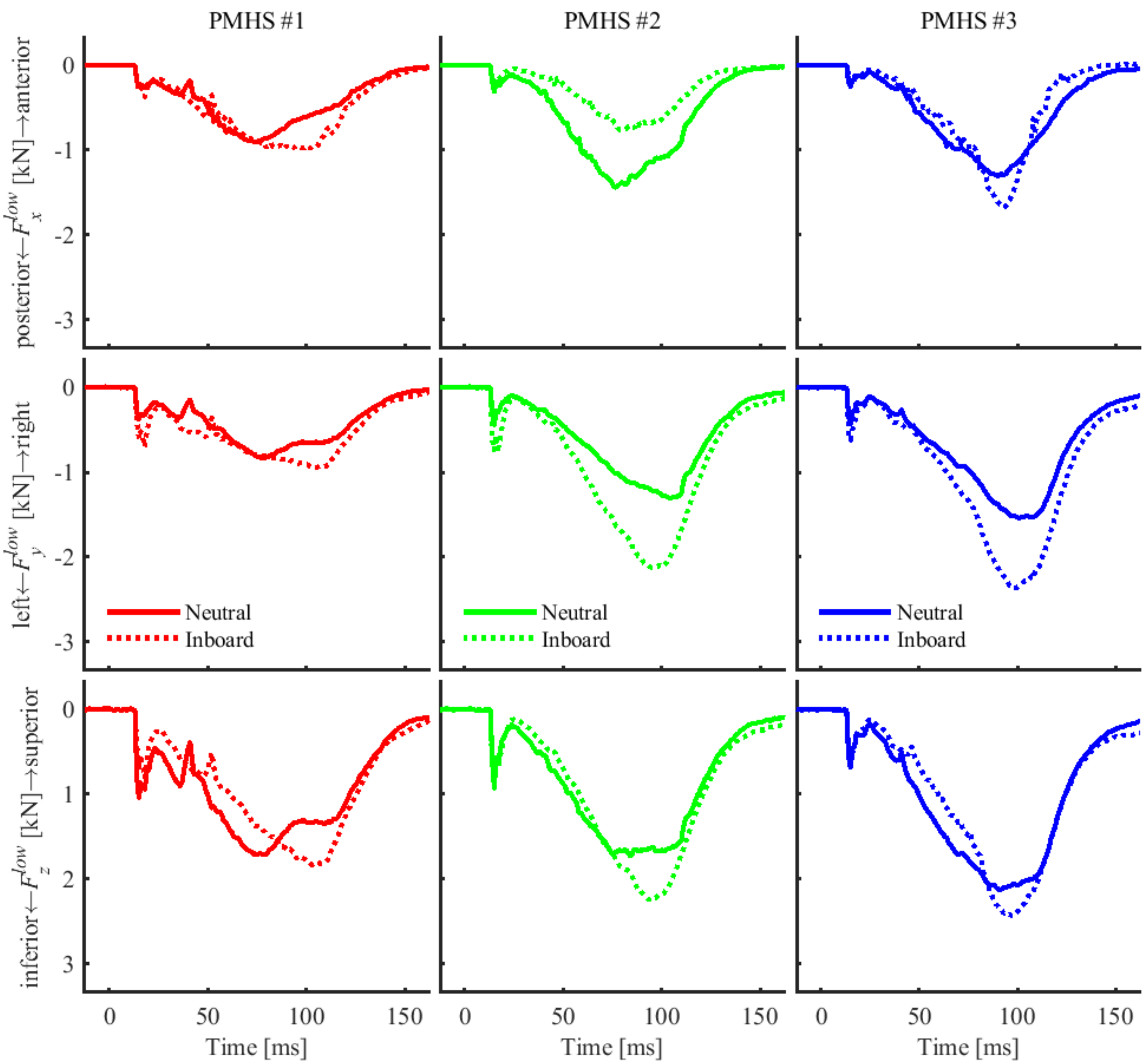

Figure 39. Lower shoulder-belt force components with respect to the T8 LCS in 30 km/h neutral and inboard PMHS tests.

Table 11. Shoulder-belt force components in neutral and inboard 30 km/h PMHS tests (T8 LCS).

			Neutral			Inboard			Inboard - Neutral			
			S1	S2	S3	S1	S2	S3	$\bar{d}$	$\bar{d}$ [%]	$s_{\bar{d}}$	p
Upper Shoulder-belt	max. [kN]	x	-2.66	-3.08	-3.34	-1.88	-2.72	-3.35	0.38	-15	0.40	0.243
		y	1.39	1.36	1.99	2.33	2.07	2.72	0.79	47	0.13	0.008
		z	-2.21	-2.53	-2.12	-0.81	-0.91	0.81	1.98	-107	0.83	0.054
	time of max. [ms]	x	100	101	108	95	101	97	-5	-5	6	0.235
		y	100	71	89	95	92	94	7	8	13	0.453
		z	74	82	91	88	86	117	15	18	11	0.148
Lower Shoulder-belt	max. [kN]	x	-0.91	-1.44	-1.31	-0.98	-0.76	-1.66	0.08	-7	0.53	0.813
		y	-0.83	-1.30	-1.54	-0.94	-2.12	-2.37	-0.59	57	0.41	0.132
		z	1.71	1.73	2.13	1.83	2.24	2.43	0.31	18	0.20	0.112
	time of max. [ms]	x	74	77	90	89	81	94	8	10	6	0.172
		y	79	105	101	105	95	98	4	4	19	0.732
		z	78	84	91	103	93	98	14	15	10	0.139

Percent mean of differences ($\bar{d}$ [%]) was calculated as $\bar{d}$/mean(Neutral)

4.4. Discussion

Seatbelt efficacy depends on the duration, location, and magnitude of forces applied by the seatbelt to the occupant (Kent & Forman, 2015). Therefore, the posture-induced differences in the duration, location, and magnitude of seatbelt forces substantially affected the ability of the seatbelt to restrain the occupant.

The duration of the force-limit plateau was less in the inboard tests than in the neutral tests. As shown in Figure 40, the decreased duration was primarily due to a delay in the start of force-limiting. The delay may in turn have been due to the initial shoulder-to-D-ring seatbelt angle, as suggested in Chapter 3 (Figure 28). In Chapter 3, the increased forward displacement of the occupant in the inboard tests was ascribed to an increased initial shoulder-to-D-ring seatbelt length. The pre-tensioner removed 59 to 74 mm and the force-limiter let out 11 to 35 mm, with no difference in either between neutral and inboard. Therefore, a significantly greater shoulder-to-D-ring seatbelt length remained in the inboard tests. However, the time over which force is applied relates to the deceleration of the occupant, and subsequently, the displacement of the occupant.

Therefore, the delay in force may have contributed to the increased forward displacement observed in the inboard tests.

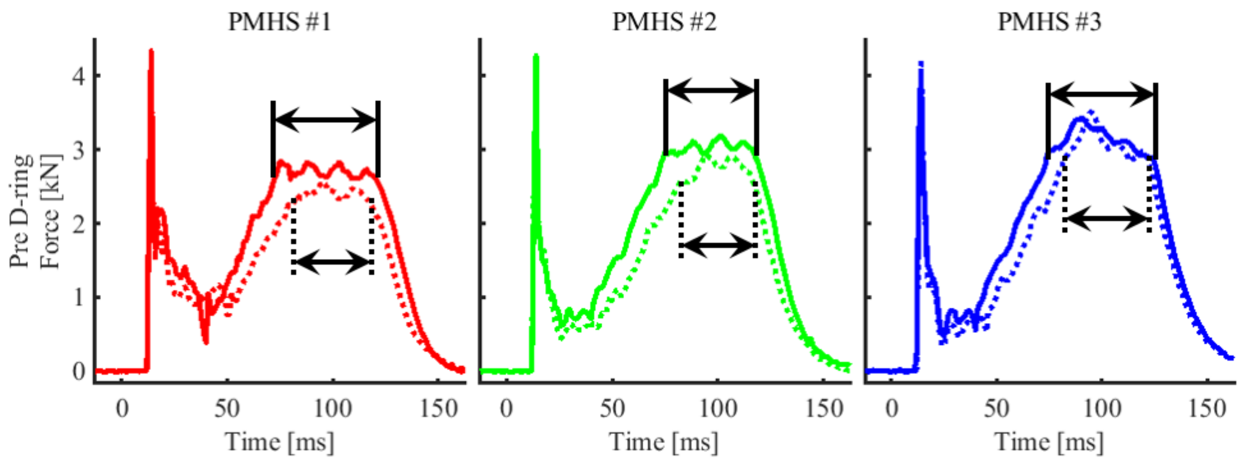

Figure 40. Pre-D-Ring force time-history from the neutral and inboard 30 km/h PMHS tests.

4.5. Conclusions

The goal of this chapter was to quantify the effect of the inboard-leaning posture on restraint loads in the PMHS tests. The inboard-leaning posture decreased the magnitude of the upper shoulder-belt force and increased the magnitude of the lower shoulder-belt force. The inboard-leaning posture also decreased the loading rate of the upper shoulder-belt force. The next chapter will integrate the restraint forces evaluated in this chapter with the occupant kinematics evaluated in the previous chapter.

Chapter 5: Findings and Implications

The goal of this thesis was to quantify the effects of an inboard-leaning posture on occupant restraint in a frontal crash. To achieve this, three PMHS were each tested in 30 km/h tests in a neutral posture and in an inboard-leaning posture. The inboard-leaning posture increased the forward displacement of the occupant (as described in Chapter 3) and increased the loading of the seatbelt on the lower left ribcage (as described in Chapter 4). This final chapter will discuss consequences for seatbelt design, interpretation of the unexpected submarining outcomes, and the limitations of this study. Finally, the conclusions and contributions of this thesis will be summarized.

5.1. Countermeasures for Inboard-Leaning Postures

The inboard-leaning posture substantially affected the restraint of the occupant. This suggests the need for a modified approach to restraining an inboard-leaning occupant both during and before the crash.

Past studies of occupant kinematics in frontal crashes have, understandably, focused on the sagittal plane (e.g., Forman et al., 2006a; Arbogast et al., 2009; Lopez-Valdes et al., 2010). However, motion of the occupant is not restricted to the sagittal plane, even in a frontal crash: Ash et al. (2012) observed non-negligible lateral displacements of the head, T1, and left acromion in frontal crash tests with eight adult male PMHS. The authors suggested that the lateral displacements may have affected the interaction of the thorax with the seatbelt, and would have affected frontal airbag deployment. Similarly, Montesinos-Acosta et al. (2016) saw shoulder rotation of a similar magnitude to that observed in the neutral tests of the present study (Figure 19). However, the studies by Ash et al. (2012) and Montesinos-Acosta et al. (2016) included a knee-bolster initially adjacent to the knees, which greatly constrained the pelvis. In the current study, no knee-bolster was used, and non-negligible lateral displacements of head, spine, and pelvis were observed even in the neutral posture (Figure 21). Since the crash was symmetric (full frontal) and the posture in these cases was symmetric (neutral), and assuming that the human body is structurally and mechanically symmetric, then the out-of-sagittal-plane motions may logically be attributed primarily to the asymmetry of the three-point seatbelt system. Thus it may be that the inboard-leaning posture exacerbated and highlighted the intrinsic asymmetry of the three-point belt, which could be mitigated by a symmetric restraint system such as a four-point seatbelt (Rouhana et al., 2003; Bostrom and Haland, 2005; Hu et al., 2018).

A four-point seatbelt offers many possible advantages over the traditional three-point seatbelt with outboard D-ring. The tolerance of the human body to injury is greatly enhanced by load distribution, which reduces local deformation and thus minimizes the risk of injury (Kent and Forman, 2015). Various four-point seatbelt configurations—double diagonal shoulder-belts, double vertical shoulder-belts—have been shown to distribute seatbelt loads across the whole ribcage and both clavicles, thus decreasing chest deflection and subsequent risk of rib fracture (Rouhana et al., 2003; Kent et al., 2004; Bostrom & Haland, 2005; Hu et al., 2018). Four-point seatbelts may also provide benefit during the pre-crash phase by reducing the possibility of shoulder-belt slip-off and minimizing the steering-induced lateral displacement of the occupant (Bostrom & Haland, 2005). Despite these possible benefits, evaluations of four-point seatbelts have found essential concomitant problems. Addition of an inboard shoulder-belt (whether diagonal or vertical) may help prevent the occupant from slipping out from under the typical outboard shoulder-belt, but at the risk of causing neck injury (States & Ryon, 1969; Kallieris & Schmidt, 1990). Added inboard support structures may mitigate this downside (e.g., Bostrom & Haland, 2005). Some four-point seatbelt configurations have been associated with an increase in local chest deflection (e.g., the "X4" seatbelt of Rouhana et al., 2003), although overall chest deflection may decrease (Kent et al., 2004). Configurations that attach the shoulder-belts to the mid-substance of the lap-belt rather than through a sliding latch-plate have been shown to increase the risk of lap-belt submarining, since the shoulder-belts may pull the lap-belt up over the pelvis (e.g., the "V4" seatbelt of Rouhana et al., 2003; the "suspender" seatbelt of Hu et al., 2018). Buckle and anchor pre-tensioning of the lap-belt may help in such cases (Hu et al., 2018), but the tolerance of the pelvis must then be accounted for: Rouhana et al. (2003) found that a non-pre-tensioned lap-belt with a "V4" configuration induced fractures of the anterior superior iliac spines (ASIS) of the pelvis. Despite these challenges, the possible benefits of a four-point seatbelt for lateral out-of-position occupants should be considered.

In the meantime, enhancement of the ubiquitous three-point seatbelt may mitigate the effects of the inboard-leaning posture on occupant displacement and restraint forces. Holt et al. (2018) evaluated the effect of pre-crash countermeasures on the lateral displacement of the head and thorax of volunteers under 0.75 g sinusoidal lateral acceleration. As a baseline, they used second-row captain's chair from a passenger van. They compared this seat to a "sculpted" seat with pronounced lateral support structures in both the seat cushion and seat back. The lateral bolsters of the seat back of the "sculpted" seat also contained inflatable cushions, which Holt et al. (2018) evaluated both uninflated and inflated. Finally, the authors added a 200 N motorized reversible pre-tensioner (a "pre-pretensioner"). They found that the pre-pretensioner reduced lateral excursions by around 45%, while the sculpted seat—whether inflated or not—reduced lateral excursions by less than 10% (Holt et al., 2018). Other studies have confirmed the ability of pre-pretensioners to reduce out-of-position displacements due to pre-crash vehicle dynamics (Arbogast et al., 2012; Ólafsdóttir et al., 2013; Östh et al., 2013; Ghaffari et al., 2018). This suggests that a pre-pretensioner may be an effective countermeasure for reducing pre-crash lateral lean; but its effect, if any, on occupant restraint in a subsequent crash is unknown and worth investigation.

5.2. Unexpected Submarining

Differences in lap-belt submarining outcome were observed across PMHS. The sudden threshold or decrease of force in the lower shoulder-belt and the lap-belt in all three tests with PMHS #1 (Figure 41) was due to submarining of the lap-belt, as was independently identified from the high-speed videos (Figure 24). That the submarining was more apparent in the lap-belt force for the inboard test and in the lower shoulder-belt force for the neutral test suggests asymmetric submarining: in the neutral test, the lap-belt may have slipped over the left iliac wing first, while in the inboard tests, the lap-belt may have slipped over the right iliac wing first. Other than this possible influence, submarining showed no sensitivity to the lateral-leaning posture examined in this study. The occurrence of submarining in PMHS #1 but in neither PMHS #2 nor PMHS #3 was surprising, since submarining has been attributed to increased abdominal soft tissue (Forman et al., 2009a). On the other hand, analysis of radiologic scans from submarining cases in the field have suggested a protective effect of increased abdominal soft tissue (Hartka et al., 2017).

High-speed video analysis showed lap-belt submarining in all three tests with PMHS #1 (Figure 24). Lap-belt submarining has been considered both a cause (e.g., Adomeit & Heger, 1975; Forman et al., 2009a) and an effect (e.g., Forman et al., 2008) of decreased forward torso rotation. In this study, lap-belt submarining manifestly caused the decreased forward torso rotation of PMHS #1 in all three test conditions: the plateau in lap-belt force that indicated the onset of submarining occurred well before the time of peak forward excursion of the pelvis (Figure 42). If the lap-belt had constrained the pelvis, then that PMHS #1's torso may have leaned farther forward than it did.

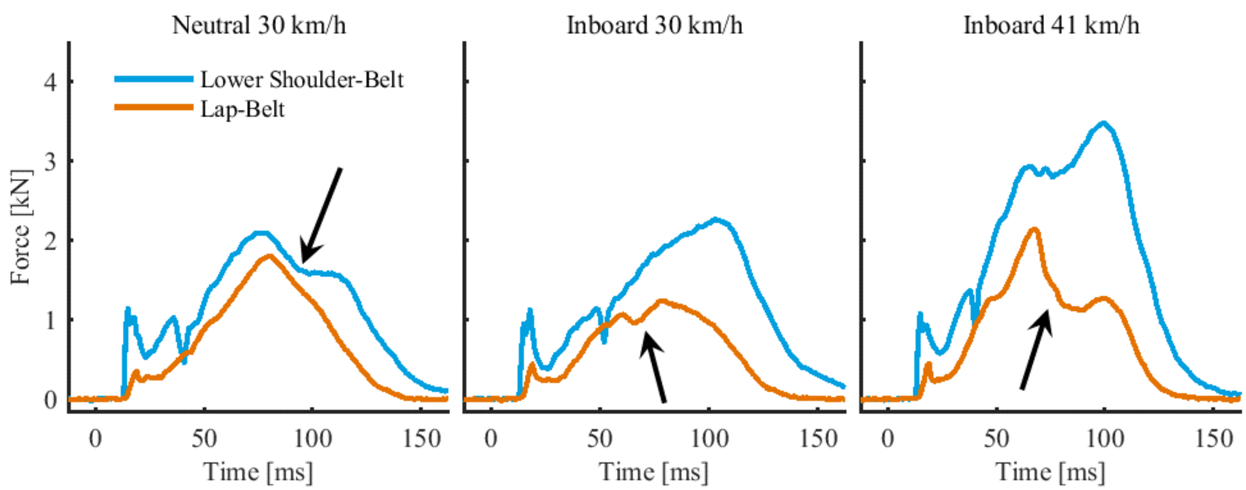

Figure 41. Lower shoulder-belt and lap-belt forces demonstrating possible posture-induced asymmetry in onset of submarining.

Increased body mass index (BMI) has been suggested as both a predilection for (Forman et al., 2009a) and a protection against (Hartka et al., 2017) submarining. In a belt-fit study with volunteers, Reed et al. (2012) found that every 10 kg/m^2 increase in BMI moved the lap-belt on average 43 mm forward and 21 mm upward from the ASIS. In contrast, Hartka et al. (2017) examined radiographically-identifiable cases of lap-belt submarining from field crashes (3-point seatbelt, front-end collision, crash velocity greater than 56 km/h), and found no statistically significant relationship between BMI and superior location of belt-induced trauma relative to the ASIS. In this study, the initial lap-belt path was around the same superior location relative to the ASIS for all three PMHS in all test conditions (Figure 43). However, the decreased abdominal depth of PMHS #1 placed the lap-belt more posteriorly than the other two PMHS. This contradicts the work of Hartka et al. (2017), who found a correlation between increasing BMI and anterior displacement of the belt-induced trauma. This also suggests that BMI alone may not suffice to predict lap-belt path and subsequent risk of submarining, whether in a neutral posture (Reed et al., 2012) or in a reclined posture (Reed & Ebert, 2018).

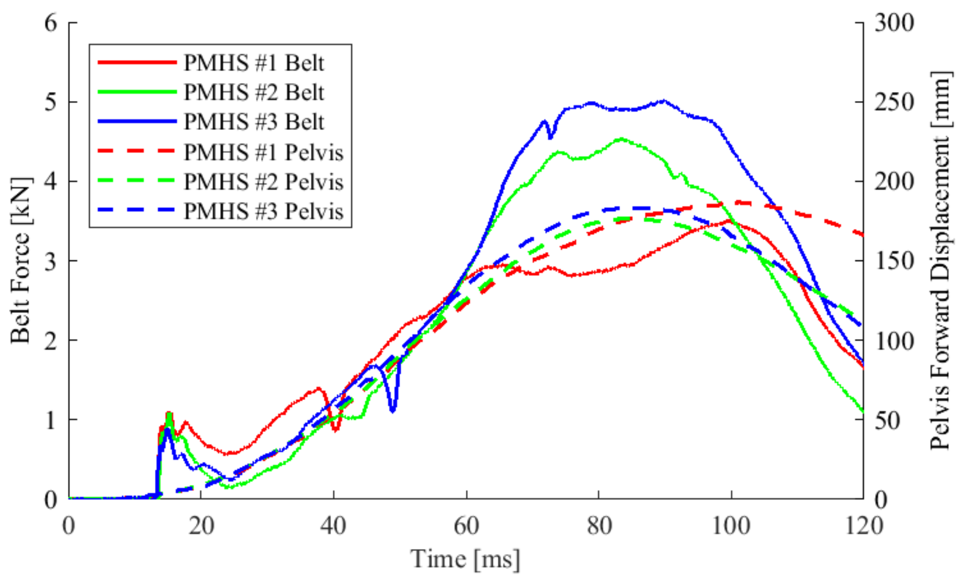

Figure 42. Pelvis displacement and lap-belt force time-histories for the 41 km/h tests.

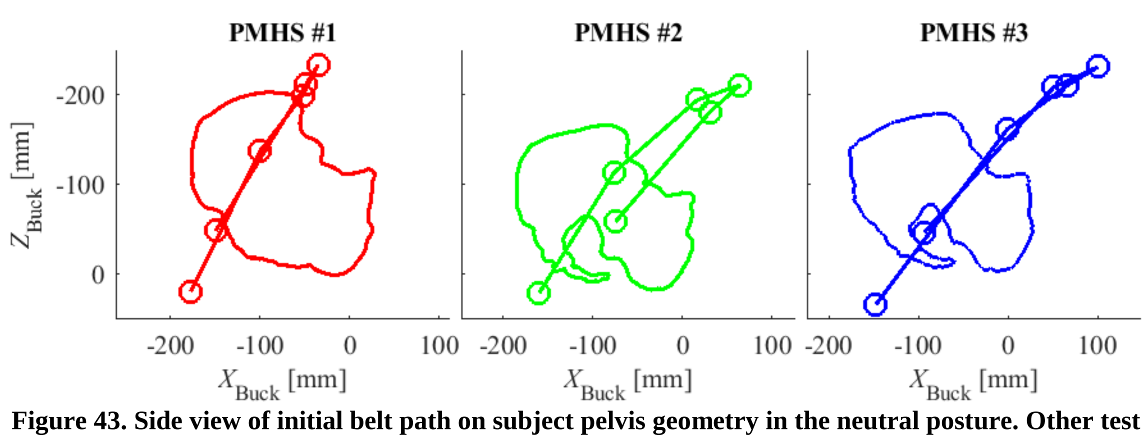

Figure 43. Side view of initial belt path on subject pelvis geometry in the neutral posture. Other test conditions yielded similar results.

5.3. Limitations

Experimental Limitations

This study used volunteer tests to quantify a pre-crash posture for PMHS tests. As noted in Chapter 2, it was discovered between the volunteer and PMHS tests that the angle of the seat bottom was steeper in the volunteer tests (21°) than in an actual vehicle (15°). The steeper seat angle in the volunteer tests may have restricted the lateral motion of the pelvis and lower extremities. Thus, the simplification of the combined lateral lean and turn observed in the volunteer tests to an isolated lateral lean in the PMHS tests may not represent actual steering-induced postures in crashes in the field. Even with the steeper seat pan angle, the addition of a lateral turning component would probably have further changed the restraint geometry and occupant motion. However, the inboard turn of the torso further secured the seatbelt on the shoulder in the volunteer tests (Figure 4), and thus at least may not have changed the fact that the seatbelt did not slip off the shoulder in the simplified posture of the PMHS tests. In contrast, the combined outboard turn and lean of the volunteers (Figure 4) may lead to shoulder-belt slip-off in a subsequent frontal crash. The changes in occupant restraint due to an inboard-leaning posture enhance rather than reduce the need for future study of an outboard-leaning posture.

The locations of the buckle and lap-belt anchor relative to the seat approximated those of a mid-track second-row seat from a passenger van. The mid-track position may not represent the most common seat position, especially for midsize adult males such as the PMHS. The restraint geometry affects the restraint effectiveness (Adomeit & Heger, 1975), so the results of this study—in particular, the submarining outcomes—may have been different if a rear-track position had been used.

Retractor Lockup and Seatbelt Spool-Out

This study found that the inboard-leaning posture increased the initial length of seatbelt webbing between the D-ring and the acromion, and that this increased initial length permitted the occupant to displace farther forward, tracing out a larger arcuate path. However, putting the seatbelt on the PMHS when they were leaning inboard required unspooling 15 mm to 75 mm more webbing (Table 10). It is possible that pre-crash swerving in a real crash would cause the inertial locking mechanism of a contemporary seatbelt retractor to activate, thus preventing the unspooling observed in the PMHS tests. However, in the simulated swerving with the target volunteer, the retractor did not lock soon enough to prevent unspooling totally: around 60 mm of seatbelt unspooled between the neutral posture (at the start of the test) and the inboard posture (at the second inboard peak) (Figure 44), although this may have been due in part to filmspooling within the retractor. Furthermore, if the volunteer tests and the PMHS tests both overestimated the amount of unspooling, then this represents a worst-case scenario and thus provides an upper bound on the effects of a swerve-induced inboard-leaning posture on occupant kinematics in a frontal impact.

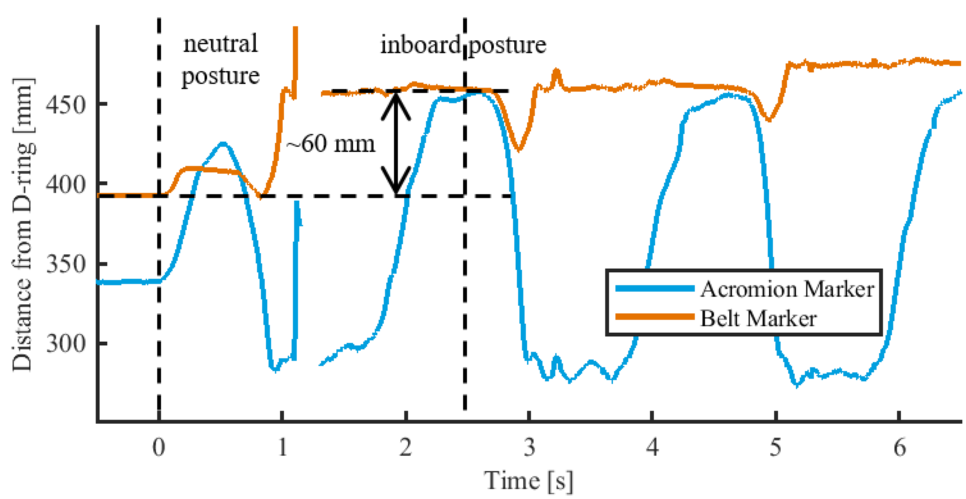

Figure 44. Distances of a marker on the right acromion and a marker on the shoulder-belt (near the shoulder) from a marker on the D-ring in the simulated swerving with volunteer Subject #42.

Population Diversity

This study only examined three midsize adult male PMHS (Table 2). While the results of this study provide some insight into the effect of an inboard-leaning posture on occupant restraint, the conclusions drawn here may not be applicable across the entire population of motor vehicle occupants. The fact that the magnitude and in some cases the direction of changes differed among PMHS suggests that postural effects may be sensitive to mass and stature, if not also to regional anthropometric variation. For example, the maximum upper and lower shoulder-belt forces increased from PMHS #1 to PMHS #2 to PMHS #3 (Figure 37a). This could have stemmed from the increasing mass of the PMHS (72 kg, 73 kg, and 83 kg), since the forces exerted on the occupant by the seatbelt have been shown to increase with the mass of the occupant (Kallieris et al., 1982; Nie et al., 2016).

Injuries and Repeated Testing

After each test, the thorax was palpated and the neck and shoulders were articulated to check for gross structural failures. No differences in stability of the ribcage, neck, or shoulders were observed after any of the lower-severity (9 g) tests. After all tests, clinical CT scans and autopsies were performed. For PMHS #1 (778), no rib or spine injuries were observed. For PMHS #2 (816), twenty-two rib fractures were observed (Table 12; Figure 45). A sternum fracture was identified just above the manubrium-body junction, passing through the upper mount screw-hole (Table 12; Figure 45). Extensive disruption of the T1-T2 functional spine unit was observed, including bilateral T1 transverse process fractures, bilateral perched facets at the T1-T2 junction with associated small fragments of bilateral inferior articular cassettes, and an anterior endplate compression fracture of T2. None of the T1-T2 injuries passed through the mount screw holes. For

PMHS #3 (899), twelve rib fractures were observed (Table 13; Figure 46). A sternum fracture was observed at the manubrium-body junction, passing through the upper mount screw-hole (Table 13; Figure 46). For PMHS #2 and #3, rib fractures occurred primarily on the left anterior aspect of the ribcage, but PMHS #2 also suffered multiple right posterior rib fractures.

In this study, each PMHS was tested multiple times. Several past studies have performed repeated tests on PMHS (e.g., Kent et al., 2004; Forman et al., 2006b; Shaw et al., 2006; Kent, 2008; Subit et al., 2010; Forman et al., 2013). Some of these studies observed injury in earlier tests that may have changed subsequent thoracic structural response. However, two studies found a low sensitivity of thoracic response to multiple or isolated rib fractures (Kent et al., 2004) or even up to 15 rib fractures (Shaw et al., 2007). Furthermore, one simulation study predicted a minimal effect on thoracic structural response for few (< 4) grouped rib fractures, and a smaller effect for anterior fractures than for lateral fractures (Zaseck et al., 2018). However, sensitivity of thorax response to sternal fractures has not been evaluated. Shaw et al. (2009) subjected eight PMHS to 40 km/h frontal tests somewhat comparable to the present study, although with an initially adjacent knee bolster and with neither pre-tensioner nor force-limiter. They observed sternal fractures as were observed in PMHS #2 and #3 of this study, but accompanied with many (5 to 27) rib fractures. If the sternal fractures of PMHS #2 and #3 occurred in their first tests, then they may have been accompanied by rib fractures, and may have altered the thoracic structural response of those PMHS.

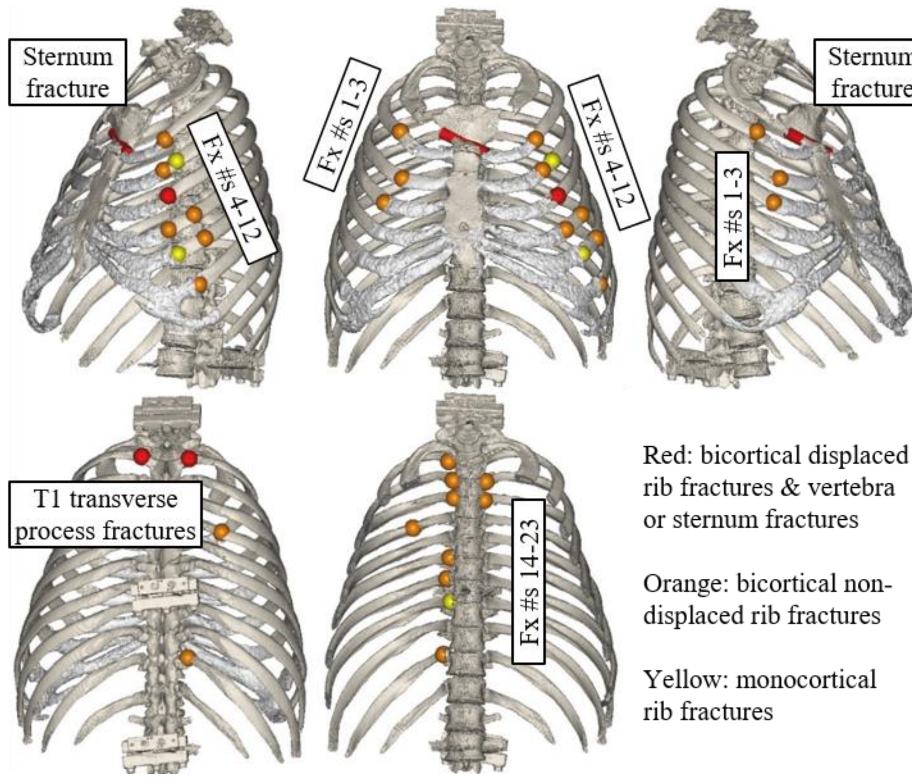

Figure 45. Locations of thoracic fractures on post-test CT reconstruction of PMHS #2 (816).

Table 12. Thoracic fracture summary for PMHS #2 (816).

Right Ribs				**Left Ribs**			
Fx #	Rib #	Fx Type	S [mm]	Fx #	Rib #	Fx Type	S [mm]
Anterior				*Anterior*			
1	2	BC ND	100	4	2	BC ND	75
2	3	BC ND	85	5	3	BC ND	80
3	4	BC ND	115	6	4	BC D	115
Posterior				7	5	BC ND	115
14	2	BC ND	30	8	5	BC ND	160
15	3	BC ND	30	9	6	MC	175
16	4	BC ND	35	10	6	BC ND	225
17	5	BC ND	100	11	7	BC ND	220
18	7	BC ND	35	12	3	MC	100
19	8	BC ND	50	*Posterior*			
20	9	MC	45	22	3	BC ND	30
21	11	BC ND	55	23	4	BC ND	55
Sternum							
13	-	-	65				

S = approximate curvilinear distance to fracture along rib from anterior sternal midline (anterior fractures), along rib from anterior spinal midline (posterior fractures), or down from sternal notch (sternum fracture)
Fracture Type: ND – Non-displaced; D – Displaced; BC – Bicortical; MC – Monocortical

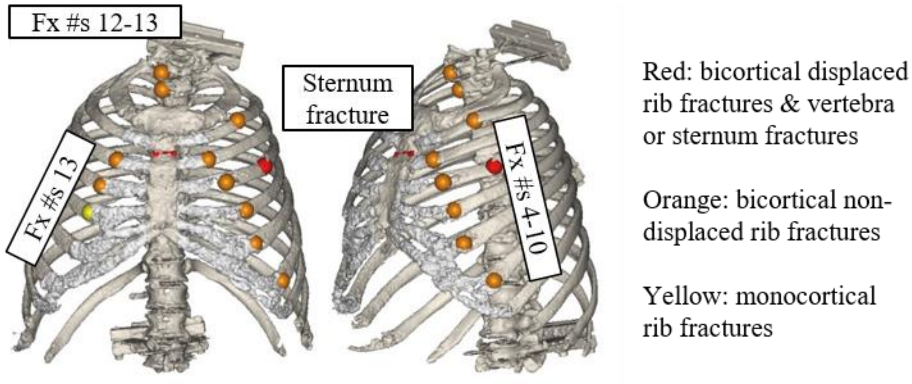

Figure 46. Locations of thoracic fractures on post-test CT reconstruction of PMHS #3 (899).

Table 13. Thoracic fracture summary for PMHS #3 (899).

Right Ribs				**Left Ribs**			
Fx #	Rib #	Fx Type	S [mm]	Fx #	Rib #	Fx Type	S [mm]
Anterior				*Anterior*			
1	3	BC ND CC	65	4	2	BC ND	95
2	4	BC ND CC	60	5	3	BC ND CC	60
3	5	MC CC	80	6	4	BC ND CC	60
Posterior				7	4	BC D	145
12	1	BC ND CV	15	8	5	BC ND CC	85
13	2	BC ND CV	25	9	6	BC ND CC	120
Sternum				10	7	BC ND CC	170
11	-	-	75				

S = approximate curvilinear distance to fracture along rib from anterior sternal midline (anterior fractures), along rib from anterior spinal midline (posterior fractures), or down from sternal notch (sternum fracture)
Fracture Type: ND – Non-displaced; D – Displaced; CC – Costochondral; CV – Costovertebral; BC – Bicortical; MC – Monocortical

The sternum and rib fractures were not observed via palpation of the chest of either PMHS #2 or PMHS #3 until after the third test. However, each PMHS was left supported in an upright seated posture between tests, and this may have inhibited palpation-based thoracic injury assessment. Whenever the sternum and rib fractures occurred, the uncertainty of their timing occludes attribution of injury outcomes to varied test conditions (posture or crash pulse). Future tests could employ complementary injury assessment methods such as mobile x-ray scanning (e.g., Crandall et al., 2000) or rib-mounted sensors (e.g., Kent et al., 2007). For the current study, radiography was avoided to accelerate the execution of the tests and reduce the effect of PMHS autolysis. Rib-mounted sensors were avoided in this study to minimize incisions on the anterior thorax. Despite these limitations, repeated testing was a necessary limitation of this study's strategy, since it was unknown whether the effect of the 20° inboard lateral lean would be masked by the expected differences among PMHS.

5.4. Conclusion

The goal of this thesis was to evaluate the effect of an out-of-position posture on restraint performance. In Chapter 2, a steering-induced 20° inboard lateral lean posture was identified in volunteer tests, and three PMHS were each tested in a neutral posture and in the inboard-leaning posture in 30 km/h frontal crash tests. In Chapter 3, it was found that the posture-induced increased length of the shoulder-to-D-ring seatbelt segment (131 mm ± 26 mm increase) and increased initial angle between this segment and the crash acceleration vector (14° ± 3° increase) caused the head of the occupant to displace farther forward (59 mm ± 13 mm increase) and to be positioned farther inboard (139 mm ± 14 mm farther inboard) at the time of maximum forward displacement. These changes in occupant motion may increase risk of injury via contact with the vehicle interior. In Chapter 4, it was further found that the change in initial posture and subsequent motion resulted in a tradeoff in the shoulder-belt forces: the maximum upper shoulder-belt force decreased (0.37 kN ± 0.32 kN decrease) and the maximum lower shoulder-belt force increased (0.57 kN ± 0.36 kN increase). These relatively small changes in restraint forces suggest that countermeasures deployed after the occupant is already out of position may not be as effective as countermeasures deployed to keep the occupant in position. Therefore, pre-crash countermeasures to maintain occupant position should be sought, and their benefits—or any counter-indications—should be evaluated.

References

Adomeit D, Heger A (1975). Motion sequence criteria and design proposals for restraint devices in order to avoid unfavorable biomechanic conditions and submarining. Stapp Car Crash Journal 19:139-65.

Arbogast KB, Balasubramanian S, Seacrist T, Maltese MR, Garcia-Espana JF, Hopely T, Constans E, Lopez-Valdes FJ, Kent RW, Tanji H, Higuchi K (2009). Comparison of kinematic response of the head and spine for children and adults in low-speed frontal sled tests. Stapp Car Crash Journal 53:329-372.

Arbogast KB, Mathews EA, Seacrist T, Maltese MR, Hammond R, Balasubramanian S, Kent RW, Tanji H, St. Lawrence S, Higuchi K (2012). The effect of pretensioning and age on torso rollout in restrained human volunteers in far-side lateral and oblique loading. Stapp Car Crash Journal 56:443-467.

Ash JH, Lessley DJ, Forman JL, Zhang Q, Shaw CG, Crandall JR (2012). Whole-body kinematics: Response corridors for restrained PMHS in frontal impacts. International Research Council on the Biomechanics of Injury:142-154.

ASTM International (2018). ASTM F2291-18 Standard practice for design of amusement rides and devices.

Augenstein J, Perdeck E, Stratton J, Digges K, Bahouth G (2003). Characteristics of crashes that increase the risk of serious injuries. 47th Annual Proceedings, Association for the Advancement of Automotive Medicine.

Bacon DGC (1989). The effect of restraint design and seat position on the crash trajectory of the Hybrid III dummy. Society of Automotive Engineers 890652.

Benson BR, Smith GC, Kent RW, Monson CR (1996). Effect of seat stiffness in out-of-position occupant response in rear-end collisions. Society of Automotive Engineers 962434.

Bohman K, Arbogast KB, Bostrom O (2011a). Head injury causation scenarios for belted, rear-seated children in frontal impacts. Traffic Injury Prevention 12(1): 62-70.

Bohman K, Stockman I, Jakobsson L, Osvalder A-L, Bostrom O, Arbogast KB (2011b). Kinematics and shoulder belt position of child rear seat passengers during vehicle maneuvers. 55th Annual Proceedings, Association for the Advancement of Automotive Medicine.

Bose D, Crandall J, Untaroiu C, and Maslen E (2008). Influence of pre-collision occupant properties on the injury response during frontal collisions. International Research Council on the Biomechanics of Injury:135-147.

Bostrom O, Haland Y (2005). Benefits of a 3+2-point belt system and an inboard torso side support in frontal, far-side and rollover crashes. International Journal of Vehicle Safety 1:181-199.

Carlsson S, Davidsson J (2011). Volunteer occupant kinematics during driver initiated and autonomous braking when driving in real traffic environments. International Research Council on the Biomechanics of Injury:125-136.

Cavanaugh JM, Jepsen K, King AI (1988). Quasi-static frontal loading of the thorax of human cadavers and the Hybrid III dummy. 16th Annual International Workshop on Human Subjects for Biomechanical Research.

Center for Disease Control and Prevention (2015). Web-based Injury Statistics Query and Reporting System (WISQARS). https://www.cdc.gov/injury/wisqars/index.html

Cesari D, Ramet M, Bloch J (1981). Influence of arm position on thoracic injuries in side impact. Stapp Car Crash Journal 25:270-297.

Crandall JR, Duma SM, Bass CR, Pilkey WD, Kuppa SM, Khaewpong N, Eppinger R (1999). Thoracic response and trauma in air bag deployment tests with out-of-position small female surrogates. Journal of Crash Prevention and Injury Control 1(2):101-112.

Crandall J, Kent R, Patrie J, Fertile J, Martin P (2000). Rib fracture patterns and radiologic detection: A restraint-based comparison. AAAM 44:235-259.

Crandall JR, Bose D, Forman J, Untaroiu CD, Arregui-Dalmases C, Shaw CG, Kerrigan, JR (2011). Human surrogates for injury biomechanics research. Clinical Anatomy 24:362-371.

Ejima S, Ito D, Satou F, Mikami K, Ono K, Kaneoka K, Shiina I (2012). Effects of pre-impact swerving/steering on physical motion of the volunteer in the low-speed side-impact sled test. International Research Council on the Biomechanics of Injury: 352-366.

Eppinger RH, Marcus JH, Morgan RM (1984). Development of dummy and injury index for NHTSA's thoracic side impact protection research program. SAE Paper 840885.

Flannagan CA, Rupp JD (2009). Comparison of distributions of key predictor variabiles in CIREN and NASS-CDS cases meeting CIREN inclusion criteria. Traffic Injury Prevention 10(5):451-457.

Forman J, Lessley D, Kent R, Bostrom O, Pipkorn B (2006a). Whole-body kinematic and dynamic response of restrained PMHS in frontal sled tests. Stapp Car Crash Journal 50:299-336.

Forman J, Lessley D, Shaw CG, Evans J, Kent R, Rouhana SW, Prasad P (2006b). Thoracic response of belted PMHS, the Hybrid III, and the THOR-NT mid-size male surrogates in low speed, frontal crashes. Stapp Car Crash Journal 50:191-215

Forman J, Michaelson J, Kent R, Kuppa S, Bostrom O (2008). Occupant restraint in the rear seat: ATD response to standard and pre-tensioning, force-limiting belt restraints. 52nd AAAM 141-154.

Forman J, Lopez-Valdes FJ, Lessley D, Kindig M, Kent R, and Bostrom O (2009a). The effect of obesity on the restraint of automobile occupants. 53rd Annual Proceedings, Association for the Advancement of Automotive Medicine:25-40.

Forman J, Lopez-Valdes FJ, Lessley D, Kindig M, Kent R, Ridella S, Bostrom O (2009b). Rear seat occupant safety: An investigation of a progressive force-limiting, pretensioning 3-point belt system using adult PMHS in frontal sled tests. Stapp Car Crash Journal 53:49-74.

Forman JL, Lopez-Valdes F, Lessley DJ, Riley P, Sochor M, Heltzel S, Ash J, Perz R, Kent RW, Seacrist T, Arbogast KB, Tanji H, Higuchi K (2013). Occupant kinematics and shoulder belt retention in far-side lateral and oblique collisions: A parametric study. Stapp Car Crash Journal 57:343-85.

Ghaffari G, Brolin K, Brase D, Pipkorn B, Svanberg B, Jakobsson L, Davidsson J (2018). Passenger kinematics in lane change and lane change with braking manoeuvres using two belt configurations: standard and reversible pre-pretensioner. International Research Council on the Biomechanics of Injury: 493-511.

Graci V, Douglas EC, Seacrist T, Kerrigan J, Mansfield J, Bolte J, Sherony R, Hallman JJ, Arbogast KB (2018). Effect of age on kinematics during pre-crash vehicle manoeuvres with sustained lateral acceleration. International Research Council on the Biomechanics of Injury: 524-535.

Haight S, Samaha RR, Biss D (2013). Analysis of seat belt positioning in recent NCAP crash tests. SAE International Journal of Transportation Safety 1(1):16-24.

Hartka TR, Carr HM, Smith BR, Melmer M, Sochor MR (2017). Does obesity affect the position of seat belt loading in occupants involved in real-world motor vehicle collisions? Traffic Injury Prevention 19(sup1):S70-S75.

Hault-Dubrulle A, Robache F, Drazetic P, Guillemot H, Morvan H (2011). Determination of pre-impact occupant postures and analysis of consequences on injury outcome—Part II: Biomechanical study. Accident Analysis and Prevention 43:75-81.

Holt C, Seacrist T, Arbogast KB, Balasubramanian S, Kerrigan J, Kent R (2017). Evaluating occupant kinematic responses in low acceleration time-extended evasive swerving events. Ohio State University Injury Biomechanics Symposium.

Holt C, Douglas E, Graci C, Seacrist T, Kerrigan J, Kent R, Balasubramanian S, Arbogast K (2018). Effect of countermeasures on adult kinematics during pre-crash evasive swerving. International Research Council on the Biomechanics of Injury: 536-548.

Horsch JD, Culver CC (1979). A study of driver interactions with an inflating air cushion. Society of Automotive Engineers 791029.

Horsch J, Lau I, Andrzejak D, Viano D, Melvin J, Pearson J, Cok D, Miller G (1990). Assessment of air bag deployment loads. Society of Automotive Engineers 902324.

Huber P, Kirschbichler S, Pruggler A, Steidl T (2014). Three-dimensional occupant kinematics during frontal, lateral and combined emergency maneuvers. International Research Council on the Biomechanics of Injury:668-669.

Huber P, Kirschbichler S, Prüggler A, Steidl T (2015). Passenger kinematics in braking, lane change and oblique driving maneuvers. International Research Council on the Biomechanics of Injury:783-802.

Jones MLH, Miller CS, Ebert S, Bonifas S, Park BKD, Reed MP, Hallman J, Sherony R (2017). Tracking occupant head movements during braking events.

Kallieris D, Schmidt G, Schuler F (1982). Thoraxbelastung und Verletzungsmuster bei der Schragkollision. Beitrage zur gerichtichen Medizin 40:275-281.

Kallieris D, Schmidt G (1990). Neck response and injury assessment using cadavers and the US-SID for far-side lateral impacts of rear seat occupants with inboard-anchored shoulder belt. Society of Automotive Engineers Technical Paper 902313.

Kemper AR, McNally C, Kennedy EA, Manoogian SJ, Duma SM (2008). The influence of arm position on thoracic response in side impacts. Stapp Car Crash Journal 52:379-420.

Kent RW, Crandall JR, Bolton JR, Duma SM (2000). Driver and right-front passenger restraint system interaction, injury potential, and thoracic injury prevention. 44th Annual Proceedings, Association for the Advancement of Automotive Medicine:261-282.

Kent R, Shaw G, Lessley D, Crandall J, Kallieris D, Svensson M (2003). Comparison of belted Hybrid III, THOR, and cadaver thoracic responses in oblique frontal and full frontal sled tests. Society of Automotive Engineers 2003-01-0160.

Kent R, Lessley D, Sherwood C (2004). Thoracic response to dynamic, non-impact loading from a hub, distributed belt, diagonal belt, and double diagonal belts. Stapp Car Crash Journal 48:495-519.

Kent R, Forman J, Parent DP, Kuppa S (2007). Rear seat occupant protection in frontal crashes and its feasibility. Society of Automotive Engineers 07-0386.

Kent R (2008). Frontal thoracic response to dynamic loading: The role of superficial tissues, viscera and the rib cage. International Journal of Crashworthiness 13(3):289-300.

Kent RW, Forman J (2015). Restraint system biomechanics. In: N. Yoganandan et al. (eds), Accidental Injury: Biomechanics and Prevention. Springer Science+Business Media New York, NY.

Kirschbichler S, Huber P, Prüggler A, Steidl T, Sinz W, Mayer C, D'Addetta GA (2014). Factors influencing occupant kinematics during barking and lane change maneuvers in a passenger vehicle. International Research Council on the Biomechanics of Injury:614-625.

Kitagawa Y, Hayashi S, Yamada K, Gotoh M (2017). Occupant kinematics in simulated autonomous driving vehicle collisions: Influence of seating position, direction and angle. Stapp Car Crash Journal 61:101-155.

Kumbfbeck M, Oertel D, Pilatus K (1999). Occupant kinematics during emergency braking: An investigation with regard to the out of position issue for passengers. IRCOBI.

Langwieder K (1999). Characteristics of car accidents in the pre-crash phase. Society of Automotive Engineers of Japan 9-12.

Lessley D, Shaw G, Parent D, Arregui-Dalmases C, Kindig M, Riley P, Purtsezov S, Sochor M, Gochenour T, Bolton J, Subit D, Crandall J, Takayama S, Ono Koshiro, Kamiji K, Yasuki T (2010). Whole-body response to pure lateral impact. Stapp Car Crash Journal 54:289-336.

Lin H, Gepner B, Wu T, Forman J, Panzer M (2018). Effect of seatback recline on occupant model response in frontal crashes. IRCOBI 386-387.

Lopez-Valdes FJ, Lau A, Lamp J, Riley P, Lessley DJ, Damon A, Kindig M, Kent R, Balasubramanian S, Seacrist T, Maltese MR, Arbogast KB, Higuchi K, Tanji H (2010). Analysis of spinal motion and loads during frontal impacts. Comparison between PMHS and ATD. 54th Annual Proceedings, Association for the Advancement of Automotive Medicine:61-78.

Lopez-Valdes FJ, Juste-Lorente O, Maza-Frechin M, Pipkorn B, Sunnevang C, Lorente A, Aso-Vizan A, Davidsson J (2016). Analysis of occupant kinematics and dynamics in nearside oblique impacts. Traffic Injury Prevention 17(sup1):S86-S92.

Luet C, Trosseile X, Drazétic P, Potier P, Vallancien G (2012). Kinematics and dynamics of the pelvis in the process of submarining using PMHS sled tests. Stapp Car Crash Journal 56:411-442.

Mackay M (1994). Smart seat belts – Some population considerations applied to intelligent restraint systems. Society of Automotive Engineers 940531.

Matsuda T, Yamada K, Hayashi S, Kitagawa Y (2018). Simulation of occupant postural changes due to evasive manoeuvres and injury predictions in vehicle frontal and side collisions. IRCOBI:512-523.

Montesinos-Acosta S, Ash JH, Lessley DJ, Shaw CG, Heltzel SB, Crandall JR (2016). Comparison of whole body response in oblique and full frontal sled tests. IRCOBI:740-754.

Muggenthaler H, Adamec J, Praxl N, Schonpflug M (2005). The influence of muscle activity on occupant kinematics. IRCOBI 313-323.

National Highway Traffic Safety Administration (1999). Laboratory procedure for FMVSS 208: Occupant Crash Protection, TP-208-09.

National Highway Traffic Safety Administration (2012). Laboratory test procedure for FMVSS No. 214, dynamic side impact protection – Moving deformable barrier test requirements using advanced test dummies, TP-214d-09.

National Highway Traffic Safety Administration (2015). Final report of New Car Assessment Program Side Impact MDB testing of 2015 Toyota Sienna L Minivan.

Nie B, Poulard D, Subit D, Donlon J-P, Forman JL, Kent RW (2016). Experimental investigation of the effect of occupant characteristics on contemporary seat belt payout behavior in frontal impacts. Traffic Injury Prediction 17(4):374-380.

Ólafsdóttir JM, Östh JKH, Davidsson J, Brolin KB (2013). Passenger kinematics and muscle responses in autonomonous braking events with standard and reversible pre-tensioned restraints. IRCOBI: 602-617.

Östh J, Ólafsdóttir JM, Davidsson J, Brolin K (2013). Driver kinematic and muscle responses in braking events with standard and reversible pre-tensioned restraints: Validation data for human models. Stapp Car Crash Journal 57:1-41.

Parenteau C, Shah M, Steffan H, Hofinger M (2002). Volunteer and dummy head kinematics in low-speed lateral sled tests. Traffic Injury Prevention 3:233-240.

Parenteau, C (2006a). A comparison of volunteers and dummy upper torso kinematics with and without shoulder belt slack in a low speed side/pre-roll environment. Traffic Injury Prevention 7:155-163.

Parenteau, C (2006b). Far-side occupant kinematics in low speed lateral sled. Traffic Injury Prevention 7:164-170.

Patrick LM, Nyquist GW (1972). Airbag effects on the out-of-position child. Society of Automotive Engineers 720442.

Poulard D, Subit D, Donlon J-P, Lessley DJ, Kim T, Park G, Kent RW (2014). The contribution of pre-impact spine posture on human body model response in whole-body side impact. Stapp Car Crash J 58:385-422.

Reed MP, Ebert-Hamilton SM, Rupp JD (2012). Effects of obesity on seat belt fit. Traffic Injury Prevention 13(4):364-372.

Reed MP, Ebert SM (2018). Effects of recline on passenger posture and belt fit. UMTRI.

Ridella SA, Rupp JD, Poland K (2012). Age-related differences in AIS 3+ crash injury risk, types, causation and mechanisms. IRCOBI: 43-60.

Riexinger LE, Gabler HC (2018). A preliminary characterisation of driver manoeuvres in road departure crashes. IRCOBI:484-492.

Rouhana SW, Bedewi PG, Kankanala SV, Prasad P, Zwolinski JJ, Meduvsky AG, Rupp JD, Jeffreys TA, Schneider LW (2003). Biomechanics of 4-point seat belt systems in frontal impacts. Stapp Car Crash Journal 47:367-399.

Rupp JD, Reed MP, Jeffreys TA, Schneider LW (2003). Effects of hip posture on the frontal impact tolerance of the human hip joint. Stapp Car Crash Journal 47:21-33.

Scanlon JM, Kusano KD, Gabler KC (2015). Analysis of driver evasive maneuvering prior to intersection crashes using event data recorders. Traffic Injury Prevention 16(sup2):S182-S189.

Schneider LW, Robbins D, Pflug MA, Snyder RG (1983). Development of anthropometrically based design specifications for an advanced adult anthropomorphic dummy family, Volume 1. University of Michigan Transportation Research Institute UMTRI-83-53-1.

Seacrist T, Kerrigan JR, Holt C, Balasubramanian S, Jordan A, Kent RW, Arbogast KB (2016). A novel methodology for evaluating occupant response in low acceleration time-extended events. IRCOBI:765-767.

Seacrist T, Douglas EC, Huang E, Megariotis J, Prabahar A, Kashem A, Elzarka A, Haber L, MacKinney T, Loeb H (2018). Analysis of near crashes among teen, young adult, and experienced adult drivers using the SHRP2 naturalistic driving study. Traffic Injury Prevention 19(sup1): S89-S96.

Searle JA, Bethell J, Baggaley G (1978). The variation of human tolerance to impact and its effect on the design and testing of automotive impact performance. Society of Automotive Engineers 780885.

Shaw JM, Herriott RG, McFadden JD, Donnelly BR, Bolte JH (2006). Oblique and lateral impact response of the PMHS thorax. Stapp Car Crash Journal 50:147-167.

Shaw G, Lessley D, Evans J, Crandall J, Shin J, Portier P, Paoloni G (2007). Quasi-static and dynamic thoracic loading tests: Cadaveric torsos. International Research Council on the Biomechanics of Injury:325-348.

Shaw G, Parent D, Purtsezov S, Lessley D, Crandall J, Kent R, Guillemot H, Ridella SA, Takhounts E, Martin P (2009). Impact response of restrained PMHS in frontal sled tests: Skeletal deformation patterns under seat belt loading. Stapp Car Crash Journal 53:1-48.

Shaw G, Lessley DJ, Ash JL, Sochor MR, Crandall JR, Luzon-Narro J, Arregui-Dalmases C (2014). Side impact PMHS thoracic response with large-volume air bag. Traffic Injury Prevention 15(1):40-47.

Shaw G, Lessley D, Ash J, Acosta S, Heltzel S, Riley P, Kim T, Crandall J (2018). Pelvic restraint cushion test evaluation of pelvic forward motion. Traffic Injury Prevention 19(3):25-255.

Society of Automotive Engineers (2007). Surface vehicle recommended practice SAE J211: Instrumentation for impact test—Part 1—Electronic instrumentation.

Stalnaker RL, Tarrière C, Fayon A, Walfisch G, Balthazard M, Masset J, Got C, Patel A (1979). Modification of Part 572 dummy for lateral impact according to biomechanical data. Society of Automotive Engineers 791031.

Stigson H, Kullgren A, Rosen E (2012). Injury risk functions in frontal impacts using data from crash pulse recorders. 56th Annual Proceedings, Association for the Advancement of Automotive Medicine:267-276.

Strother CE, James MB, Gordon JJ (1994). Response of out-of-position dummies in rear impact. Society of Automotive Engineers 941055.

Subit D, Duprey S, Lau S, Guillemot H, Lessley D, Kent R (2010). Response of the human torso to lateral and oblique constant-velocity impacts. 54th Annual Proceedings, Association for the Advancement of Automotive Medicine.

Talmor D, Legedza ATR, Nirula R (2010). Injury thresholds after motor vehicle crash—Important factors for patient triage and vehicle design. Accident Analysis and Prevention 42: 672-675

Thomas C, Perron T, Le Coz J-Y, Aguade V (1996). What happens on the road before fatal car crashes? 40th Annual Proceedings, Association for the Advancement of Automotive Medicine.

Tornvall FV, Svensson MY, Davidsson J, Flogard A, Kallieris D, Haland Y (2005). Frontal impact dummy kinematics in oblique frontal collisions: Evaluation against post mortem human subject test data. Traffic Injury Prevention 6:340-350.

Uriot J, Potier P, Baudrit P, Trosseille X, Petit P, Richard O, Compigne S, Masuda M, Douard R (2015). Reference PMHS sled tests to assess submarining. Stapp Car Crash Journal 59:203-223.

van Rooij L, Pauwelussen J, Op den Camp O, Janssen R (2013a). Driver head displacement during (automatic) vehicle braking tests with varying levels of distraction. Society of Automotive Engineers 19-0403.

van Rooij L, Elrofai H, Philippens MMGM, Daanen HAM (2013b). Volunteer kinematics and reaction in lateral emergency maneuver tests. Stapp Car Crash Journal 57:313-342.

Vezin P, Buyere-Garnier K, Bermond F, Verriest JP (2002). Comparison of Hybrid III, Thor-α and PMHS response in frontal sled tests. Stapp Car Crash Journal 45:1-26.

Viano DC, Parenteau C (2003). Case study of vehicle maneuvers leading to rollovers: Need for a vehicle test simulating off-road excursions, recovery and handling. Society of Automotive Engineers 2003-01-0169.

Viano DC, Parenteau CS, Burnett R, Prasad P (2018a). Occupant responses in conventional and ABTS seats in high-speed rear sled tests. Traffic Injury Prevention 19(1):54-59.

Viano DC, Parenteau CS, Burnett R (2018b). Thoracic and lumbar spine responses in high-speed rear sled tests. Traffic Injury Prevention 19(5):523-528.

World Health Organization (2015). Global status report on road safety 2015.

Zaseck LW, Chen C, Hu J, Reed MP, Rupp J (2018). The influence of pre-existing rib fractures on Global Human Body Models Consortium thorax response in frontal and oblique impact. Journal of Biomechanics 69:54-63.

Zhang L, Chen L, Vertiz A, Balci R (2004). Survery of front passenger posture usage in passenger vehicles. Society of Automotive Engineers 2004-01-0845.

Appendix A. PMHS anthropometry

Table 14. Subject information and supine anthropometry.

General Information			
Cadaver ID No.	778	816	899
Age at Time of Death	19	37	51
Sex	Male	Male	Male
Cause of Death	Suicide by Helium	Alcoholic Cirrhosis	Unknown
Preservation Method	Freezing	Freezing	Freezing
Immunology			
HIV Assay	Negative	Negative	Negative
Hepatitis B	Negative	Negative	Negative
Anthropometry (cm unless otherwise noted)			
Body Mass (kg)	72	73	82
Stature	182	178	175
Vertex-to-Symphision Length	99	103	92
Top-of-Head to Trochanterion	92	92	87
Shoulder (Acromial) Height	159	156	154
Waist Height (at Umbilicus)	109	106	99
Waist Depth (at umbilicus)	16.5	21.4	22.5
Waist Breadth	29.2	32.0	38
Shoulder Breadth (Biacromial)	42.3	38	41.3
Chest Breadth – 4th Rib	31.7	35.3	39
Chest Breadth – 8th Rib	29.2	34.2	38
Chest Depth – 4th Rib	15.0	20.2	23.2
Chest Depth – 8th Rib	15.6	23	25.5
Hip Breadth	27.0	32.2	37
Buttock Depth	15.5	19.1	18.7
Shoulder-to-Elbow	39	37	37
Forearm-to-Hand	not measured: hands amputated at forearm		
Tibiale Height	50	46	48
Ankle Height (Outside)	8	8	9
Foot Breadth	9.3	9.2	8.5
Foot Length	25.5	23	25.5
Head Length	18.3	19.3	18.4
Head Breadth	15.5	15.5	14.5
Head Height	21.7	21.4	22.8
Head Circumference	54.5	56	57
Neck Circumference	38.7	39	54
Chest Circumference – 4th Rib	86.3	95	109
Chest Circumference – 8th Rib	78.0	103	112
Waist Circumference – At Umbilicus	71.2	95	107.5
Waist Circumference – 8cm above Umbilicus	72.3	98	113.5
Waist Circumference – 8 cm below Umbilicus	85.3	91	102
Buttock Circumference	93.9	94	100
Thigh Circumference	51.6	45.5	50
Lower Thigh Circumference	36.2	36	40
Knee Circumference	35.6	37.5	41
Calf Circumference	34.0	30	33
Ankle Circumference	21.8	21	21
Scye (Armpit) Circumference	45.5	42	41
Bicep Circumference	28.9	26	29
Elbow Circumference	27.5	24	32
Forearm Circumference	27.5	24	24.5
Wrist Circumference	not measured: hands amputated at forearm		

Appendix B. Initial position photographs of PMHS.

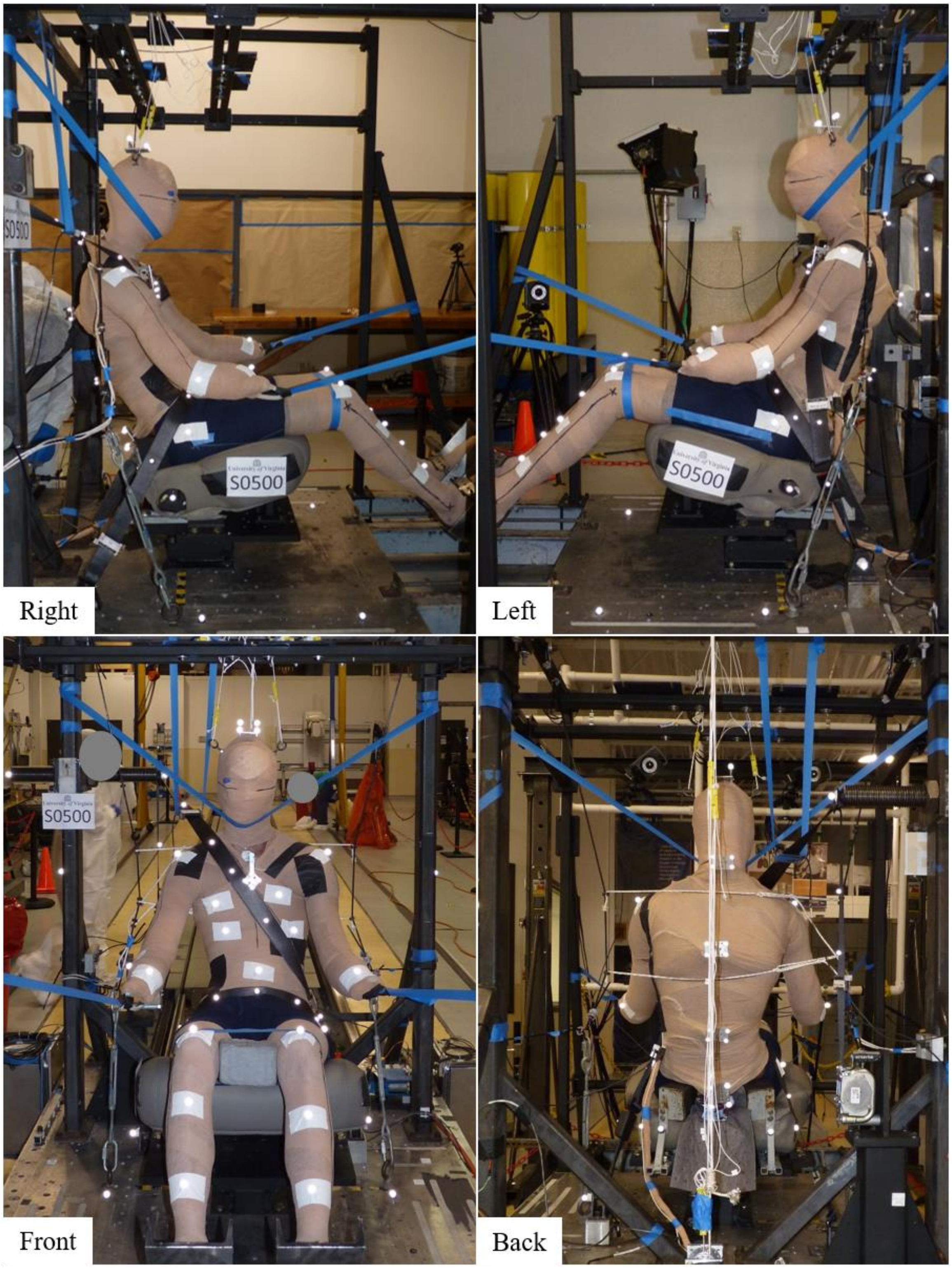

Figure 47. Initial position of PMHS #1 in the Neutral 9 g test.

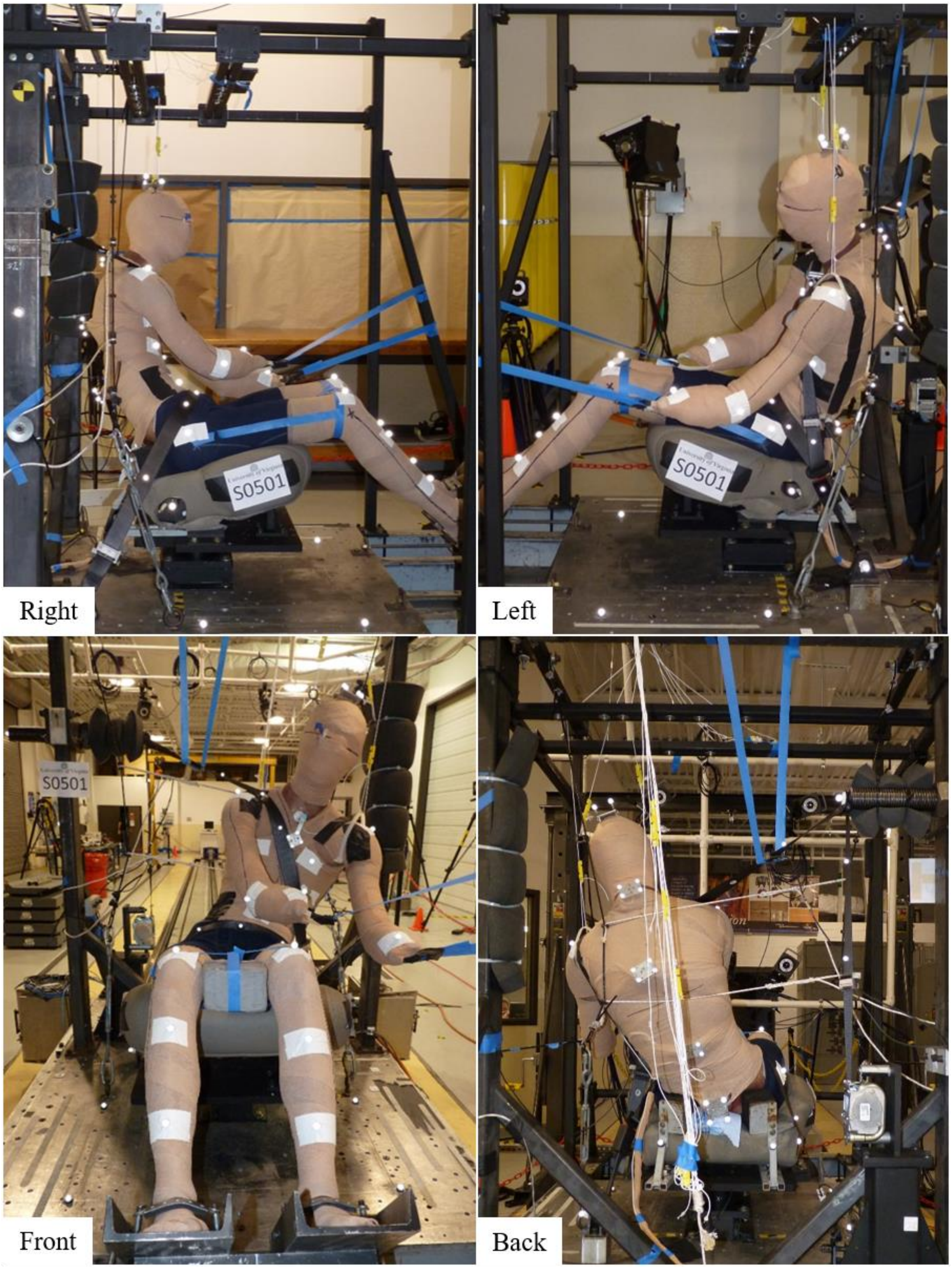

Figure 48. Initial position of PMHS #1 in the Inboard 9 g test.

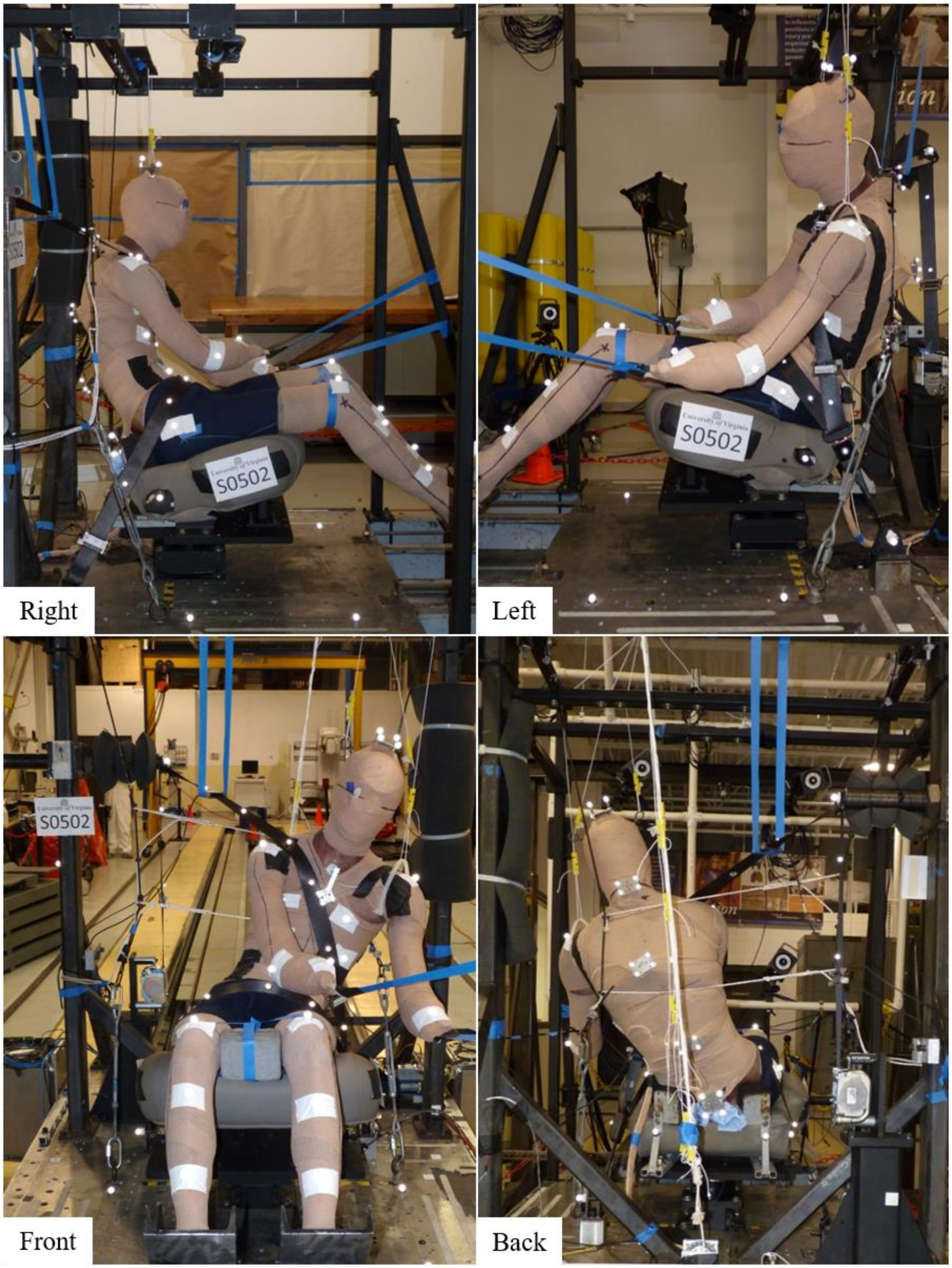

Figure 49. Initial position of PMHS #1 in the Inboard 14 g test.

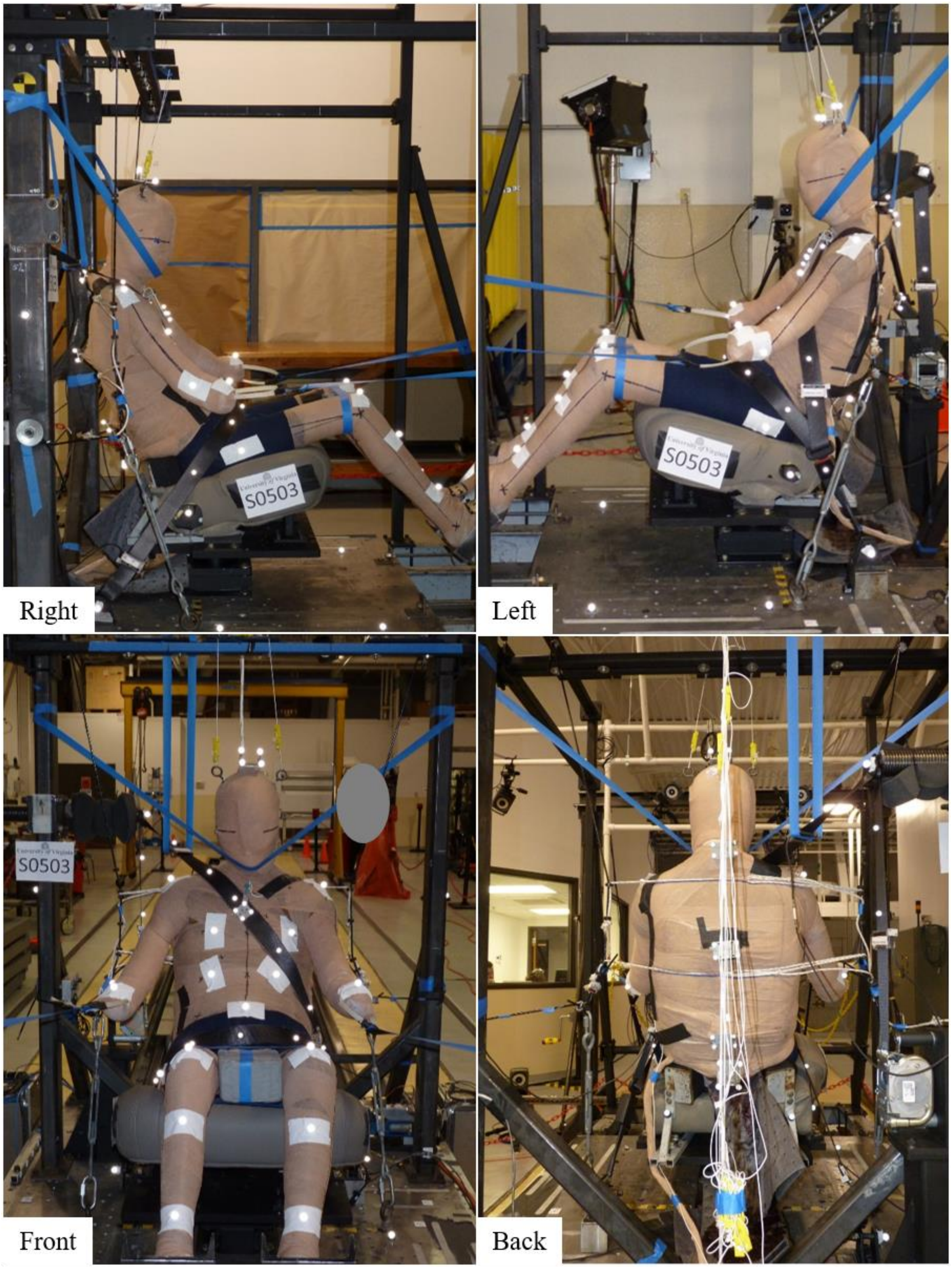

Figure 50. Initial position of PMHS #2 in the Neutral 9 g test.

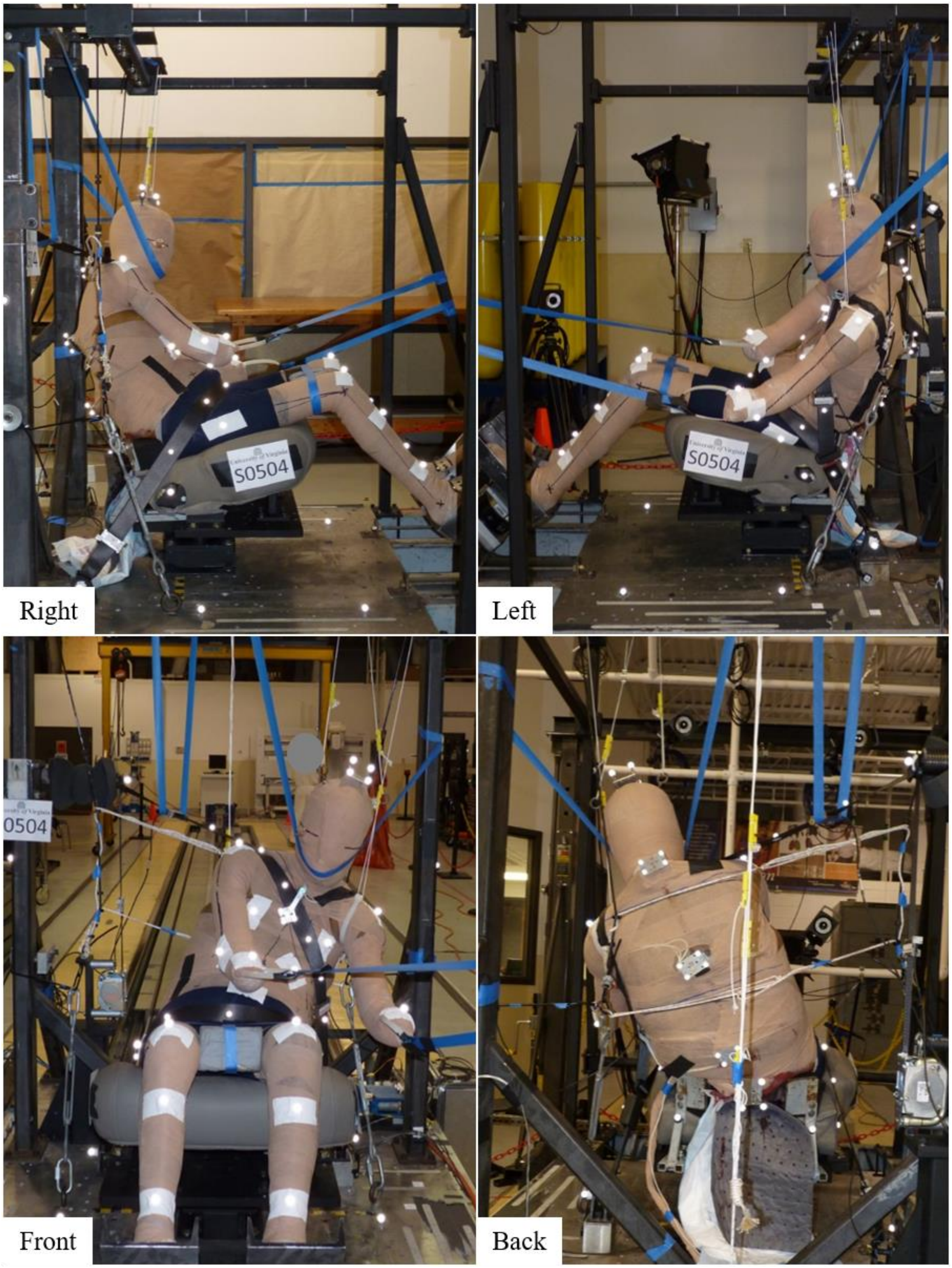

Figure 51. Initial position of PMHS #2 in the Inboard 9 g test.

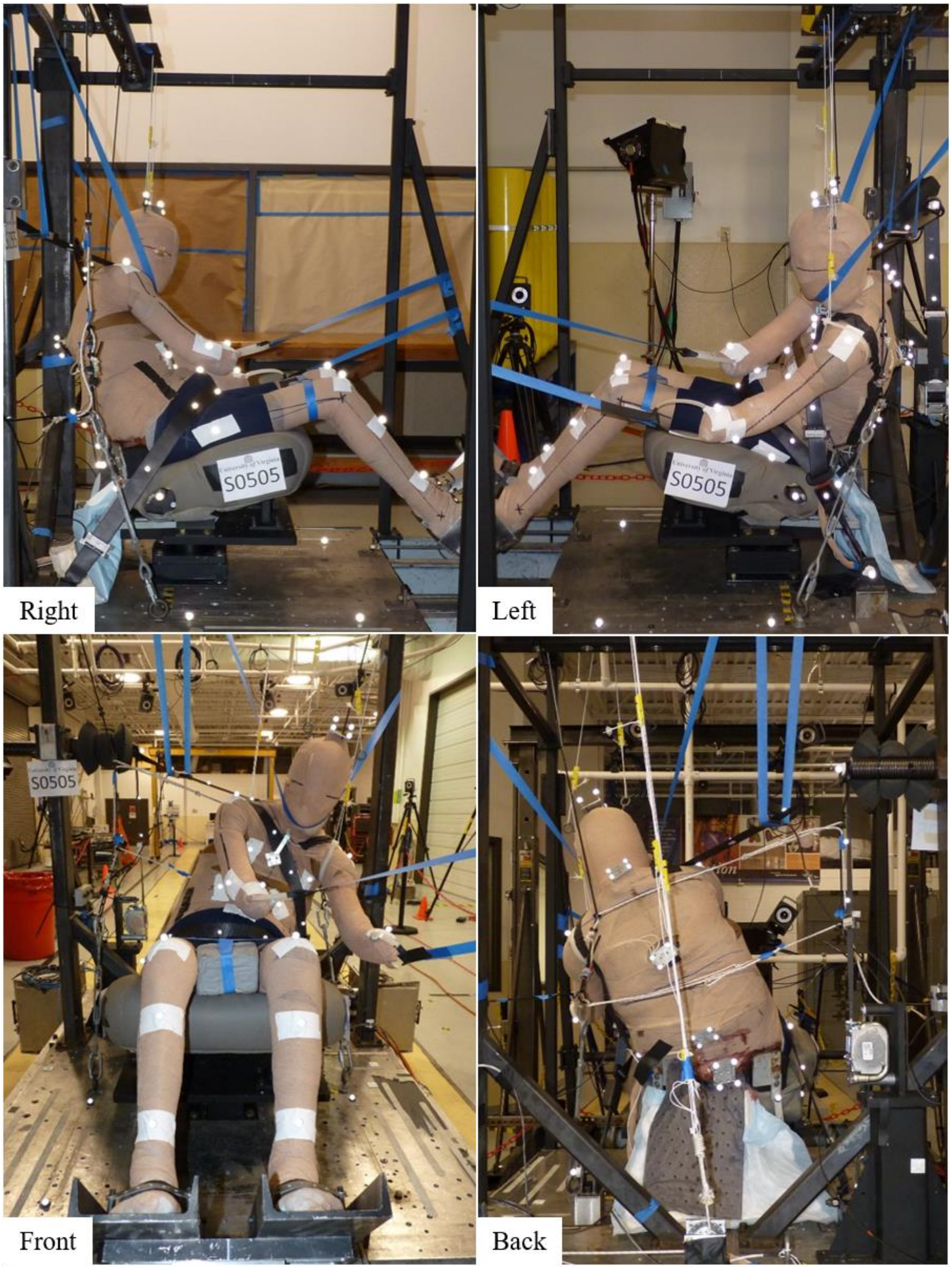

Figure 52. Initial position of PMHS #2 in the Inboard 14 g test.

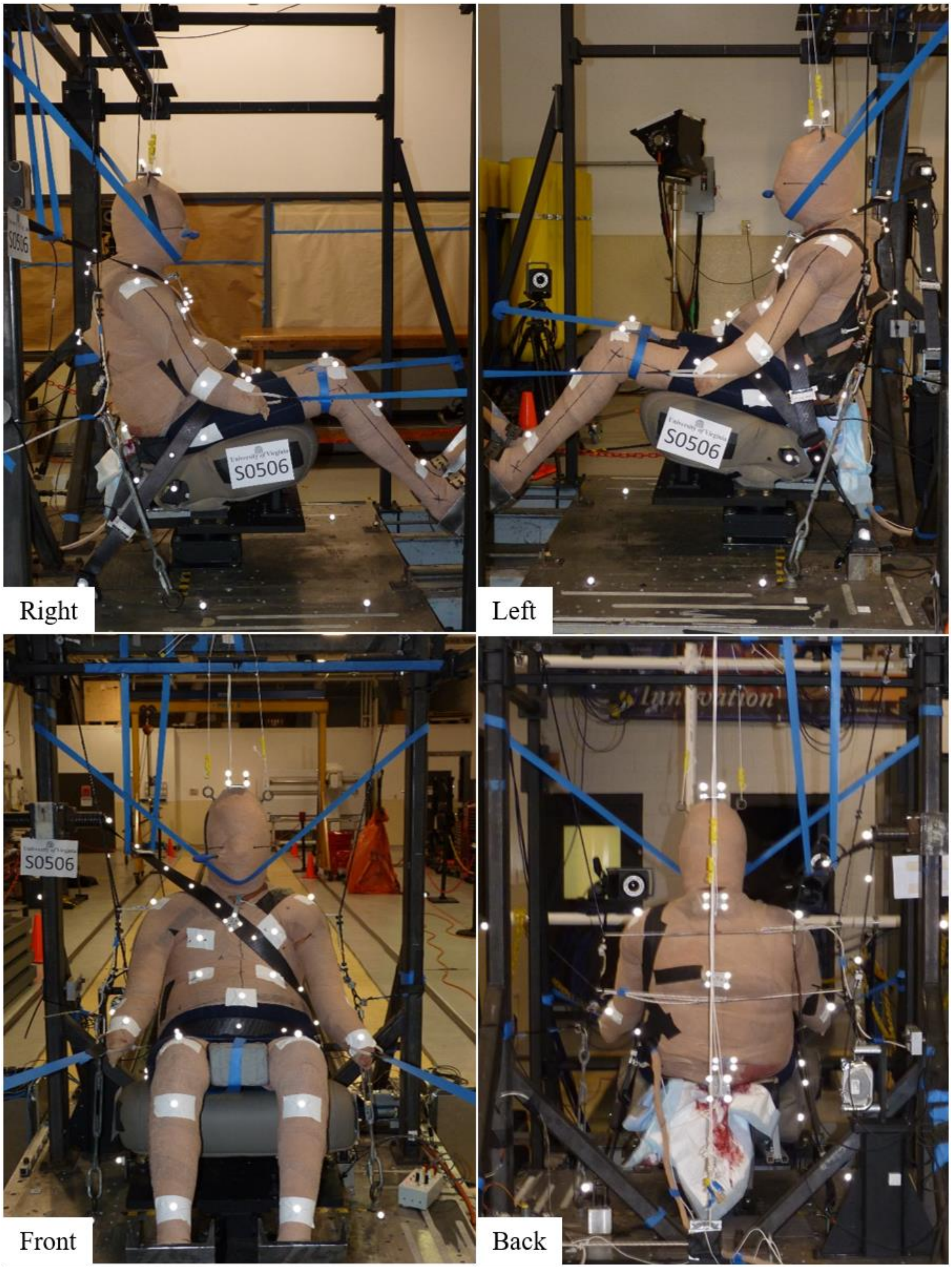

Figure 53. Initial position of PMHS #3 in the Neutral 9 g test.

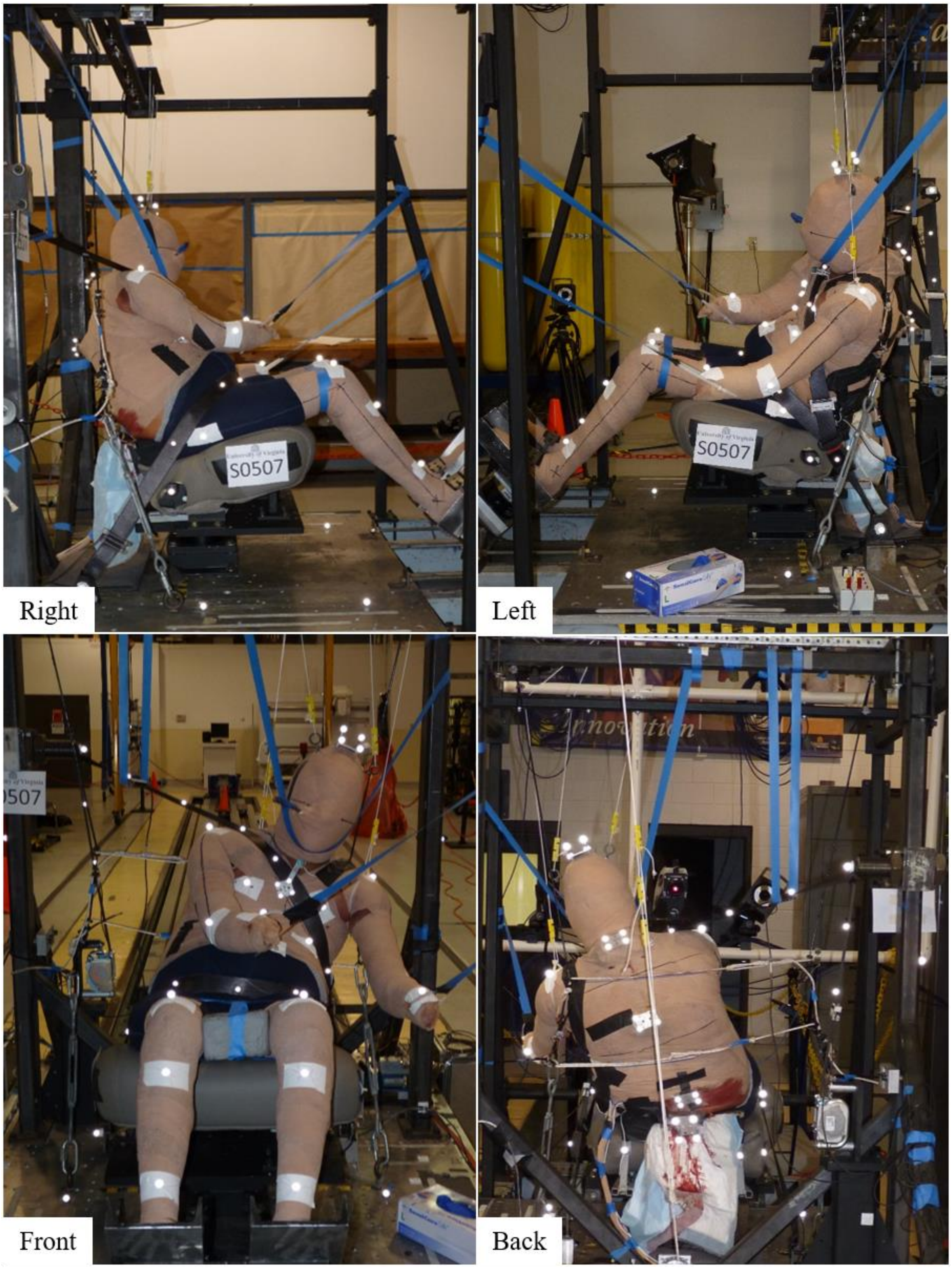

Figure 54. Initial position of PMHS #3 in the Inboard 9 g test.

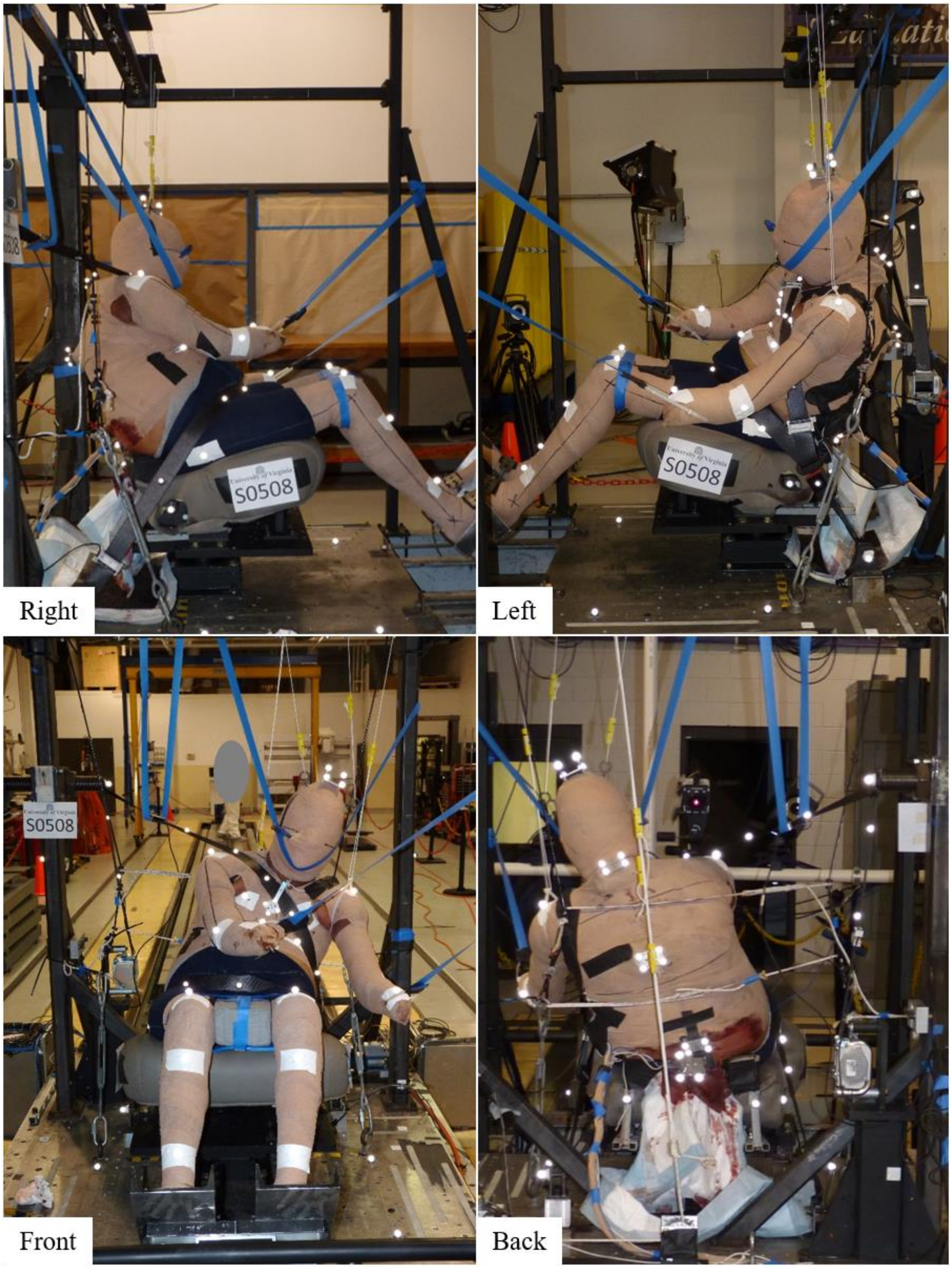

Figure 55. Initial position of PMHS #3 in the Inboard 14 g test.

Appendix C. Definitions of Local Coordinate Systems on Bones

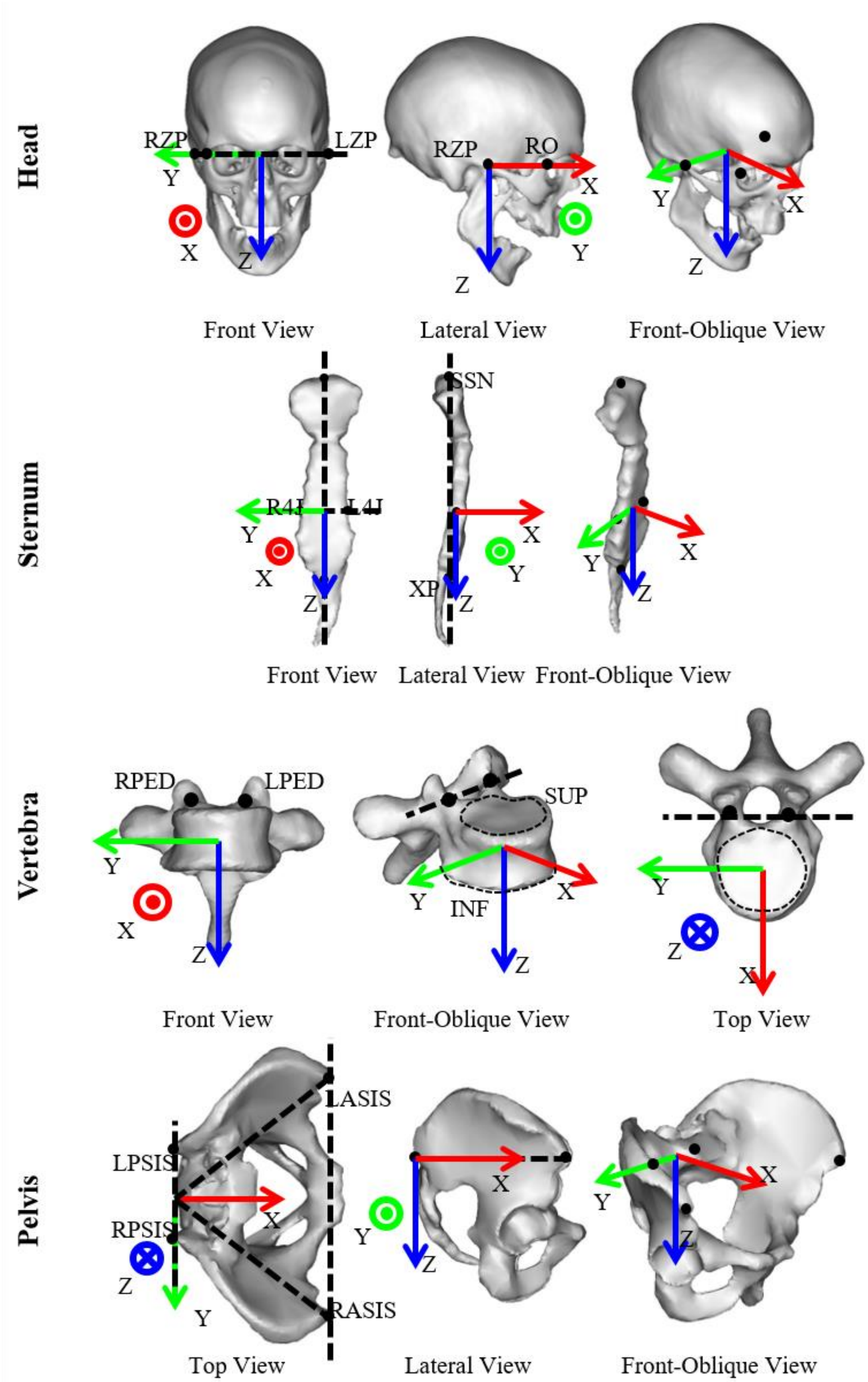

Appendix D. High-speed video frames showing the motion sequences of the PMHS

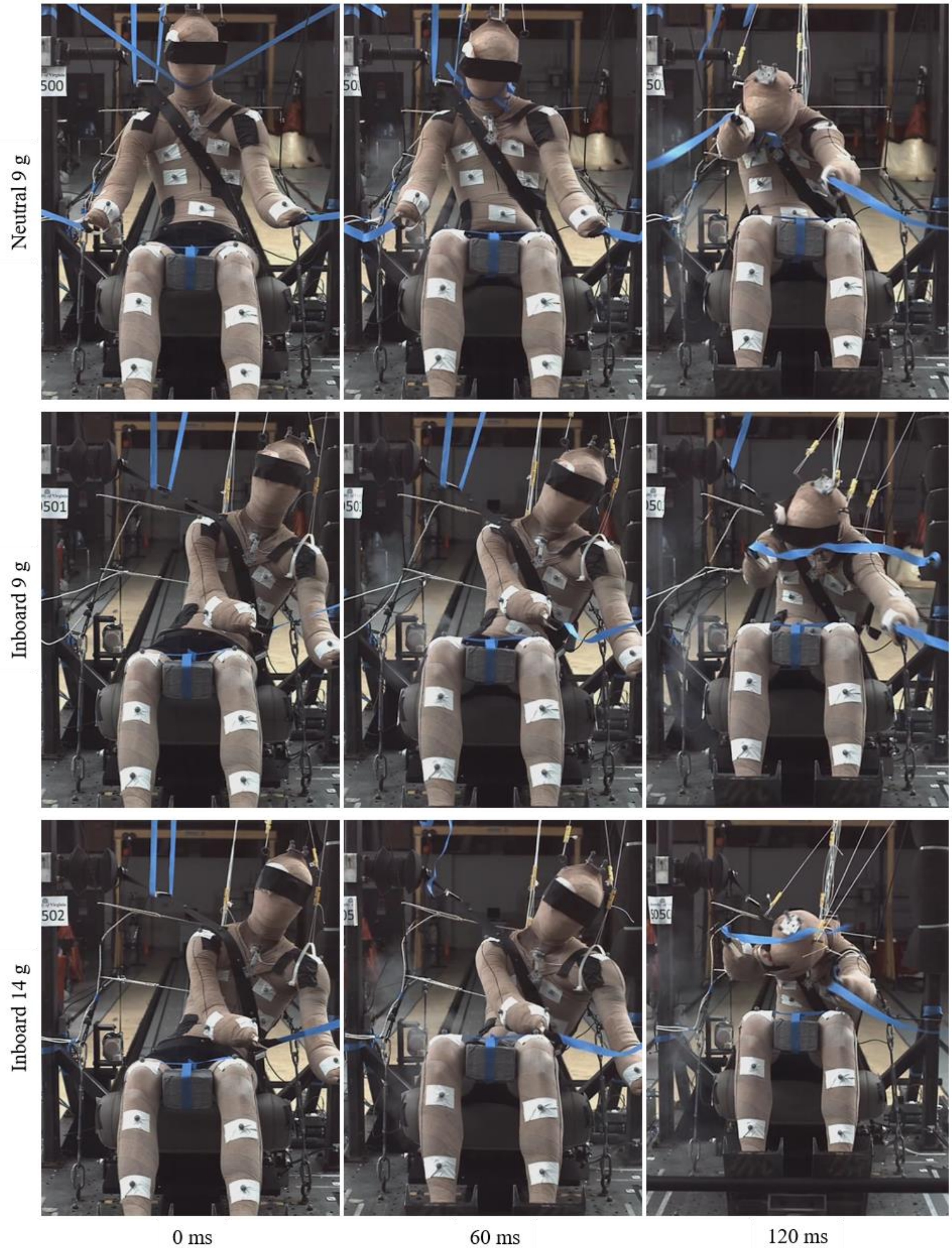

Figure 56. High-speed frontal video frames showing the motion sequences up to the time of maximum forward excursion in the neutral 9 g (top), inboard 9 g (middle), and inboard 14 g (bottom) tests for PMHS #1.

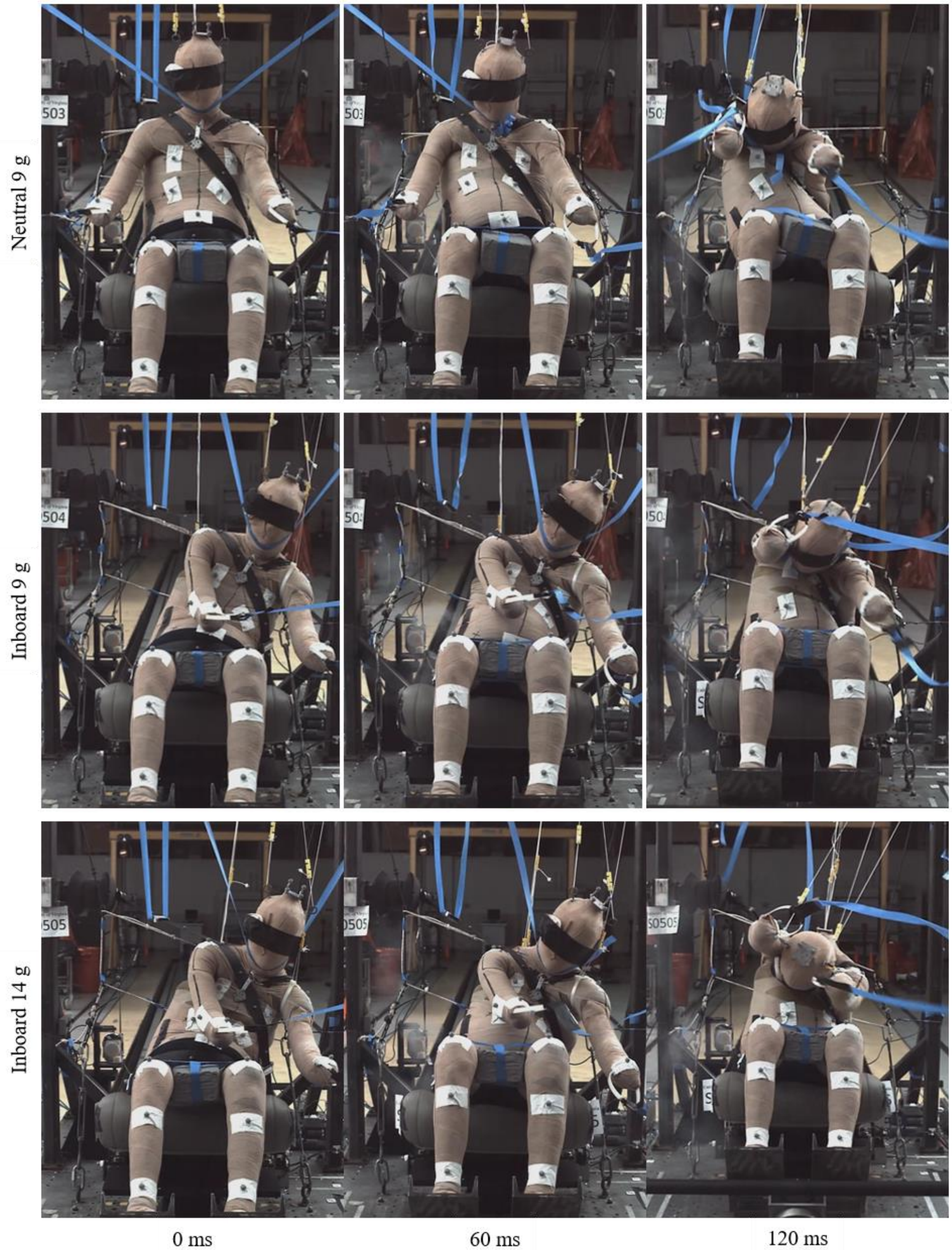

Figure 57. High-speed frontal video frames showing the motion sequences up to the time of maximum forward excursion in the neutral 9 g (top), inboard 9 g (middle), and inboard 14 g (bottom) tests for PMHS #2.

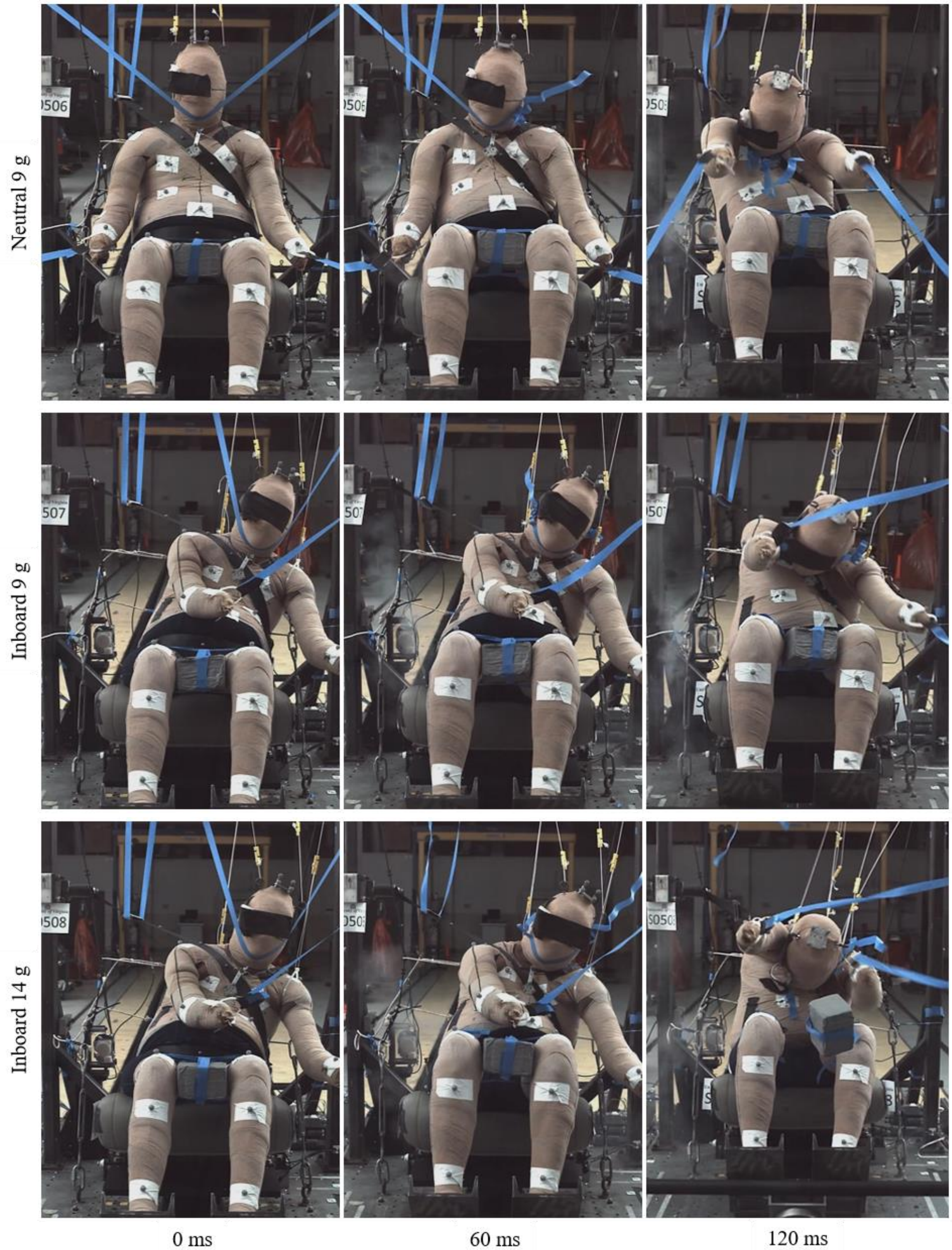

Figure 58. High-speed frontal video frames showing the motion sequences up to the time of maximum forward excursion in the neutral 9 g (top), inboard 9 g (middle), and inboard 14 g (bottom) tests for PMHS #3.

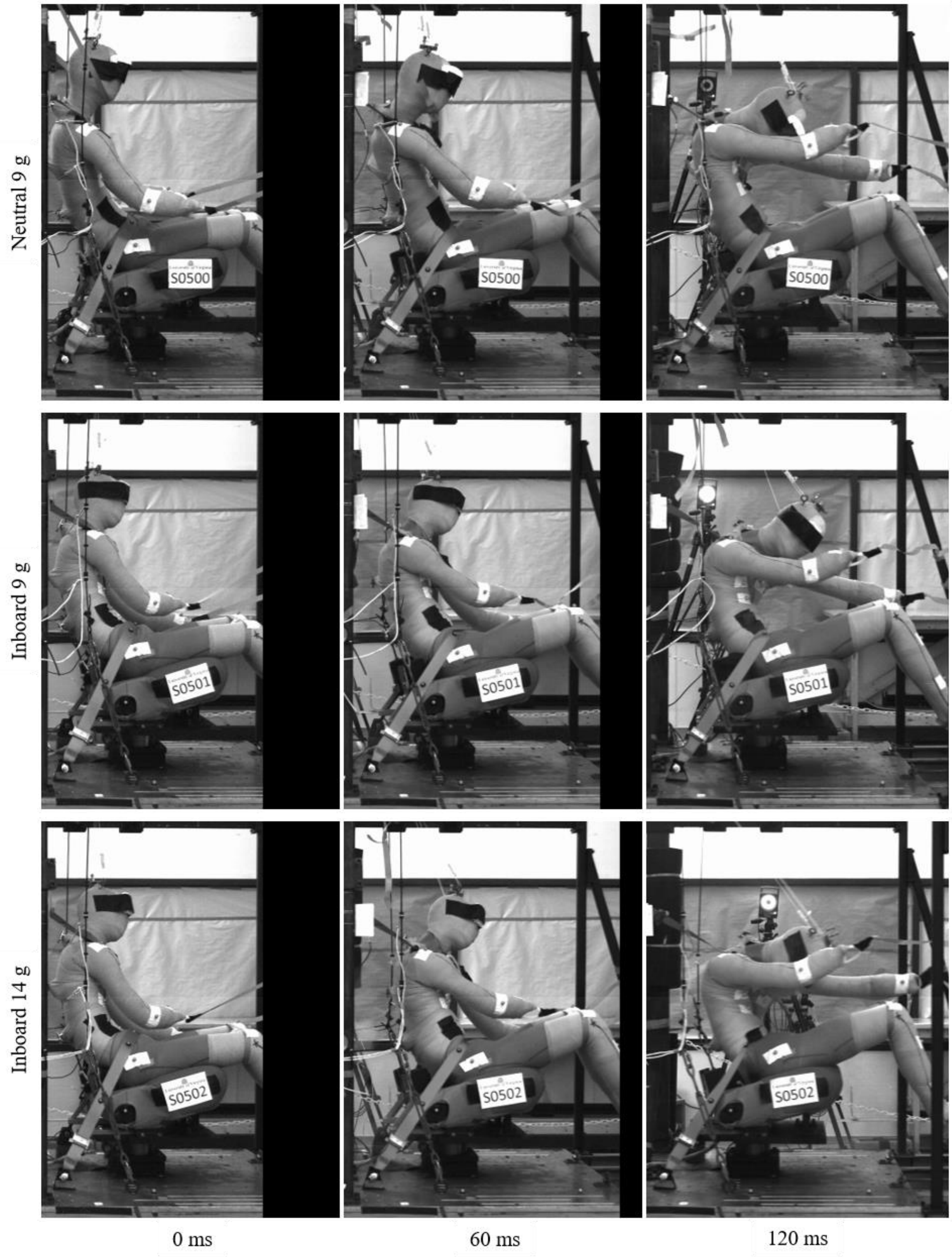

Figure 59. High-speed passenger-side video frames showing the motion sequences up to the time of maximum forward excursion in the neutral 9 g (top), inboard 9 g (middle), and inboard 14 g (bottom) tests for PMHS #1.

Neutral 9 g

Inboard 9 g

Inboard 14 g

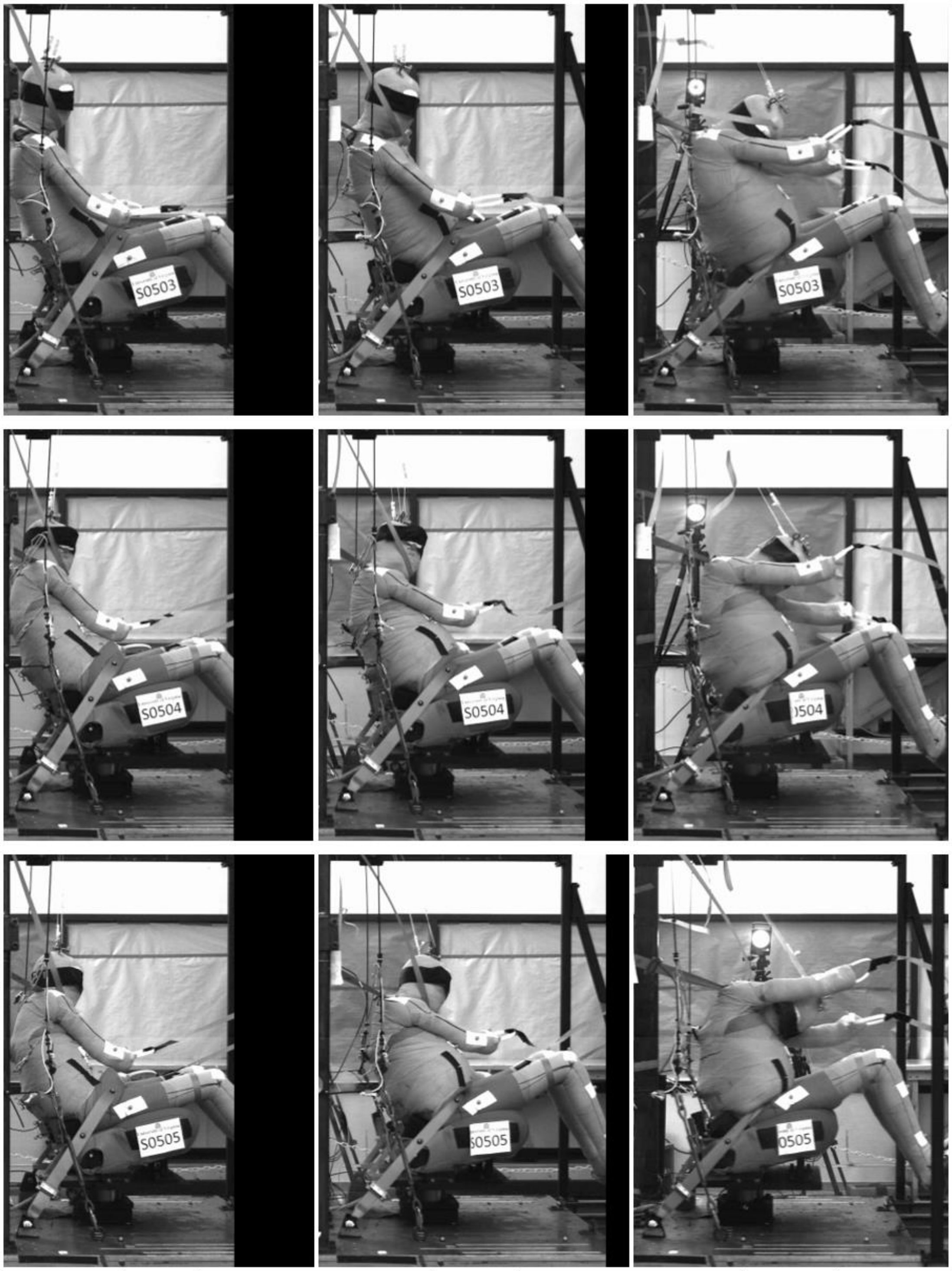

0 ms 60 ms 120 ms

Figure 60. High-speed passenger-side video frames showing the motion sequences up to the time of maximum forward excursion in the neutral 9 g (top), inboard 9 g (middle), and inboard 14 g (bottom) tests for PMHS #2.

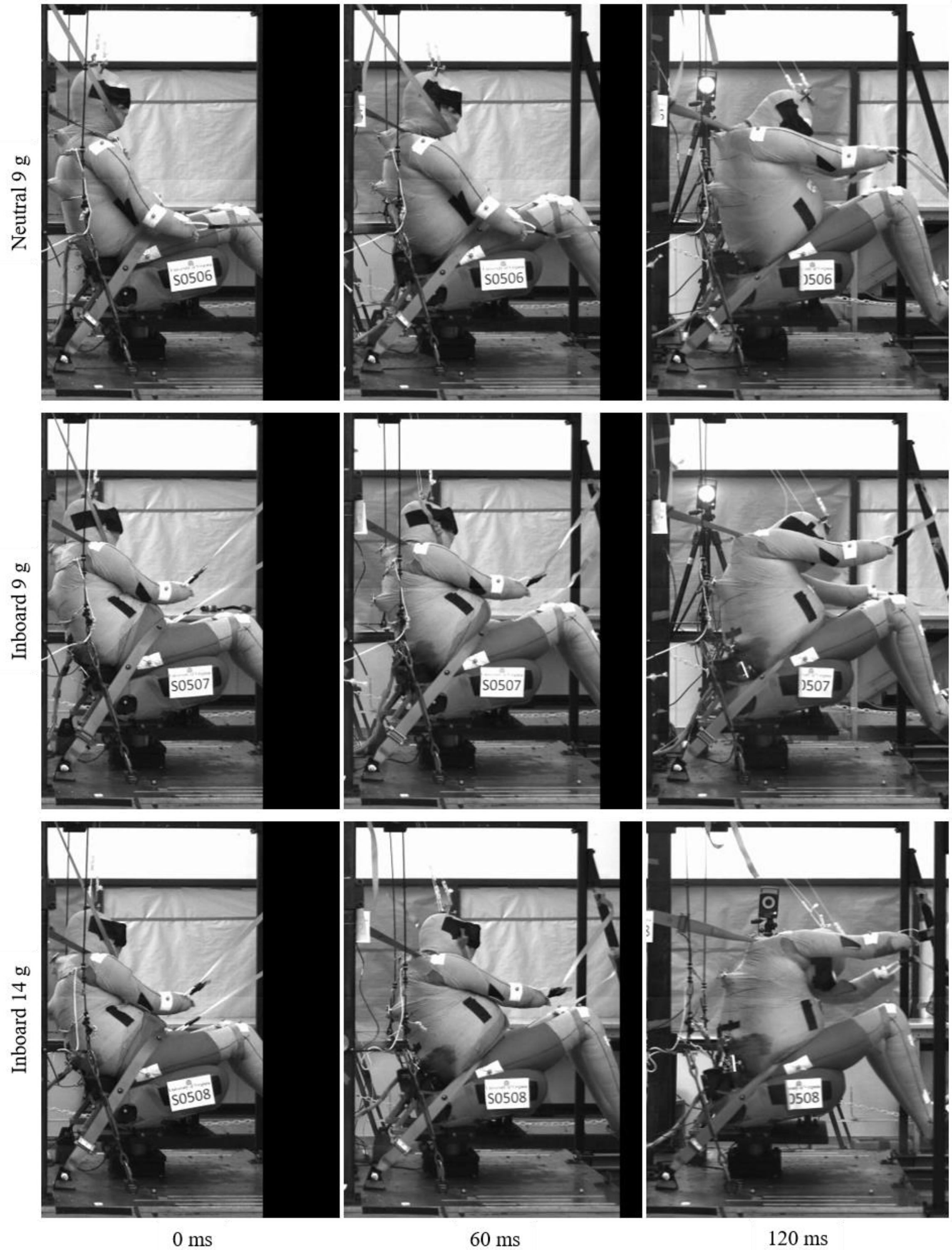

Figure 61. High-speed passenger-side video frames showing the motion sequences up to the time of maximum forward excursion in the neutral 9 g (top), inboard 9 g (middle), and inboard 14 g (bottom) tests for PMHS #3.

Figure 62. High-speed driver-side video frames showing the motion sequences up to the time of maximum forward excursion in the neutral 9 g (top), inboard 9 g (middle), and inboard 14 g (bottom) tests for PMHS #1.

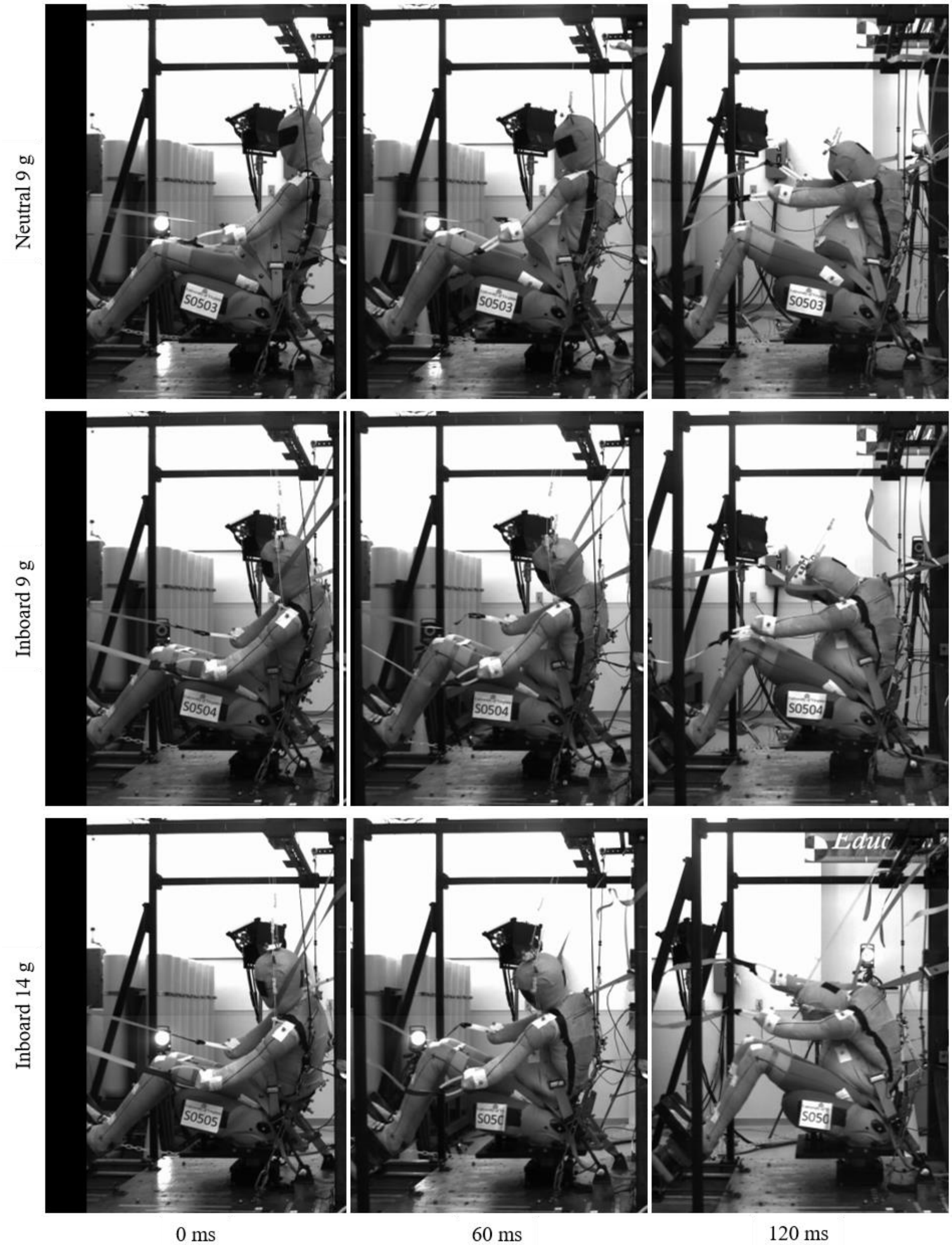

Figure 63. High-speed driver-side video frames showing the motion sequences up to the time of maximum forward excursion in the neutral 9 g (top), inboard 9 g (middle), and inboard 14 g (bottom) tests for PMHS #2.

Figure 64. High-speed driver-side video frames showing the motion sequences up to the time of maximum forward excursion in the neutral 9 g (top), inboard 9 g (middle), and inboard 14 g (bottom) tests for PMHS #3.

Appendix E. Transformation of accelerations to the head center-of-gravity

Input:

- linear accelerations of the orthogonal accelerometers
- angular velocities of the orthogonal angular rate sensors

Output:

- linear accelerations of the body segment in its own coordinate system (CS)

Method:

1. Debias input signals by subtracting out the average of the signal over time t = [-0.1,0].
2. Filter input linear accelerations with a CFC 1000 filter and input angular velocities with a CFC 180 filter.
3. Differentiate the filtered angular velocities to calculate the angular accelerations.

$$\boldsymbol{\alpha}_i(t_i) = \frac{\boldsymbol{\omega}_i(t_i) - \boldsymbol{\omega}_{i-1}(t_{i-1})}{t_i - t_{i-1}}$$

i Data index

t Time

$\boldsymbol{\omega}$ Angular velocities

$\boldsymbol{\alpha}$ Angular accelerations

4. Transform the linear accelerations of the sensors into the sensor-package CS:

$$\boldsymbol{a}_{sj/p} = \boldsymbol{a}_{sj/sj} - \boldsymbol{\omega} \times \left(\boldsymbol{\omega} \times \boldsymbol{r}_{sj/p}\right) - \boldsymbol{\alpha} \times \boldsymbol{r}_{sj/p}$$

$\boldsymbol{r}_{sj/p} = [x_{sj/p} \quad y_{sj/p} \quad z_{sj/p}]^T$ Position of the *j*th sensor with respect to the sensor-package CS (from sensor-package schematics)

$\boldsymbol{a}_{sj/sj}$ Linear accelerations measured by the *j*th sensor in its own CS

$\boldsymbol{a}_{sj/p}$ Linear accelerations measured by the *j*th sensor in the sensor-package CS

$\boldsymbol{\omega} = [\omega_1 \quad \omega_2 \quad \omega_3]^T$ Angular velocities of the rigid body

Since each sensor only measures along a single axis, we select from each $\boldsymbol{a}_{sj/p}$ only the component which was measured:

$$\boldsymbol{a}_{p/p} = \begin{bmatrix} (a_1)_{s1/p} \\ (a_2)_{s2/p} \\ (a_3)_{s3/p} \end{bmatrix}$$

$\boldsymbol{a}_{p/p}$ Linear accelerations of the sensor-package in its own CS

$(a_j)_{sj/p}$ *j*th component of the linear acceleration of the *j*th sensor in the sensor-package CS

These components are expanded below:

$$\boldsymbol{a}_{p/p} = \begin{bmatrix} a_{s1} - \left(\omega_1\omega_2 y_{s1/p} + \omega_3\omega_1 z_{s1/p} - x_{s1/p}(\omega_2^2 + \omega_3^2)\right) - \left(\alpha_2 z_{s1/p} - \alpha_3 y_{s1/p}\right) \\ a_{s2} - \left(\omega_2\omega_3 z_{s2/p} + \omega_1\omega_2 x_{s2/p} - y_{s2/p}(\omega_3^2 + \omega_1^2)\right) - \left(\alpha_3 x_{s2/p} - \alpha_1 z_{s2/p}\right) \\ a_{s3} - \left(\omega_3\omega_1 x_{s3/p} + \omega_2\omega_3 y_{s3/p} - z_{s3/p}(\omega_1^2 + \omega_2^2)\right) - \left(\alpha_1 y_{s3/p} - \alpha_2 x_{s3/p}\right) \end{bmatrix}$$

By defining the sensor-package such that its origin coincides with that of sensor S3 and its axes are parallel to those of sensors S1, S2, and S3 (Figure 1), these components are simplified to

$$\boldsymbol{a}_{p/p} = \begin{bmatrix} a_{s1} + x_{s1/p}(\omega_2^2 + \omega_3^2) \\ a_{s2} + y_{s2/p}(\omega_3^2 + \omega_1^2) \\ a_{s3} \end{bmatrix}$$

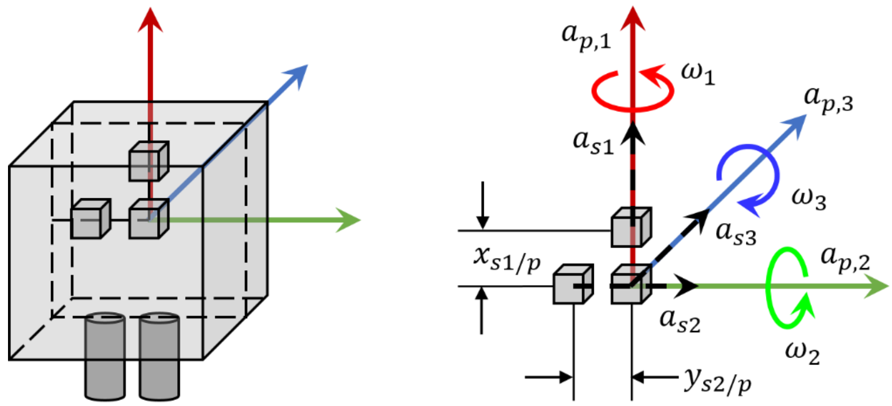

Figure C1. Locations of linear accelerometers in the DTS 6DX Pro (left) and with respect to the sensor package CS (right).

Table C1. Locations of linear accelerometers in the DTS 6DX Pro with respect to the sensor package CS.

Sensor	Axis	[in]	[mm]
s1	x	0.233	5.92
	y	0	0
	z	0	0
s2	x	0	0
	y	-0.233	-5.92
	z	0	0
s3	x	0	0
	y	0	0
	z	0	0

5. Transform the linear accelerations of the sensor-package into the body segment CS:

$$\boldsymbol{a}_b = \boldsymbol{R}_{p/b}\left[\boldsymbol{a}_p - \boldsymbol{\omega} \times \left(\boldsymbol{\omega} \times \boldsymbol{P}_{p/b}\right) - \boldsymbol{\alpha} \times \boldsymbol{P}_{p/b}\right]$$

$$\boldsymbol{T}_{p/b} = \begin{bmatrix} \begin{bmatrix} \boldsymbol{R}_{p/b} \\ (3 \times 3) \end{bmatrix} & \begin{bmatrix} \boldsymbol{P}_{p/b} \\ (3 \times 1) \end{bmatrix} \\ 0 \quad 0 \quad 0 & 1 \end{bmatrix}$$ Transformation matrix of the sensor-package CS

with respect to the body segment CS (from CT scan and mount schematics)

$\boldsymbol{a}_b$ Linear accelerations of the body segment CS

$\boldsymbol{a}_p$ Linear accelerations of the sensor-package CS

$\boldsymbol{\omega}$ Angular velocities of the rigid body